NTNU – Trondheim
Norwegian University of
Science and Technology

Radial Consolidation of Pore Pressure Induced by Pile Driving

Knut-Helge Bergset

Civil and Environmental Engineering
Submission date: June 2015
Supervisor: Gudmund Reidar Eiksund, BAT

Norwegian University of Science and Technology
Department of Civil and Transport Engineering

NORWEGIAN UNIVERSITY OF SCIENCE AND TECHNOLOGY

DEPARTMENT OF CIVIL AND TRANSPORT ENGINEERING

Report Title: Radial consolidation of pore pressure induced by pile driving	Date: 09.06.2015 Number of pages (incl. appendices): 131			
	Master Thesis	X	Project Work	
Name: Knut-Helge Bergset				
Professor in charge/supervisor: Gudmund Eiksund				

Abstract:

Pile installation is recognized to significantly disturb the surrounding clay and cause changes in total and effective stresses around the pile. In this thesis, a numerical model is used to simulate pile installation and subsequent pore pressure dissipation. Pile installation is modelled in Plaxis 2D by the expansion of a cylindrical cavity. The Modified Cam-Clay model is used as a constitutive model. Four different cases are studied, with soil parameters for normal and overconsolidated clay with low and high plasticity. The resulting effective stresses at the pile shaft, normalized by the undrained shear strength from Direct Simple Shear test, are similar for the four cases studied. The predicted consolidation time is shortest for the overconsolidated low-plastic case, and longest for the normally consolidated case with high plasticity. Close to the pile, the soil experience primary loading during dissipation of the excess pore pressure. Outside this zone, the soil experience unloading/reloading type stress changes and behave much stiffer. The radial effective stress at the pile surface decrease with increasing difference in stiffness in these two zones.

Keywords:

1. Pile installation
2. Cavity Expansion Method
3. Plasticity index
4. Overconsolidation ratio

Knut-Helge Bergset

Knut-Helge Bergset

NTNU
Faculty of Engineering Science and Technology
Institute of Civil and Transport Engineering

MASTER DEGREE THESIS

Spring 2015
for

Student: Knut Helge Bergset

Radial consolidation of pore pressure induced by pile driving

BACKGROUND

When a pile is installed in a saturated clay, excess pore pressures are generated around the pile. Pile driving causes large soil deformations and affects the stress- strain- and strength characteristics of the clay. The stress state of the soil surrounding the pile is very different from the original soil state and is difficult to determine. Dissipation of excess pore pressure leads to pile set-up as the effective stresses in the soil increase. However, prediction of pile set-up is challenging due to the large shear strains and excess pore pressures generated from pile installation.

Pile load tests show that the shaft friction of piles installed in clay is strongly dependent on the overconsolidation ratio (OCR) and plasticity index (I_P) for the clay. The physical explanation for these relations is not fully understood.

TASK

The main task of this thesis is to analyse the pore pressure dissipation process after pile installation. The analysis should be performed with soil parameters for normal and over consolidated clay with both low and high plasticity.

Task description

The task will be to analyse the pile installation process, and subsequent dissipation of pore pressures. The pile may installation process can be simplified by assuming simultaneous radial displacement of the pile along the entire pile length. The finite element program PLAXIS may be used for the calculations of pore pressure distribution after pile installation and dissipation of pore pressure with time.

Objective and purpose

The objective of this study is to investigate the impact of plasticity index and OCR on the lateral stress and pore pressures in the clay surrounding a driven pile.

Subtasks and research questions

A literature survey on theories for assessing pore pressure build up induced by pile installation and pile set-up with time should be carried out.

Description and evaluation of soil models to be used in the FEM analysis.

The plasticity index is not a material parameter in the soil models. The possibilities for representing the plasticity index with the other soil parameters should be discussed.

Professor in charge: Gudmund Eiksund

Department of Civil and Transport Engineering, NTNU
Date: 05.06.2015

Professor in charge (signature)

Preface

This master thesis in geotechnics is part of a five-year integrated Master's program in Civil and Environmental Engineering at NTNU, Trondheim. The work was carried out during the spring semester of 2015.

The work presented herein include a literature study and a numerical case study, utilizing theory from the literature survey.

I want to express gratitude to my supervisor, Professor Gudmund Eiksund, for discussions, suggestions, and guidance throughout the study.

Trondheim, 2015-06-09

Knut-Helge Bergset

Summary

When installing or driving a pile into a clay under undrained conditions, large excess pore pressures are generated close to the pile. Pile driving causes significant shearing and disturbance of the soil. The pile capacity will be significantly reduced immediately after pile installation. Increase in effective stress over time as the excess pore pressure dissipate, will lead to pile set-up. Increase in pile capacity over time may also be due to thixotropy and creep effects.

In this thesis, Plaxis 2D is used to simulate pile installation and subsequent pore pressure dissipation. Pile installation is modelled in the finite element program by the expansion of a cylindrical cavity (Cavity Expansion Method). The Modified Cam-Clay model is used as a constitutive model. Four cases are studied, with soil parameters for normal and overconsolidated clay with both low and high plasticity. It is decided to represent the plasticity index (I_p) by flexibility and permeability parameters in the soil model. The compressibility index and swelling index are found to generally increase with increasing plasticity index. The permeability generally decrease with increasing plasticity index.

The resulting effective stresses at the pile shaft, normalized by the undrained shear strength from Direct Simple Shear test (s_{ud}), are similar for the four cases studied. The predicted excess pore pressure, normalized by s_{ud}, is lowest for the overconsolidated high plasticity case, and greatest for the normally consolidated case with low plasticity. Compared with field measurements, the excess pore pressure at the pile shaft is somewhat underpredicted for the normally consolidated cases, and overpredicted for the overconsolidated cases. The generated excess pore pressure field decrease linearly with the logarithm of the radius from the pile. The radial extent of the excess pore pressure field decrease with increasing plasticity index and OCR. As the extent of the generated excess pore pressure is shorter for the overconsolidated cases, shorter consolidation times are predicted for these cases. Further, the consolidation time tend to increase with increasing plasticity index.

The large impact of OCR and plasticity index on the ultimate shaft friction should be reflected in the predicted radial effective stress acting on the pile. The numerical model overpredicts the radial effective stress acting on the pile shaft when comparing with field measurements. Greater radial effective stress is predicted for the overconsolidated cases than the normally consolidated cases. However, there is no distinction in the magnitude of the predicted radial effective stress for different plasticity indexes. In particular, the model fails to predict the low radial effective stress observed in clays with low OCR and low plasticity index.

Close to the pile, the soil experience primary loading during dissipation of the excess pore pressure. Outside this inner zone, the soil experience unloading/reloading type stress changes and behave much stiffer. The radial effective stress at the pile surface decrease with increasing difference in stiffness in these two zones.

Samandrag

Peleramming forårsakar store skjærtøyningar og endringar i jordstrukturen. For pelar i leire kan bæreevna være betydelig redusert like etter ramming. Installasjon av pel i leire fører til oppbygging av poreovertrykk rundt pelen. Pelens bæreevne vil auke i samband med at effektivspenninga aukar over tid når poreovertykket minkar. Auke i bæreevne kan også være på grunn av kryp og "thixotropy".

I denne oppgåva er elementmetodeprogrammet Plaxis 2D brukt til å simulere peleramming og påfølgande konsolideringsfase. Peleramming er modellert ved utviding av eit sylindrisk holrom ("Cavity Expansion Method"). Modified Cam-Clay er brukt som jordmodell. Fire tilfelle er studert med parameterar for normalkonsolidert og overkonsolidert leire med både lav og høg plastisitetsindeks. Plastisitetsindeksen er representert ved hjelp av stivheit og permeabilitet i jordmodellen. Kompressibilitetsindeksen og svelleindeksen aukar med aukande plastisitetsindeks, medan permeabiliteten reduserast med aukande plastisitetindeks.

Effektivspenningane ved peleoverflata, normalisert med udrenert skjærstyrke frå enkle direkte skjærforsøk (s_{ud}), er lik for dei fire studerte tilfella. Det estimerte poreovertrykket, normalisert med s_{ud}, er lavast for den overkonsoliderte leira med høg plastisitetsindeks, og størst for den normalkonsoliderte leira med lav plastisitetsindeks. Samanlikna med feltmålingar, blir poreovertrykket underestimert for dei normalkonsoliderte tilfella og overestimert for dei overkonsoliderte tilfella. Poreovertrykket minkar lineært med logaritmen av avstanden frå pelen. Utstrekkinga av poreovertrykket blir mindre med aukande plastisitetsindeks og overkonsolideringsratio (OCR). Sidan poreovertrykkutstrekkinga er kortare for dei overkonsoliderte tilfella, er konsolideringstida også kortare. I tillegg er konsolideringstida kortare for leirer med lav plastisitetsindeks sidan dei har høgare permeabilitet.

Den store innverknaden frå OCR og plastisitetsindeks på sidefriksjonen bør visast igjen i den estimerte radielle effektivspenninga ved pelen. Den numeriske modellen overestimerer den radielle effektivespenninga samanlikna med feltmålingar. Større radiell effektivspenning er estimert for dei overkonsoliderte tilfella enn dei normalkonsoliderte tilfella. Derimot er det ingen forskjell i dei estimerte radielle effektivspenningane for ulik plastisitetsindeks. Den numeriske modellen viser dermed ikkje dei svært lave effektivspenningane målt i leirer med lav plastisitetsindeks og lav OCR.

I konsolideringsprosessen opplever jorda primærlasting i ei sone nærast pelen. Utanfor denne indre sona oppfører jorda seg mykje stivare, sidan jorda opplev avlasting/gjenlasting. Den radielle effektivspenninga som verkar på pelen blir redusert med aukande forskjell i stivheit i desse to sonene.

Table of Contents

List of Figures

List of Tables

1 Introduction

1.1 Background

Installation of a pile in a saturated clay causes significant shearing and disturbance of the surrounding soil. During pile driving, excess pore pressure will develop around the pile. As the excess pore pressure dissipates, the effective stresses around the pile will increase and as a result, the bearing capacity of the pile will increase. Increase in pile capacity with time is known as pile set-up. In design, it is crucial to be able to predict the pile capacity and the pile set-up times. Significant cost reductions in projects involving pile foundations in clay can be obtained by considering the time for pile set-up.

Pile load tests show that the shaft friction of piles installed in clay is strongly dependent on the overconsolidation ratio (OCR) and plasticity index (I_p) for the clay. Karlsrud (2012) propose two new procedures for predicting the ultimate shaft friction of piles, which takes these relations into account. One of the main observations in Karlsrud's work is that low plasticity clays have very low bearing capacity after pile installation. The physical explanation to this observation is not fully understood.

This thesis investigates the impact of plasticity index and OCR on the earth and pore pressures in the clay surrounding a driven pile.

Literature review

Hill (1950) presented an analytical solution to determine the stress changes caused by pile installation. The solution was based on plasticity theory and the expansion of a cylinder, and is referred to as the Cavity Expansion Method (CEM). In the late 1970's, the CEM theory was expanded and more advanced soil models was included in the analysis of pile installation (Carter et al., 1978, Carter et al., 1979, Randolph et al., 1979, Randolph and Wroth, 1979). This was accompanied by the use of the Finite Element Method (FEM). Randolph et al. (1979) carried out a parametric study on the effect of OCR on the stress changes in the soil due to pile installation.

The Strain Path Method (SPM) presented by Baligh (1985), assumes that the soil flow around a penetrating pile is similar to the flow of a viscous liquid. In the SPM, soil deformations and strains are independent of the actual constitutive properties of the soil.

To validate numerical models, small scale testing on instrumented piles have been carried out by researchers in both the laboratory and in field. A number of large scale test program was

also carried out, as dealt with in detail by Karlsrud (2012). In combination, numerical models and instrumented pile load tests have led to analytical methods that account for pile installation effects on the clay surrounding a pile. However, the typically used pile design methods are semi-empirical.

1.2 Objective

The main objective of this study is:

- To investigate the impact of plasticity index and OCR on the lateral stress and pore pressure in the clay surrounding a driven pile.

Secondary objectives are:

- To study the effect of pile installation on the stress-, strain- and strength characteristics of clays.
- To choose a suitable soil model for a FEM analysis and determine parameters that may represent the plasticity index

1.3 Approach

Separate approaches are selected to meet the objectives stated above.

For the main objective:

- Finite element modelling in Plaxis 2D will be carried out to predict the earth and pore pressures generated in the clay surrounding a pile from installation and reconsolidation phases, including the required consolidation time. A case study will be carried out, with soil parameters for normal and overconsolidated clay with both low and high plasticity. The predictions will be compared with field measurements collected from a literature survey.

For the secondary objectives:

- A literature study on analytical and numerical methods for predicting the stress- and strain changes in the clay due to pile installation will be carried out. Processes that can influence the shaft friction along a pile will be discussed. In addition, the procedures for estimating shaft friction by Karlsrud (2012) will be presented.

- The chosen constitutive model shall be described and evaluated. Representative soil parameters for the plasticity index shall be determined from general correlations found in literature.

1.4 Limitations

This study is limited to pile driving in saturated clay. That is, pile installation is assumed to occur sufficiently rapid to ensure that little or no drainage occur in the clay surrounding the pile during installation.

Attention in this work is devoted to installation of closed-ended piles. Any differences with open-ended piles are briefly discussed where it is felt appropriate.

1.5 Structure of the Report

This report consists of two main parts. The first part concerns a literature review. Chapter 2 concerns pile foundations; when they are applied, how they are installed and installation effects on the surrounding soil. The processes that may influence the shaft friction by time will be discussed. The Modified Cam-Clay (MCC) model will be reviewed in Chapter 3, and the Cavity Expansion Method (CEM) is presented in Chapter 4. The MCC model and the CEM will be used in the numerical analysis. A review of literature on the CEM coupled with the elastic, perfectly plastic (EP) soil model and the Modified Cam-Clay (MCC) model is included in Chapter 4. In Chapter 5, the Strain Path Method (SPM) is introduced. The procedures for predicting shaft friction proposed by Karlsrud (2012), are presented in Chapter 6. Chapter 6 can be seen as the background to carry out a case study.

A case study is carried out in the second part of this study. Four different cases are studied. Soil parameters for the MCC model are determined for normal and overconsolidated clay with both low and high plasticity in Chapter 7. A numerical analysis is carried out for the cases studied in Chapter 8. Results from finite element modelling in Plaxis 2D are compared to field measurements. Further, a parametric study on the virgin compression index and the swelling index is conducted. Discussion of results are given in Chapter 9. Finally, conclusions and recommendations for further work are presented in Chapter 10.

A list of symbols and abbreviations are given in the back of this report. When expressions or figures are taken from other sources, the symbols may differ from what is given in this list, but are then defined within the text.

Appendix A presents the undrained shear strength obtained from Direct Simple Shear Test in Plaxis 2D for the different cases studied. Appendix B presents a “thin slice” model tried in Plaxis 2D that gave unsatisfactory results. In Appendix C, circumferential and vertical stresses from a parametric study carried out in section 8.5.2 are presented.

2 Pile Foundations

When shallow foundations are inadequate to support a structure, deep foundations (pile foundations) are required to transfer the structural loads to soils at deeper depth. A pile is a slender, structural member, normally consisting of steel, concrete, timber or plastic. The selection of material depends on the magnitude of the structural loads, the availability of material, and the environment at the site. According to Budhu (2008), pile foundations are typically used when:

- The soil close to the ground surface does not have sufficient capacity to support the structural loads.
- The estimated total settlement or the estimated differential settlement exceeds tolerable limits
- The structural loads consist of large horizontal loads, moments or uplift forces.
- The excavations to construct a shallow foundation are difficult or expensive.

2.1 Pile Installation

Piles can either be driven into the ground (driven piles), or they can be bored (bored piles). Pile driving may produce excessive noise from the hammering. In addition, pile driving may lead to ground vibration, which can damage adjacent structures. In some cases, especially in urban areas, pile driving may induce intolerable noise and vibration.

A pile that displaces a large volume of soil is called a displacement pile**.** Driven piles with solid sections, such as closed-ended piles, are displacement piles. A pile that displaces less than 10 % of soil volume relative to the pile's external volume is called a non-displacement pile (e.g. open-ended piles) (Budhu, 2008).

2.2 Effects of Pile Installation

Pile installation has a pronounced effect on the stresses and strains in the nearby soil. Sand and clay behave differently, only clay soils are considered in the work presented herein.

When displacement piles are driven into a saturated clay under undrained conditions, it causes significant shearing and disturbance of the surrounding soil. This affected area around the pile is referred to as the disturbed zone. During installation, the soil fails due to the imposed shear

stress at the interface of the pile and soil, and radial compression to the soil mass adjacent to the pile (Budhu, 2008).

After pile installation, the following processes can influence the shaft friction along a pile by time:

- Increased shaft friction due to dissipation of excess pore pressures and increasing effective stress.
- Increased shaft friction due to thixotropy.
- Increased strength due to ageing effects, or creep.

2.2.1 Dissipation of Excess Pore Pressure

At the end of pile driving, an excess pore pressure field will exist around the pile. The excess pore pressure is primarily due to increase in total stress as the soil is pushed outwards. In addition, changes in mean effective stress due to shearing and partial remoulding of the soil contribute to the excess pore pressure. Shearing of the soil will produce positive excess pore pressures for lightly overconsolidated clay, and negative pore pressures for potentially dilatant, heavily overconsolidated clay (Randolph, 2003).

After pile installation, the disturbed soil will reconsolidate as the excess pore pressure dissipates. During the reconsolidation process, the effective stress increases, and thus the soil strength increases. As the permeability may be very low in fine-grained soils, the reconsolidation process may last for a very long time.

The stresses and strains induced by the pile installation may alter the physical properties of the clay, and thereby significantly affect the pile capacity. Work has been done in identifying the processes that occur in the soil surrounding the pile, but quantification of the changes in stress and fabric is not straight forward (Randolph, 2003). Randolph (2003) argues that any scientific approach to predict the pile shaft friction must consider the three main phases during history of a driven pile (Figure 2.1). The main phases are the installation process, equilibration of excess pore pressures (reconsolidation) and loading of the pile.

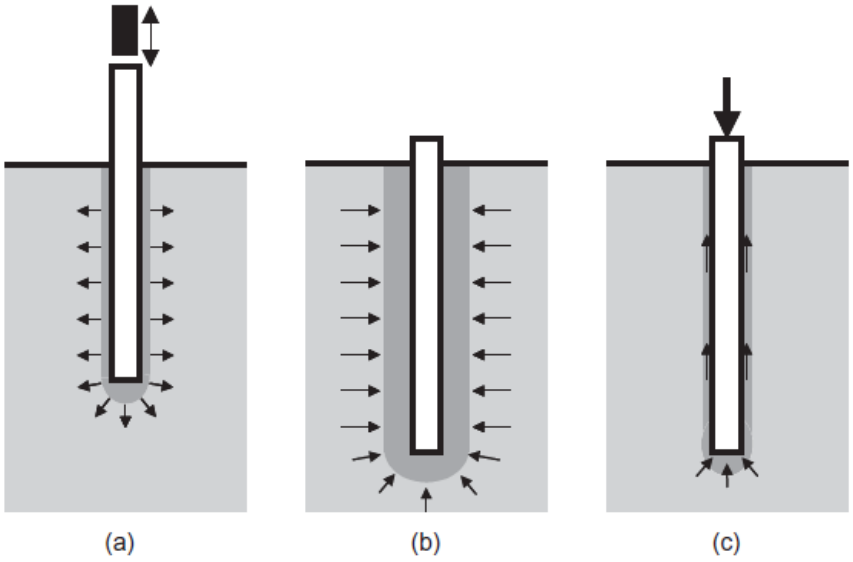

Figure 2.1: Main phases: (a) installation; (b) equilibration of excess pore pressures; (c) loading (Randolph, 2003)

2.2.2 Thixotropy

Mitchell (1961) define thixotropy as a process of softening caused by remoulding, followed by a time dependent return to the original state at a constant water content and constant porosity. In a fully thixotropic material, this process is completely reversible.

Thixotropy is a geochemical effect that involves a strength increase under constant effective stress and volume. The thixotropy strength ratio, C_t, is the ratio between the shear strength after a certain time with thixotropic strength gain and the shear strength just after remoulding. Skempton and Northey (1952) studied the sensitivity of clays and found that natural clays exhibited a significant strength increase by time. The thixotropy of clays is likely to depend strongly on their mineral composition. Figure 2.2 by Andersen and Jostad (2002) present the thixotropy strength ratio as a function of plasticity index. The figure is based on data from literature (Skempton and Northey, 1952, Mitchell, 1961). The thixotropy strength ratio increases with plasticity index, but the scatter in Figure 2.2 is large. Figure 2.2 also illustrate that the thixotropy strength ratio increases with time after remoulding. The data is based on clays with sensitivity higher than 2.8. There is insufficient data on overconsolidated clays to conclude if the OCR has an effect on the thixotropy.

The thixotropy effect means that a clay may exhibit a strength after installation that is higher than the remoulded shear strength, even before pore pressure dissipation occurs. The strength will be equal to the remoulded shear strength multiplied by the thixotropy strength ratio. It is generally assumed that strength gain from thixotropy and pore pressure dissipation occur independently of each other. The two process are not additive, as the interaction between thixotropy and effective stress is unknown (Andersen and Jostad, 2002).

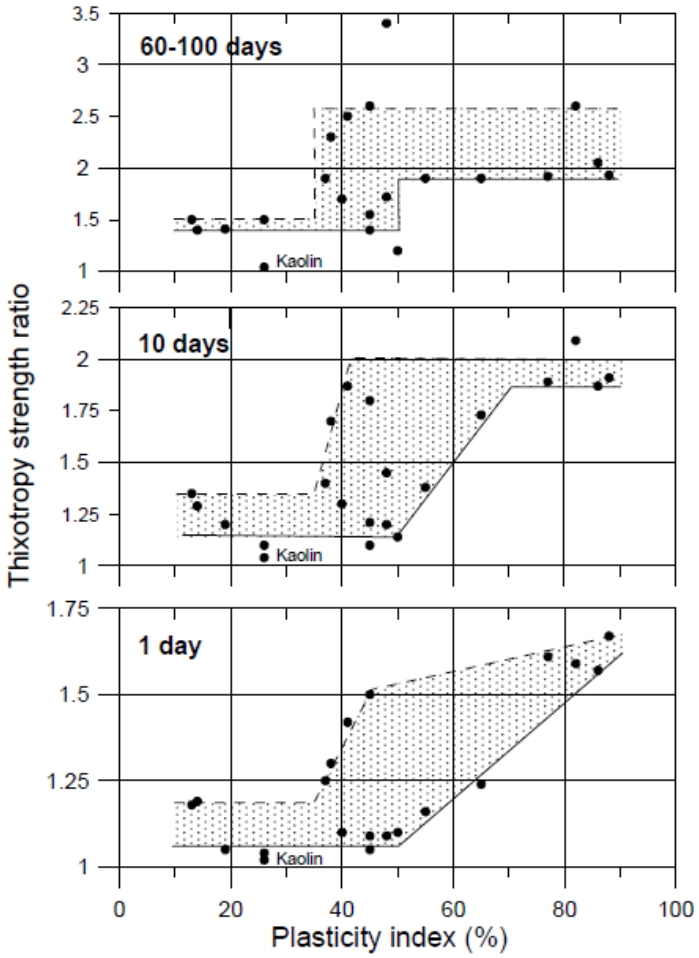

Figure 2.2: Thixotropy strength ratio as a function time and plasticity index (Andersen and Jostad, 2002)

2.2.3 Creep

Pile tests have shown that the ultimate shaft friction may continue to increase with time after the excess pore pressure has dissipated. This may be due to chemical bonding (thixotropy), as discussed, or a further increase in total and effective stress due to creep effects. Creep, or secondary compression, is the change in volume of a clay soil caused by the adjustment of the soil fabric (Budhu, 2008).

Mesri (1973) reported that it exists a relationship between the coefficient of secondary compression C_α and I_p. C_α is defined as the ratio of decrement in void ratio to the logarithm of time during secondary compression ($C_\alpha = \Delta e/\Delta \log t$). Figure 2.3 show a relationship between C_α and the plasticity index as found by Nakase et al. (1988). The data from Nakase et al. (1988) suggests that the coefficient of secondary compression increase with increasing I_p.

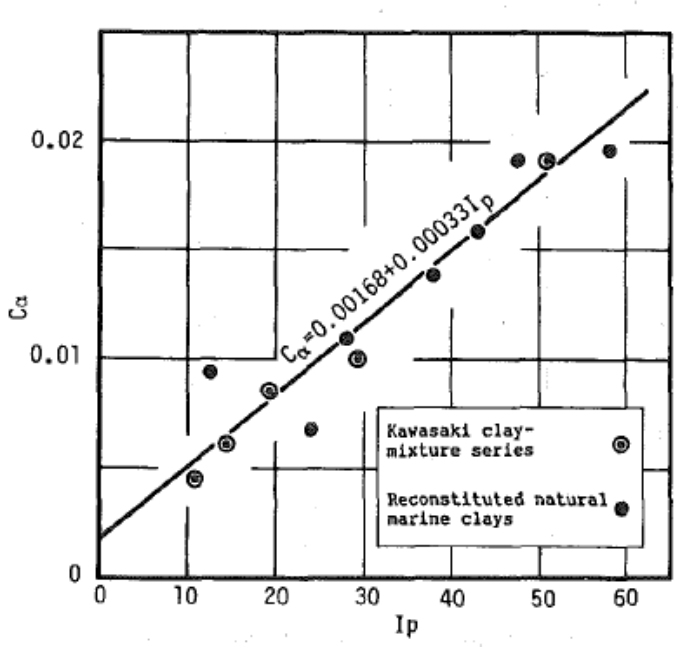

Figure 2.3: Correlation between Secondary Compression Index and Plasticity Index (Nakase et al., 1988)

3 The Modified Cam-Clay Model

The Modified Cam-Clay (MCC) model is based on critical state soil mechanics and is similar to the model suggested by Roscoe and Burland (1968). A critical state is a state where unlimited shear strains may occur without any change in effective stress, volume or shear stress (Roscoe et al., 1958). Critical state theory suggests that every soil fails on a unique surface in (p, q, e) space. The failure stress state is thus not sufficient for failure, as the soil also must reach a critical void ratio. The mean effective stress, p', and the equivalent shear stress, q, can be calculated in terms of principal stresses as in equation (3.1) and (3.2) respectively. For triaxial states with $\sigma'_2 = \sigma'_3$, the deviatoric stress is reduced to $q = (\sigma'_1 - \sigma'_3)$.

$$p' = \frac{1}{3}(\sigma'_1 + \sigma'_2 + \sigma'_3) \tag{3.1}$$

$$q = \sqrt{\frac{1}{2}((\sigma'_1 - \sigma'_2)^2 + (\sigma'_2 - \sigma'_3)^2 + (\sigma'_3 - \sigma'_1)^2)} \tag{3.2}$$

The MCC model is a work-hardening elastic-plastic soil model, that allow for the strength of the soil to change as the water content changes during consolidation. In the MCC model, the critical state condition is given by the critical state line (CSL), defined as

$$q = Mp' \tag{3.3}$$

M is the inclination of the CSL, but it also determines the shape of the yield surface and influences the coefficient of lateral earth pressure K_0^{nc}. The preconsolidation stress p_c' determines the size of the yield surface (Figure 3.1). The yield surface for the MCC model represents an ellipse in p'-q plane defined in equation (3.4). Only elastic strain increments occur for stress paths within the ellipse, while both elastic and plastic strains generally occur for stress paths that cross the boundary.

$$q^2 - M^2\{p'(p'_c - p')\} = 0 \tag{3.4}$$

Figure 3.1 illustrate the yield ellipse in p'-q plane. On the "dry side" of the CSL, plastic yielding involves softening, and thus failure. Brinkgreve et al. (2014) say that in this region, the values of q can become unrealistically large in numerical analysis. On the right hand side of the yield ellipse (the "wet side" of the CSL), plastic yielding is associated with expansion of the yield surface. This is represented by strain hardening.

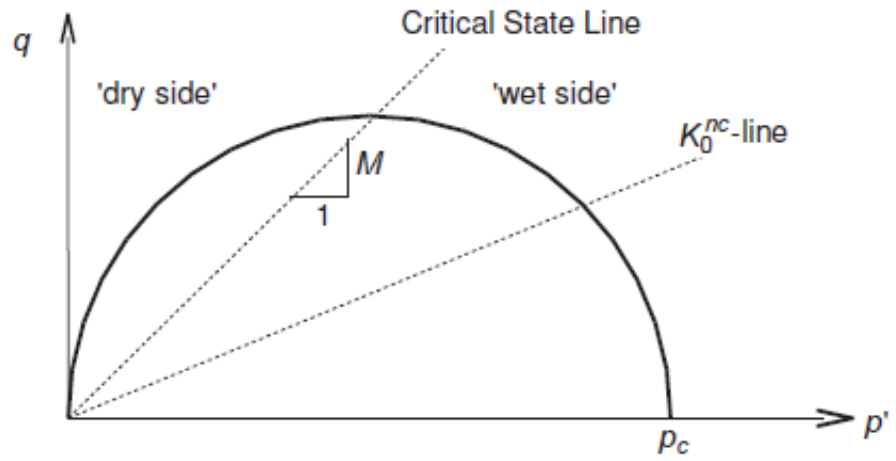

Figure 3.1: Yield surface of the MCC model in p'-q space (Brinkgreve et al., 2014)

A natural logarithmic relation between void ratio *e* and the mean effective stress *p'* is assumed in the MCC model. During virgin isotropic ($\sigma'_1 = \sigma'_2 = \sigma'_3 = p'$) compression, the preconsolidation stress increases as stress increases, resulting in elastoplastic deformations following the λ-line. During isotropic unloading and reloading, the preconsolidation level remain constant, resulting in only elastic volumetric deformations following the κ-line. The compression index, λ, and the swelling index, κ, can be obtained from oedometer tests. Relations to the compression index, C_c, and recompression index, C_r, are:

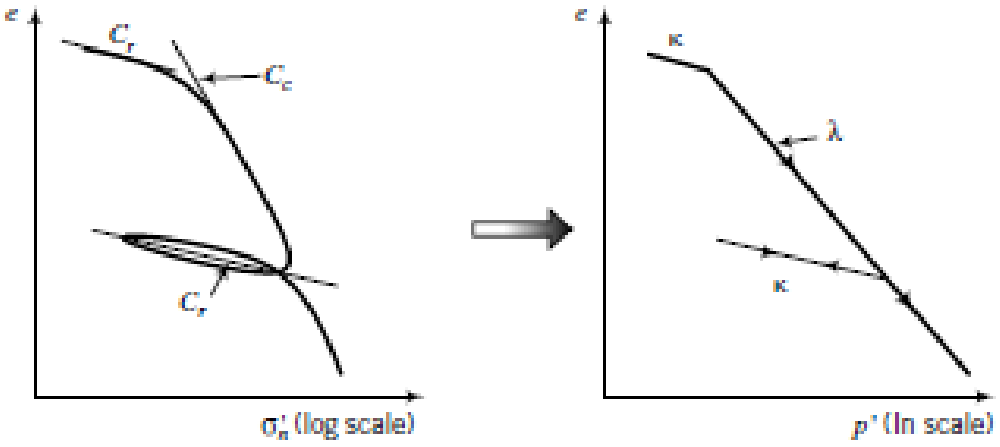

Figure 3.2: Relation between consolidation parameters (Budhu, 2008)

$$\lambda = \frac{C_c}{2.3} \tag{3.5}$$

$$\kappa \approx \frac{2\,C_r}{2.3} \tag{3.6}$$

There is no exact relation between κ and C_r as shown in equation (3.6), because the ratio between horizontal and vertical stresses changes during one-dimensional unloading (Brinkgreve et al., 2014). The factor 2.3 is obtained from the ratio between logarithm of base 10 and the natural logarithm.

A nonlinear elastic volumetric modulus is used in the MCC model. The bulk modulus can be calculated as

$$K = \frac{vp}{\kappa} \tag{3.7}$$

Where v is specific volume ($v = 1 + e$), p is mean stress, and κ is the swelling index.

The MCC formulation requires specification of either the shear modulus G or Poisson's ratio ν_{ur}. The Poisson's ratio is the negative ratio of transverse to axial strain. In Plaxis, the Poisson's ratio is given as an input parameter. The relation between G and ν_{ur} is

$$G = \frac{3(1 - 2\nu_{ur})}{2(1 + \nu_{ur})} K \tag{3.8}$$

In order to obtain the correct shear strength, the inclination of the critical state line, M, should be based on the friction angle φ'. Equation (3.9) give the relation between M and the Coulomb friction angle. The (+) sign is valid for triaxial extension and the (-) sign is valid for triaxial compression. The M parameter for compression should be used as an input parameter in the MCC model in Plaxis (Brinkgreve et al., 2014).

$$M = \frac{6\ sin\varphi'}{3 \pm sin\varphi'} \tag{3.9}$$

In addition, the initial void ratio, e_0, need to be determined in the MCC model in Plaxis. To summarize, the MCC model is based on the following input parameters:

ν_{ur}: Poisson's ratio

λ: Cam-Clay compression index

κ: Cam-Clay swelling index

M: Tangent of the critical state line

e_0: Initial void ratio

4 The Cavity Expansion Method

When a pile is driven into a soil, it displaces a volume of soil equal to the volume of the pile. At small penetrations, some heave of the ground surface is expected. Most of the ground heave occurs during initial penetration up to about twelve times the pile radius (Cooke and Price, 1973). At larger depths however, the soil is mainly displaced outwards in the radial direction. Studies of the displacement pattern near the tip of the pile have shown the displacement behavior to be midway between the expansion of a spherical cavity and the expansion of a cylindrical cavity (Roy et al., 1975). However, studies have shown that little further vertical movement of soil occurs at any level once the tip of the pile has passed that level. Stress changes in the soil close to the pile (except for near the tip of the pile and the ground surface) is therefore claimed to be similar to those produced from the expansion of a cylindrical cavity.

The Cavity Expansion Method (CEM) assumes that the strains induced from pile installation comes from ideal expansion of a cylindrical cavity. For closed-ended piles, the expansion is assumed to occur from zero initial cavity radius to the outer radius, r_0, of the pile. Solutions for open-ended piles involves expanding from the inner radius, r_i, to the outer radius. If the pile partially plugs, it may however be assumed that the expansion is larger than the pile wall thickness. On the other hand, if the clay for some reason enters the pile more easily inwards into the pile than outwards, an expansion smaller than the full wall thickness may be assumed. Figure 4.1 show measurements of radial displacement of soil induced from installation of closed-ended piles. The radial displacement is plotted against the radial position before pile driving. Measured results compares well with the theoretical prediction made from assuming plane strain and cylindrical deformation at constant volume. The radial displacement, v, of a soil particle initially at a distance r from the pile axis is here given by:

$$\frac{v}{r_0} = \left[\left(\frac{r}{r_0}\right)^2 + \rho\right]^{1/2} - \frac{r}{r_0} \tag{4.1}$$

Where ρ is the area ratio defined by Carter et al. (1978) as:

$$\rho = 1 - \left(\frac{r_i}{r_o}\right)^2 \tag{4.2}$$

Where r_i is the inner radius of a pile, and r_o is the outer radius. This means that $\rho = 1$ for closed-ended piles.

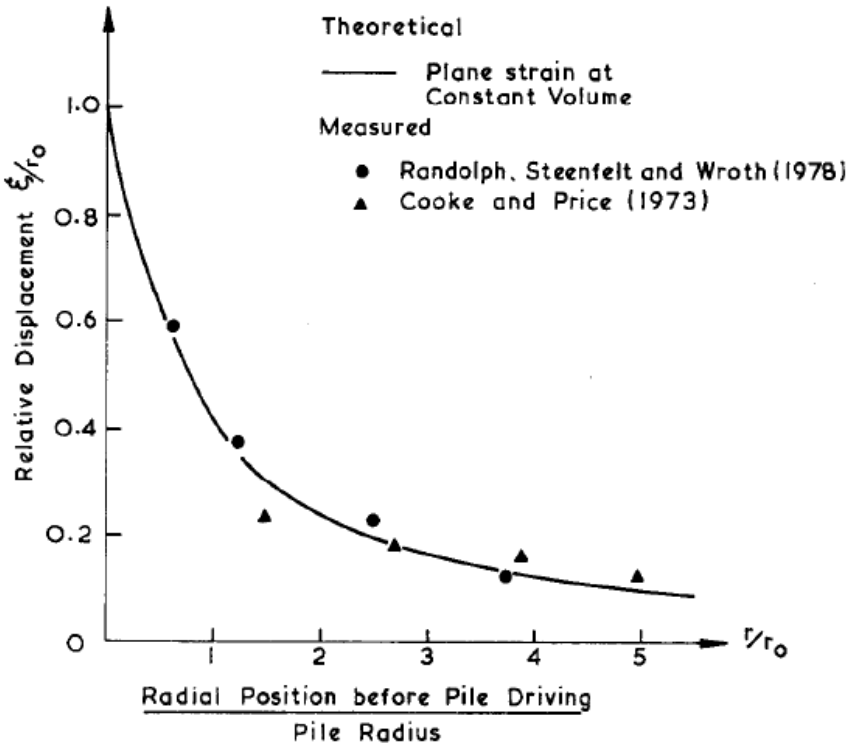

Figure 4.1: Comparison of measured and theoretical radial soil displacement (Randolph et al., 1979)

To predict the stress changes in the soil due to the imposed strains from the cavity expansion, the CEM method has been coupled with various constitutive models. In the following, solutions for the elastic, perfectly plastic (EP) and the Modified Cam-Clay (MCC) model are presented

4.1 CEM-EP

4.1.1 Pile Installation

Randolph and Wroth (1979) present a solution based on the assumption of expansion of a cylindrical cavity in an ideal elastic, perfectly plastic (EP) type soil model. They assume conditions of axial symmetry and plane strain, this implies that only radial displacement of soil particles occur. The equations of radial and vertical equilibrium in terms of total stresses are:

$$\frac{\delta\sigma_r}{\delta r} + \frac{\sigma_r - \sigma_\theta}{r} = 0 \tag{4.3}$$

$$\frac{\delta\sigma_z}{\delta z} = \gamma \tag{4.4}$$

Characterized by a shear modulus *G* and undrained shear strength s_u, the expressions for the stresses around an expanded cavity are given by Hill (1950) and Gibson and Anderson (1961). For a cavity expanded from zero radius to a radius r_0, the radial and circumferential stress changes within the plastic zone are given by:

$$\Delta\sigma_r = s_u\left[1 + ln\left(\frac{G}{s_u}\right) - 2\ln\left(\frac{r}{r_0}\right)\right] \tag{4.5}$$

$$\Delta\sigma_\theta = s_u\left[-1 + ln\left(\frac{G}{s_u}\right) - 2\ln\left(\frac{r}{r_0}\right)\right] \tag{4.6}$$

Close to the pile, in the plastic zone, the shear stress exceeds the undrained shear strength of the soil. The width of the plastic zone (plasticized radius) is given by

$$r_p = r_0\left[\frac{G}{s_u}\right]^{1/2} \tag{4.7}$$

Further, Randolph and Wroth (1979) estimate the excess pore pressure by assuming that the mean effective stress remains constant under undrained conditions. The excess pore pressure will then equal the change in mean total stress, as expressed in equation (4.8).

$$\Delta u = \frac{1}{3}(\Delta\sigma_r + \Delta\sigma_\theta + \Delta\sigma_v) = s_u\left[ln\left(\frac{G}{s_u}\right) - 2\ln\left(\frac{r}{r_0}\right)\right] \tag{4.8}$$

Outside the plasticized radius, the excess pore pressure will be zero since

$$\Delta\sigma_\theta = -\Delta\sigma_r = s_u\left(\frac{r_p}{r}\right)^2 \tag{4.9}$$

$$\Delta\sigma_v = 0 \tag{4.10}$$

The distribution of the initial excess pore pressure can then be written as

$$\Delta u_0 = 2\,s_u\ln\left(\frac{r_p}{r}\right), \qquad r_0 \le r \le r_p \tag{4.11}$$

$$\Delta u_0 = 0, \qquad r_p \le r \le r^* \tag{4.12}$$

Where r_p is given by equation (4.7). The maximum excess pore pressure at the pile shaft will be

$$\Delta u_{max} = s_u \ln\left(\frac{G}{s_u}\right) \tag{4.13}$$

For the EP soil model, the radial effective stress increase at the pile shaft after installation can now be found from equations (4.5) and (4.13) to correspond to $\Delta\sigma'_r = s_u$.

The excess pore pressure distribution immediately after installation for open-ended piles is as for closed-ended piles. For open-ended piles however, the cavity expands from initial radius r_i to the outer radius r_0. The radius of the plastic zone is therefore given by

$$r_p = r_0 \left(\frac{r_0^2 - r_i^2}{r_i^2}\right)\left[\frac{G}{s_u}\right]^{1/2} \tag{4.14}$$

Figure 4.2 illustrate the excess pore pressure around the pile in the plastic region (*R* corresponds to r_p).

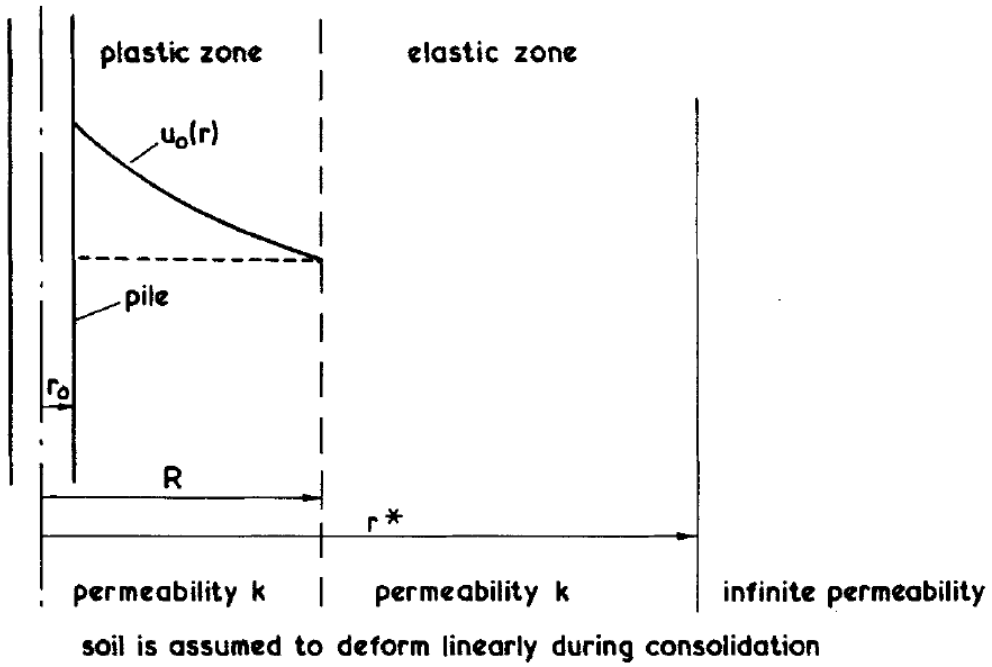

Figure 4.2: Excess pore pressure around a driven pile (Randolph and Wroth, 1979)

Ladanyi (1963) point out that the limiting pressure needed to expand a cylindrical cavity may be calculated from the solution for an elastic, perfectly plastic material, provided a reasonable secant shear modulus is chosen. Figure 4.3 show how the secant shear modulus is defined. The secant shear modulus at 50 % mobilization (G_{50}) of the soil strength is often used as an

equivalent linear stiffness. For triaxial tests, where undrained loading starts at an initial shear stress, the degree of shear strength mobilization refers to the applied increase in shear stress, $\Delta\tau_f$. Ladanyi (1963) suggest a secant modulus taken over the stress range from zero up to half the ultimate shear stress.

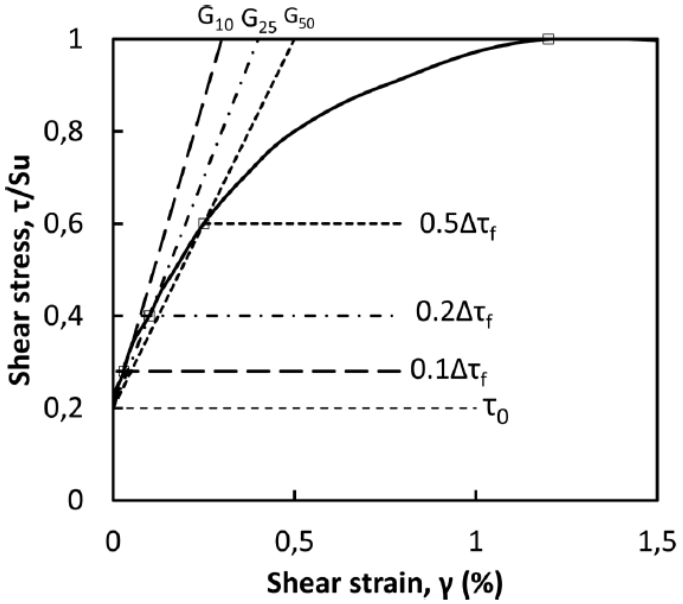

Figure 4.3: Definition of secant shear modulus (Karlsrud and Hernandez-Martinez, 2013)

Figure 4.4 shows a typical range of normalized shear modulus, G_{50}/s_{uc}, as seen on consolidated anisotropic undrained compression tests (CAUC) on high quality block samples (Karlsrud, 2012). The highest values of G_{50}/s_{uc} is observed for marine clays with water content in the range 30-40%, which typically means clays with plasticity index in the range 12-20 % according to Karlsrud (2012). Lower values of G_{50}/s_{uc} are observed for more plastic clays with water content around 60-70 %. Based on the average shear modulus from Figure 4.4, Figure 4.5 show: a) the normalized excess pore pressures at the pile shaft, and b) the plasticized radius, for the CEM-EP model (Karlsrud, 2012). Both the normalized excess pore pressure and the plasticized radius decrease with increasing OCR. The excess pore pressure will increase with depth as the undrained shear strength increase with depth. The plastic zone is constant with depth as it only depends on the ratio G/s_u. G and s_u are assumed to increase with depth in a similar way; linearly with the mean effective stress (Randolph et al., 1979).

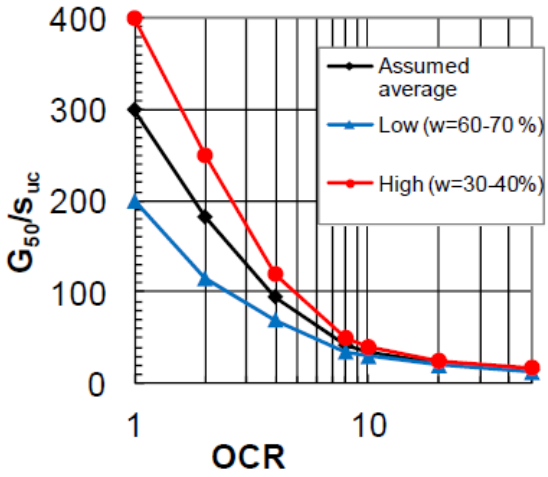

Figure 4.4: Typical range of normalized G50/suc- values obtained from CAUC triaxial tests on high quality block samples (Karlsrud, 2012)

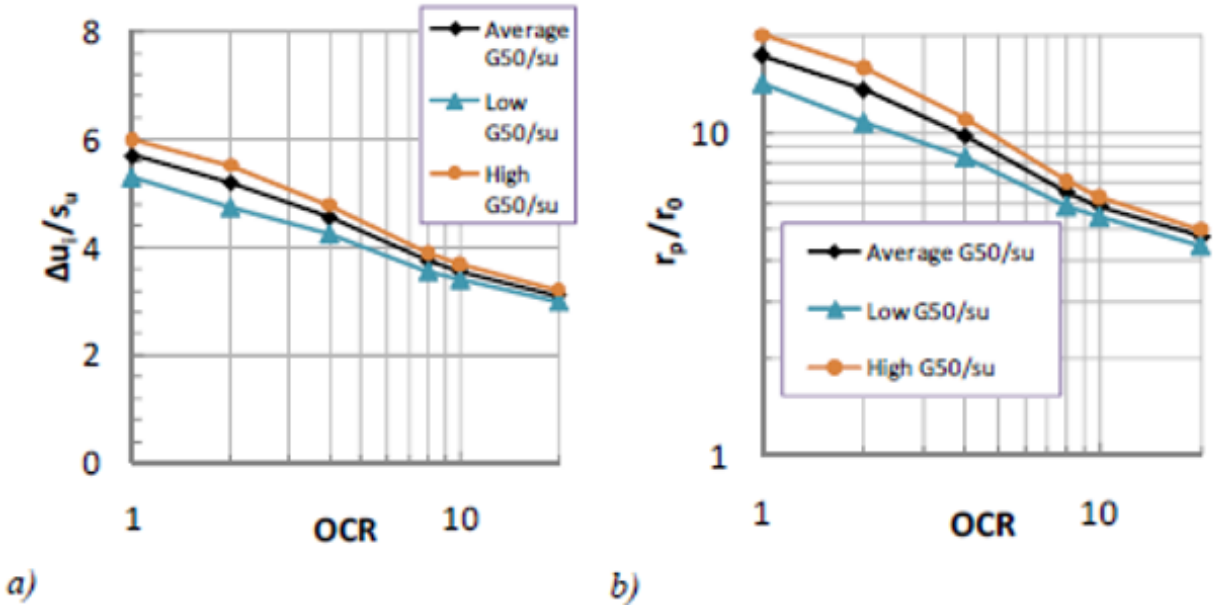

Figure 4.5: a) Normalized maximum excess pore pressures based on CEM-EP model; b) Normalized installation plasticized radius based on CEM-EP model. (From Karlsrud (2012))

4.1.2 Reconsolidation

Randolph and Wroth (1979) assume that consolidation takes place primarily by pore water flow radially outwards from the pile. The pile is presumed rigid and impermeable. During consolidation, the soil particles will move inwards towards the pile under conditions of plane strain and axial symmetry. Since the soil originally have been displaced outwards during

driving, most of the soil will go through a process of unloading in shear. Thus, Randolph and Wroth (1979) assume that the soil deforms elastically during the reconsolidation. Figure 4.2 illustrate the plastic region during pile installation. In the plasticized zone, the soil reaches failure in shear during pile driving. However, all of the soil is assumed to deform elastically during consolidation. Only considering axisymmetric radial flow, the governing consolidation equation reduce to the same form as Terzaghi's one-dimensional consolidation equation (Terzaghi, 1943)

$$\frac{\partial u}{\partial t} = c_h\left(\frac{\partial^2 u}{\partial r^2} + \frac{1}{r}\frac{\partial u}{\partial r}\right) \tag{4.15}$$

where c_h is the coefficient of consolidation in the horizontal or radial direction. For an elastic soil, c_h is constant and can be defined as

$$c_h = \frac{k}{m_v \gamma_w} = \frac{k}{\gamma_w}\frac{2G(1-\nu')}{1-2\nu'} \tag{4.16}$$

Where k is the hydraulic conductivity (permeability) of the soil, m_v is the coefficient of volume compressibility, γ_w is the specific weight of water, G is the elastic shear modulus and ν' is Poisson's ratio in terms of effective stress.

The rate of consolidation depend on the coefficient of consolidation, the radius of the pile, and the size of the maximum pore pressure. From equation (4.13), the initial excess pore pressure at the pile shaft is proportional to s_u, and it also depends on the ratio G/s_u. Soderberg (1962) found a suitable non-dimensional time variable to be

$$T = \frac{C_h t}{{r_0}^2} \tag{4.17}$$

Figure 4.6 show the variation of excess pore pressure at the pile shaft with time for different ratios of G/s_u. Both the excess pore pressure at the pile shaft and the consolidation time, increase with increasing ratio G/s_u.

The total stress change is zero during consolidation for the EP soil model, thus the radial effective stress increase can be found by equation (4.5). At the pile shaft, the increase in radial effective stress after dissipation of excess pore pressure is $\Delta\sigma'_r = s_u \cdot (1+\ln(G/s_u))$.

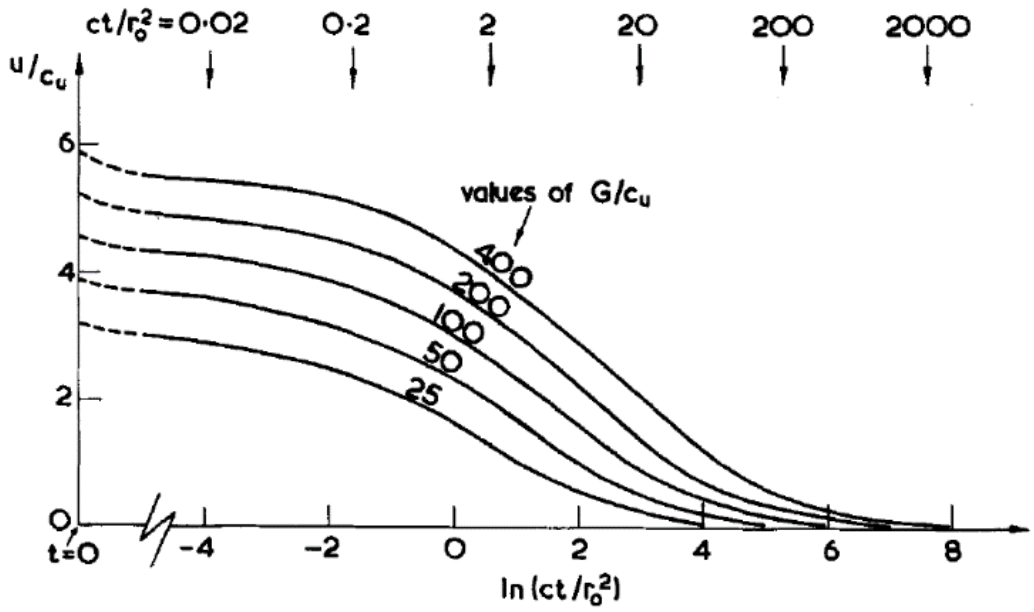

Figure 4.6: Variation of excess pore pressure at the pile shaft with time (Randolph and Wroth, 1979)

In order to check the assumption of the soil deforming elastically during consolidation, Randolph and Wroth (1979) examine the principal stress changes. The stress changes are also important in estimating the bearing capacity of a pile at any given time during consolidation. The predicted change in effective radial stress during consolidation is assumed to be equal to the change in pore pressure, i.e. the total radial stress change is zero. In other words, the full limiting pressure needed to expand the cylindrical cavity will at the end of consolidation act as effective stress against the pile. Stress changes at the pile surface in terms of the change in pore pressure are:

$$\Delta\sigma'_r = -\Delta u \tag{4.18}$$

$$\Delta\sigma'_\theta = \frac{\nu}{1-\nu}(-\Delta u) \tag{4.19}$$

$$\Delta q = \Delta\sigma'_r - \Delta\sigma'_\theta = \frac{(1-2\nu)}{(1-\nu)}(-\Delta u) \tag{4.20}$$

$$\Delta p' = \frac{1}{3}(\Delta\sigma'_r + \Delta\sigma'_\theta + \Delta\sigma'_v) = \frac{(1+\nu)}{3(1-\nu)}(-\Delta u) \tag{4.21}$$

$$\frac{\Delta q}{\Delta p'} = \frac{3(1-2\nu)}{(1+\nu)} \tag{4.22}$$

Randolph and Wroth (1979) argue that the ratio of deviatoric stress to mean effective stress casts doubt of the validity of the assumption that the soil deforms elastically. The ratio is positive and greater than one for Poisson's ratios less than about 0.3. This does not fit with the assumption that the soil is unloading (Δq is negative). However, the deviatoric stress increment is found to be negative at radii greater than about two or three times the pile radius. Most of the soil is then in fact unloading in shear, while the mean effective stress is increasing. The solution for consolidation will therefore be accurate as the process is mainly controlled by pore water flow through the large volume of soil at intermediate radii.

The assumptions of plane strain and axisymmetry by Randolph and Wroth (1979) allows for simplifications in the analysis of pile installation. However, when using more complex and realistic soil models, the possibility of obtaining closed form solutions becomes more remote. When prediction of soil behaviour both during and after cavity expansion is of interest, a numerical technique is preferable.

4.2 CEM-MCC

A closed-form solution is possible for the cavity expansion problem when using an elastic perfectly plastic soil model. However, Randolph et al. (1979) argue that the model has two important shortcomings. The first shortcoming is that pore pressure generated due to pure shear is not taken into account. Randolph et al. (1979) point out that it is an over-simplification to assume that the excess pore pressure is equal to the octahedral stress change. Even for the idealized CEM, the induced shear stresses will generate additional pore pressure. Shearing of the soil is expected to produce positive excess pore pressure in low and moderately overconsolidated clays. Negative pore pressure is expected in heavily overconsolidated clays due to dilation. The second shortcoming is that the elastic, perfectly plastic soil model does not correctly relate the strength of the soil with the current effective stress state and stress history of the soil. To avoid these shortcomings, the Modified Cam-Clay (MCC) soil model is utilized by Randolph et al. (1979).

4.2.1 Parametric Study of OCR

By means of the finite element method, the stress and pore pressure changes due to a cylindrical cavity expansion is investigated by Randolph et al. (1979). Axial symmetry and plane strain

conditions is assumed, and pile installation is modelled as the undrained expansion of a cylindrical cavity. The initial excess pore pressure generated by pile installation is assumed to dissipate as outward radial flow of pore water. A parametric study of the effect of overconsolidation ratio (OCR) on the stress changes due to pile installation is carried out by Randolph et al. (1979). Parameters for the MCC model is determined to simulate a deposit of soil like Boston Blue Clay. Numerical values of the parameters for Boston Blue Clay with different degree of overconsolidation are given in Table 4.1. This soil was considered to be initially one-dimensionally consolidated with a value of K_0 = 0.55 before removal of overburden stress. A number of cases with different OCR is considered.

Table 4.1: Parameters for Boston Blue Clay with different OCR (Randolph et al., 1979)

$\lambda = 0{\cdot}15$, $\kappa = 0{\cdot}03$, $e_{cs} = 1{\cdot}744$, $M = 1{\cdot}2$

Case	OCR	K_0	G/c_u	$G/\sigma_z'(0)$	$G/p'(0)$
A	1	0·55	74	25	36
B	2	0·7	83	50	63
C	4	1·0	91	101	100
D	8	1·35	100	201	164
E	32	2·75	118	806	372
F	8	1·35	22	44	36

A similar initial void ratio is chosen so that that the clays will have the same initial undrained shear strength. The initial void ratio is e_0 = 1.16 for each case. All cases had virgin compression index, λ = 0.15 and, swelling index, κ = 0.03. When choosing a suitable value for the elastic shear modulus G at different values of OCR, Randolph et al. (1979) select an approach that take stress history into account. G is set to be

$$G = 0.5 \cdot K_{max} \tag{4.23}$$

K_{max} is the maximum value of the elastic bulk modulus that has been reached during the history of the soil. K_{max} is determined from

$$K_{max} = \frac{1 + e_{min}}{\kappa} p'_{max} \tag{4.24}$$

Where p'_{max} is the maximum past value of the effective mean stress, and e_{min} is the corresponding minimum past void ratio. The chosen approach for calculating G entails that G

increase with increasing OCR. This implies that an overconsolidated soil is stiffer in shear than a normally consolidated soil at the same effective vertical stress.

The MCC model is primarily meant for near normally consolidated clays, and its suitability for modelling heavily overconsolidated clays has been questioned. For overconsolidated stress states where the stress path crosses the critical state line, the MCC model may allow for unrealistic high shear stresses. Furthermore, the MCC model predict a softening behaviour for stress states on the "dry side" of the yield surface. The softening behaviour may lead to mesh dependency of a finite element analysis. Randolph et al. (1979) argue that the main features of the behaviour of heavily overconsolidated clay are preserved by the MCC model. The model accounts for the large elastic range of OC soils, and the tendency of increasing mean effective stress near failure as the soil is sheared under undrained conditions.

4.2.2 Modelling the Creation of a Cylindrical Cavity

The installation of a closed-ended pile, is in theory modelled by the expansion of a cylindrical cavity with an initial radius of zero. In contrast, numerical calculations must begin with a finite cavity radius to avoid infinite circumferential strains. Solutions for the expansion of a cavity with a finite initial size are compared in Figure 4.7 by Carter et al. (1979). Figure 4.7 show the internal cavity pressure, ψ, plotted against the current radius, a, for a soil characterized by $G/s_u = 50$ and $\nu' = 0.3$. Numerical results from calculations of undrained (constant volume) cavity expansion are plotted together with a closed form solution presented by Gibson and Anderson (1961). The two solutions are compatible. Hill (1950) presents a solution for the expansion from zero initial cavity radius in an elastic, perfectly plastic soil (equation (4.5)). In Hill's solution, the limit pressure is reached immediately, before any displacement occurs. The numerical solution for when a pre-existing cavity is expanded, asymptotically approaches Hill's solution at larger cavity radii. After a doubling of the cavity size, the internal pressure is within 6 % of the ultimate limit pressure. Carter et al. (1979) found that doubling the cavity radius is adequate for both the EP and MCC soil models. Expanding a cavity from a_0 to $2a_o$ can approximate the cavity expansion from $r = 0$ to r_o, i.e. model the installation of a pile of radius r_o. The main effect of expanding beyond $a = 2a_o$ is to increase the annular region of yielded soil. Assuming undrained expansion, the relation between r_o and a is:

$$a_0 = r_0/\sqrt{3} \tag{4.25}$$

Clearly, no knowledge is gained on the stress and pore pressures for the soil inside of the cylindrical surface at $r = 2a_o = (2/\sqrt{3})r_0 \approx 1.15r_o$. This information can only be obtained by means of extrapolating, as shown in Figure 4.8.

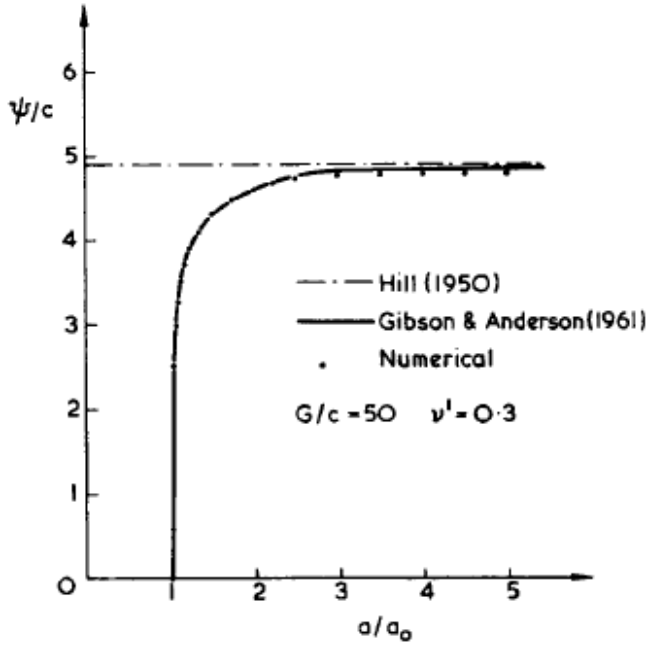

Figure 4.7: Solutions for the expansion of a cylindrical cavity in an elastic, perfectly plastic model (Carter et al., 1979)

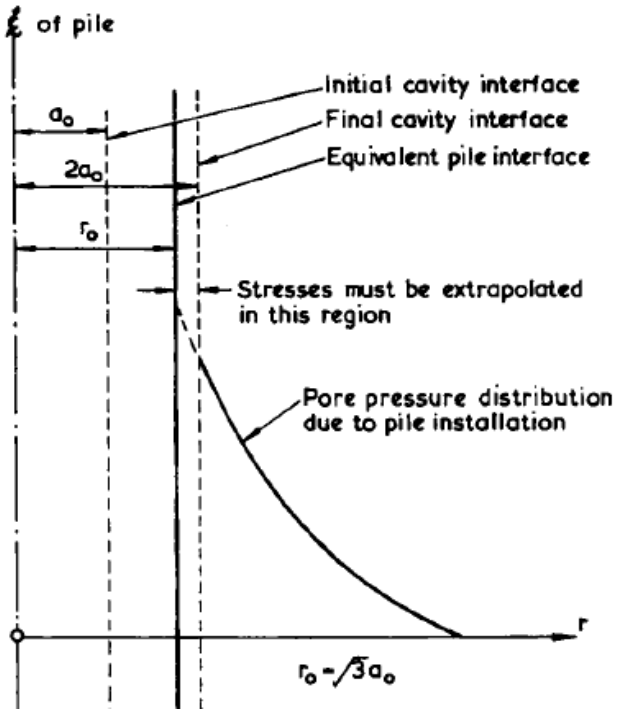

Figure 4.8: Cavity expansion as a model for pile installation (Carter et al., 1979)

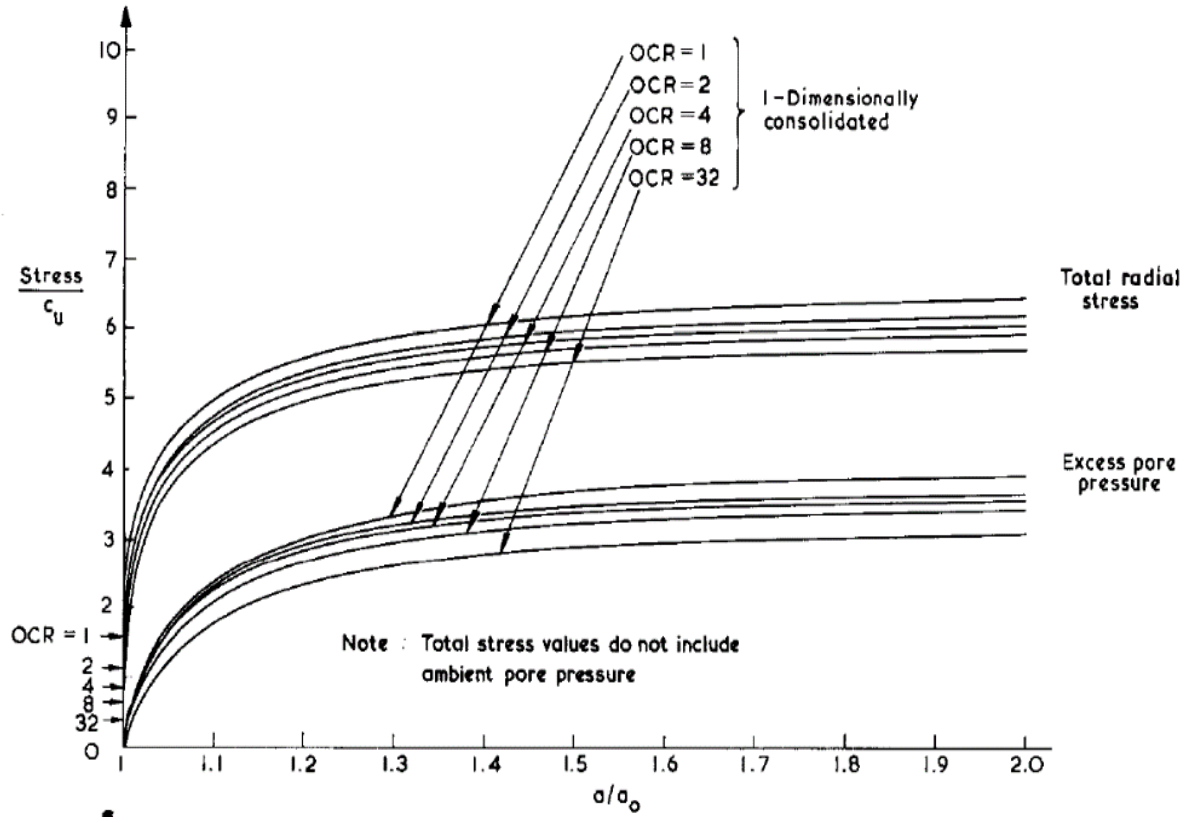

Figure 4.9: Total radial stress and excess pore pressure generated close to the pile (at r = 1.15r_o) during cavity expansion (Randolph et al., 1979)

Figure 4.9 show plots of total radial stress and excess pore pressure at the cylindrical cavity surface, as functions of the cavity radius *a*. The radial stress and the excess pore pressure are approaching limiting values as the cavity is expanding. A doubling of the cavity is sufficiently accurate for all cases (A to E). It is observed that the ratio of these limiting values to the initial undrained shear strength (c_u) of the soil is nearly independent of the consolidation history needed to achieve the value of c_u. The undrained shearing caused by pile installation has erased the memory of the soil close to the pile. Only a small decrease in the excess pore pressure (normalized by c_u) is observed at increasing values of OCR.

Randolph et al. (1979) state that for soils with OCR greater than 1, the shear stress-strain curve is linear until nearly failure, and the increase in mean total stress at the pile shaft is closely given by

$$\Delta p = s_u \ln\left(\frac{G}{s_u}\right) \tag{4.26}$$

The total stress path is similar as for the ideal elastic, perfectly plastic soil model. Even though the total stress path is largely independent of the soil model, the effective stress path and pore pressure are not (Randolph et al., 1979). For the MCC model, the value of the mean effective stress changes during shearing. The distribution of the initial excess pore pressure generated in the region of the soil which reaches failure, can be written as

$$\Delta u_0 = \left(p_i' - p_f'\right) + 2\, s_u \ln\left(\frac{r_p}{r}\right), \qquad r_0 \le r \le r_p \tag{4.27}$$

Where r_p is given by equation (4.7), and p_i' and p_f' are the initial and final mean effective stress. The maximum excess pore pressure at the pile shaft after cavity expansion will then be

$$\Delta u_{max} = \left(p_i' - p_f'\right) + s_u \ln\left(\frac{G}{s_u}\right) \tag{4.28}$$

As the value of OCR increases, so does G/s_u (see Table 4.1), but the value of p_i'-p_f' reduces. In fact, p_i'-p_f' becomes negative for OCR values larger than 2, as the clays tend to dilate on shearing. These two effects almost cancel each other out, and only a small decrease in the excess pore pressure at increasing values of OCR is observed in Figure 4.9.

The method Randolph et al. (1979) choose to define variation of shear modulus *G* with OCR is partly the reason why the excess pore pressures show little sensitivity to variation in OCR. If the shear modulus was tied to the current effective stress level rather than to the past maximum stress level, lower pore pressures would be generated at larger values of OCR. Lower excess pore pressures are generated when using a lower shear modulus.

4.2.3 Reconsolidation

At radii greater than about two or three times the pile radius, the soil is unloading in shear during reconsolidation. Thus, Randolph and Wroth (1979) argue that the solution based on an elastic soil furnishes realistic estimates of consolidation time. However, the soil closer to the pile undergoes further increase in shear strain as the pile prevents inward movement of the soil. Randolph et al. (1979) say that a real soil will continue to yield close to the pile and thus a more realistic soil model, like the MCC model, should be used to predict the stress changes.

A consolidation analysis is performed by Randolph et al. (1979) with starting conditions corresponding to those immediately after cavity expansion. All of the cases end expansion and begin consolidation at the same effective stress state ($\sqrt{3}\, s_u, p_f'$) in a p-q plot, this is because all

soil samples were chosen to have the same initial value of undrained shear strength. In undrained plane strain conditions, $s_u = \sigma'_1 - \sigma'_3 = q_f/\sqrt{3}$, because the intermediate principal stress is equal to the average of the major and minor principal stresses. Since the soil adjacent to the pile is at failure immediately after pile driving, the effective stresses at the pile surface can be calculated from the critical state condition in the MCC model. All of the effective stress paths reach critical state when $q = \sqrt{3}s_u$, and $p' = q/M$. The stresses at failure are only dependent on the slope of the critical state line, M, and the undrained shear strength s_u, by

$$\sigma'_r = \left(\frac{\sqrt{3}}{M} + 1\right) s_u \tag{4.29}$$

$$\sigma'_v = \left(\frac{\sqrt{3}}{M}\right) s_u \tag{4.30}$$

$$\sigma'_\theta = \left(\frac{\sqrt{3}}{M} - 1\right) s_u \tag{4.31}$$

The finite element solution by Randolph et al. (1979) relate the compressibility of the soil to the compression index if the soil is yielding, and to the swelling index if the soil is consolidating inside the current yield surface. The volumetric compressibility is:

$$m_v = \frac{\lambda}{(1+e)\sigma'_v} \text{ or } \frac{\kappa}{(1+e)\sigma'_v} \tag{4.32}$$

As most of the soil will be unloading, the value of m_v will mostly depend on κ rather than λ. In addition, the major principal stress will be σ'_r instead of σ'_v.

Results from Randolph et al. (1979) indicate that the value of OCR only have a small effect on the consolidation time. To some extent, this result is believed to be due to the manner in which the elastic shear modulus *G* has been chosen based on OCR. For soils with larger values of *G*, excess pore pressures are generated over a wider zone during cavity expansion and the consolidation time will be longer.

The distribution of stress in the soil once consolidation is complete, is presented in Figure 4.10 for soils with OCR of 1 and 8. Pile installation has clearly affected the stresses in the soil out to about 20 times the pile radius. For all the cases A to E in Table 4.1, the radial effective stress at the pile shaft has a value of about five times the shear strength. The circumferential and vertical effective stresses at the pile shaft are approximately three times the shear strength.

Close to the pile, the memory of the soil has been erased as the soil is completely remoulded. After the consolidation process, the stress condition in all soil samples consist of equal minor principal stresses and the radial effective stress is the major principal stress. The ratio between the minor principal stresses to the radial effective stress after consolidation is approximately, K_i'=0.65. The radial effective stress decreases approximately logarithmic with the radius until it reaches the in situ shear strength at about 20 times the pile radius. It may be noted that the increase in radial effective stress during consolidation is approximately 2.5 times the initial undrained shear strength regardless of OCR.

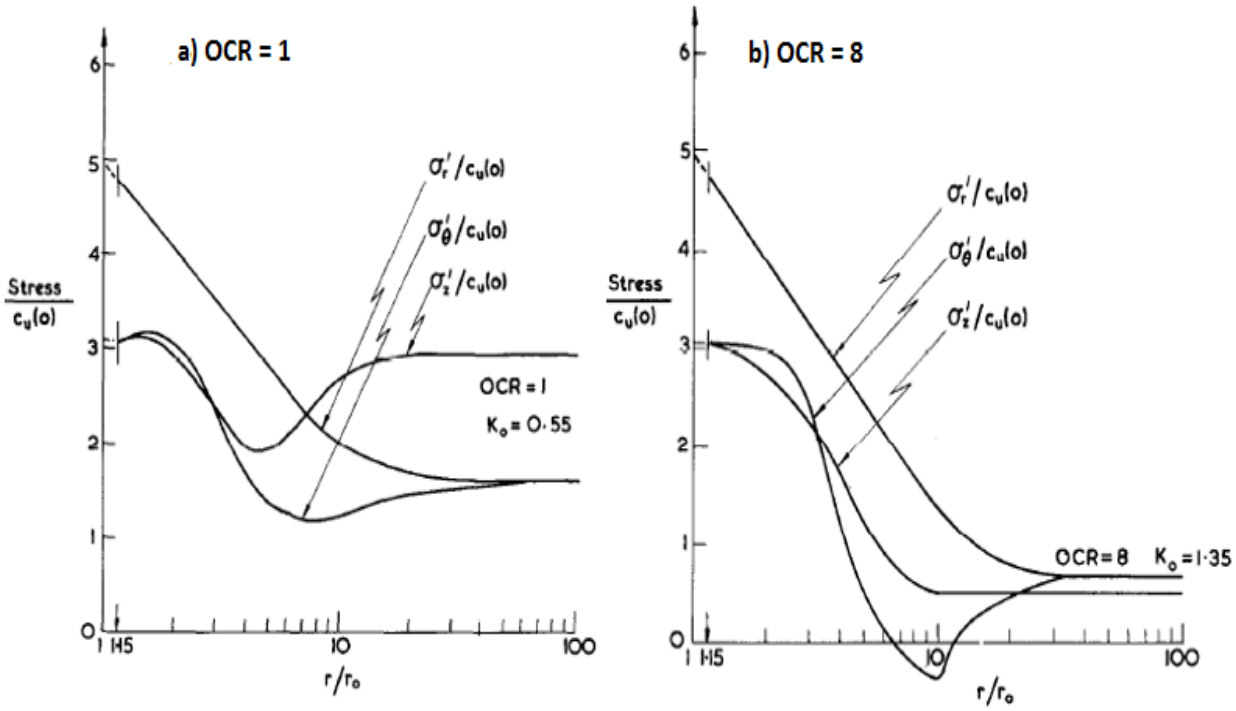

Figure 4.10: Distribution of stresses at end of consolidation for: a) OCR=1; and b) OCR=8. (Randolph et al., 1979)

Randolph et al. (1979) assume plane strain conditions in the analysis, and thus ignored shear stresses in r-z planes. In reality, shear stresses will be present due to residual driving stresses, and to balance vertical stresses caused by pile installation. Excess pore pressure generated from pile installation have been measured in the field to be as great as the effective overburden pressure. The changes in total vertical stress must be balanced by shear stresses around the pile to maintain vertical equilibrium (Randolph et al., 1979).

4.2.4 Effect of Soil Structure

Factors influencing soil behaviour that can not be accounted for by void ratio and stress history, such as cementation and ageing, may be referred to as soil structure (Leroueil and Vaughan, 1990). The intact state of a natural clay is developed during deposition and consolidation. Processes such as erosion, aging, leaching and weathering, affect the intact state. Due to structure, natural clays typically have significant anisotropy when it comes to undrained shear strength. When an intact clay is subjected to volumetric or shear deformation such that the original clay structure is partially broken, a destructured state is produced. In a remoulded state, the strength of the clay is reduced to a minimum (Leroueil et al., 1985). Soil structure is lost in remoulded and reconstituted samples, and partly lost in disturbed samples. The isotropic normal consolidation line in the MCC model represents a remoulded and reconsolidated clay. In other words, destructuration and anisotropy are not included in the MCC model. Generally, soil structure expands the boundary surface and destructuration shrinks the boundary surface. A rotated ellipse are used in critical state models that include anisotropy effects.

Castro and Karstunen (2010) carried out numerical simulations investigating the installation effects of stone columns in a natural clay. In the analysis, the S-CLAY1 (Wheeler et al., 2003) and S-CLAY1S (Karstunen et al., 2005) soil models are used. These models account for anisotropy, and destructuration and anisotropy, respectively. Castro and Karstunen (2010) conclude that the destructuration caused by column installation erase all bonding between soil particles at the column surface. In addition, the initial horizontal anisotropy changes towards planes perpendicular to the radial axis. The destructuration and change in anisotropy was limited to clay closer than about five times the column radii from the column axis. At the column surface, lower radial effective stress are generated due to the destructuration.

Immediately after pile installation, the strength of the soil close to the pile will be equal to the remoulded strength and not the peak undrained shear strength. The reduction in soil strength to the remoulded strength has not been accounted for in the analysis presented so far. The ratio between the peak strength and the remoulded strength is referred to as the sensitivity of the soil. Sensitivity of clays can partly be explained by thixotropy, but there are also other factors contributing to the sensitivity of clays, like cementation or leaching (Andersen and Jostad, 2002). The sensitivity may vary from unity to between five and ten for a typical sensitive clay. Normal or lightly overconsolidated clay tend to have higher sensitivity than heavily overconsolidated clay (Randolph et al., 1979).

Randolph et al. (1979) illustrate the difference between shearing a sensitive and insensitive clay to failure in Figure 4.11. The critical state line is parallel to the virgin consolidation line when projected onto the e-In p' plane. λ_i is the consolidation path for an insensitive clay, and λ_s is meant to represent the path for a sensitive clay. An insensitive clay will reach equilibrium at a lower void ratio for a given mean effective stress than a sensitive clay. If a sensitive soil is normally consolidated at point *E* and is then sheared undrained, it will reach a peak shear strength at point *F*. Subsequently, the structure collapses and the remoulded strength is given by point *G* on the critical state line. Shearing of a sensitive clay results in large generated pore pressures as the soil is remoulded and the effective stress reduces from point *E* to point *G* in Figure 4.11.

Equivalent to position *F* in Figure 4.11, the clay will be at its peak strength at a distance $r = r_p$ from the pile. While at the pile wall, $r = r_0$, the soil will be completely remoulded (point *G* in Figure 4.11). It is believed that severe remoulding is restricted to a region close to the pile.

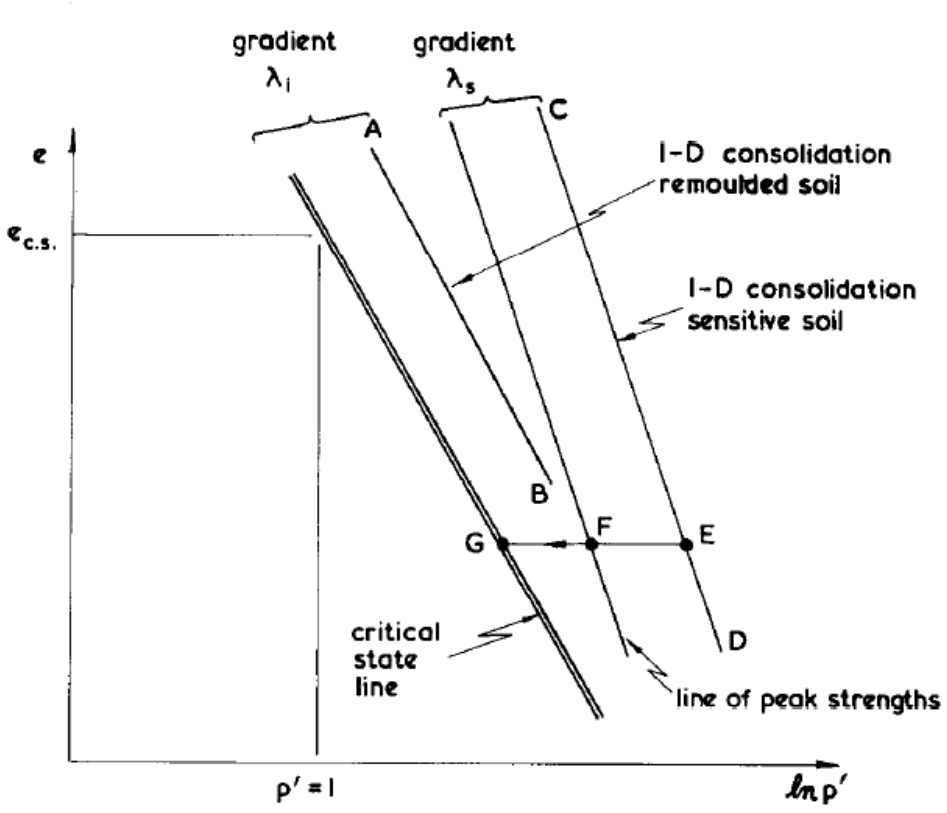

Figure 4.11: Lines for consolidation, peak strengths and critical states for a sensitive soil (Randolph et al., 1979)

5 Strain Path Method

Based on observations of soil deformations caused by deep undrained penetration of rigid objects in saturated clays, Baligh (1975) argues that soil deformations and strains are independent of the shearing resistance of the soil. This means that such problems are mainly strain-controlled. The Strain Path Method (SPM) is based on the assumption that soil flow around a penetrating pile is similar to the flow of a viscous liquid. That is, soil particles are assumed to move along streamlines around the pile. Initially, the solution consists of obtaining deformations and strains at soil elements along the streamlines. Subsequently, by utilizing generalized soil models, stress changes can be calculated from the relationship between stress and strains in the soil. Exact stress changes can only be obtained if the estimated soil deformations are identical to actual soil deformation.

Figure 5.1 illustrate soil deformations for; (a) spherical cavity expansion, and (b) penetration of "Simple Pile". The soil deformations behind the tip of the pile in (b) is not equal to the deformations from the spherical cavity solution (a). Nor are the deformations around the pile shaft far from the tip similar to the cylindrical cavity expansion solution. The cylindrical CEM assumes radial soil deformation in a cylindrical coordinate system, meaning that vertical soil deformations are neglected. Baligh (1985) argues that the SPM provide a more realistic prediction to soil behaviour during pile installation than the CEM.

Baligh (1985) predict strain paths for an ideal solution he called "simple pile". The tip of the "simple pile" is rounded to ensure smooth laminar flow around the object and a uniform velocity field is implemented. This enabled a mathematical formulation of the displacements to be made. The strain paths of soil elements during undrained axisymmetric penetration in saturated clays are illustrated in Figure 5.2 by Baligh (1985). Three deviatoric strains components (E_1, E_2, E_3), which are defined in Figure 5.2, are used to describe the strain. The vertical strain, E_1, corresponds to shearing strain from conventional triaxial testing. Further, E_2 corresponds to strain from a cylindrical cavity expansion, and E_3 is similar to strain imposed from a DSS test. Maximum straining levels in these laboratory tests are about 15% (Baligh, 1985). Figure 5.2 shows the strain paths during penetration for three soil elements initially located at r_0/R = 0.2, 0.5, and 1 (where R is radius of the pile, and r_0 is distance from the z-axis).

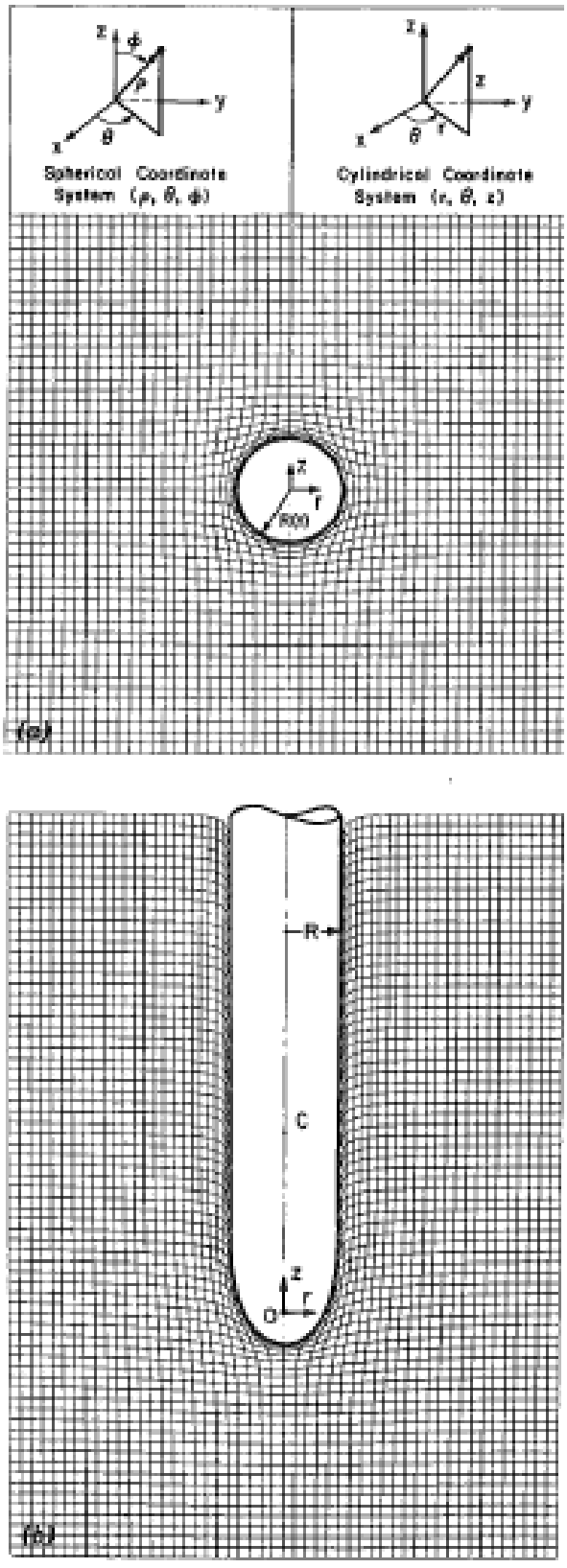

Figure 5.1: Deformation of square grid in saturated clays; (a) During Spherical Cavity Expansion; (b) During Penetration of "Simple Pile" (Baligh, 1985)

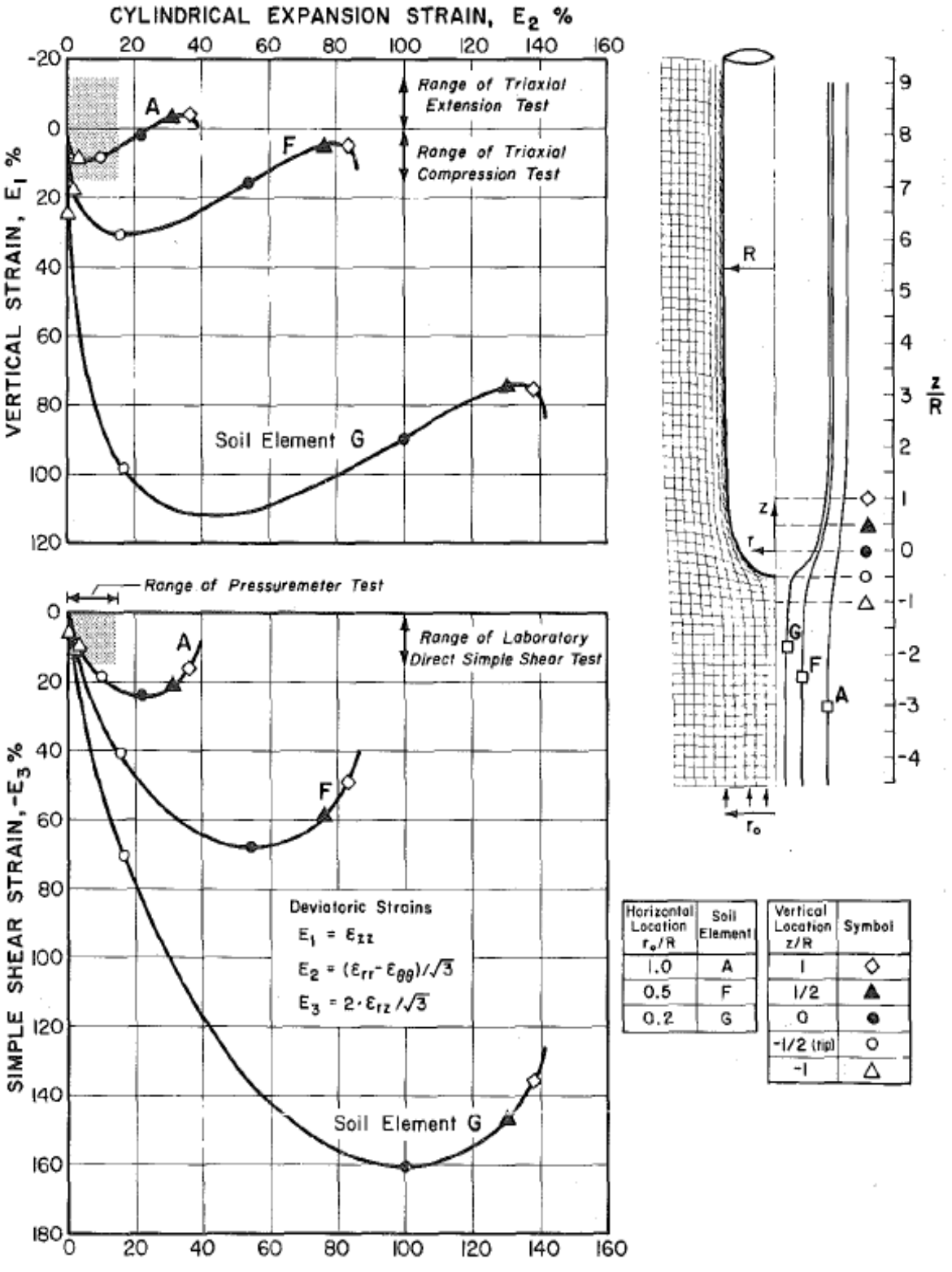

Figure 5.2: Deviatoric strain paths during "Simple Pile" penetration for a closed-ended pile, according to SPM (Baligh, 1985)

The following is noted from Figure 5.2:

- The strain levels induced by pile penetration are much greater than what is encountered in common laboratory testing. Therefore, the post peak behaviour of the clay should be considered when computing stresses and pore pressures close to the pile.
- The "vertical" simple shear strain is larger than the cylindrical expansion strain close to the pile. Since the peak strength is reached at relatively low strains, Figure 5.2 indicate that initial failure close to the pile is due to vertical compression (E_1) and shear straining (E_3), well before cylindrical cavity expansion (E_2) contributes.
- Both the E_1 and E_3 strains curves of and decreases during penetration. In other words, strains induced by pile driving are reversible in the SPM.

The SPM have been coupled with various constitutive models by researchers, e.g. Whittle (1987) and Whittle (1993). Finite element analysis with the SPM, coupled with the MIT-E3 model (Whittle, 1987), can reasonably well predict the ultimate shaft friction for normally consolidated to lightly overconsolidated clays. However, its predictions become progressively less reliable for OCR larger than 4–8 (Whittle and Sutabutr, 1999). The MIT-E3 model also fails to predict the low radial effective stress observed in low plasticity clays. Generally, the SPM leads to lower effective stresses and pore pressures at the pile shaft than the CEM model (Karlsrud, 2012).

6 Ultimate Shaft Friction

Karlsrud (2012) propose two new procedures for predicting the ultimate shaft friction, respectively the α- and β-approach. The procedures are based on the collection and analysis of data from numerous instrumented pile load tests. Instrumentation of the piles include measurement of the pore pressure, earth pressure and shaft friction along the pile shafts. In-situ and laboratory testing have generally been carried out together with the fully instrumented load tests. On this basis, the two procedures tie the local ultimate shaft friction along a pile to the undisturbed in-situ undrained strength as determined from Direct Simple Shear Tests, the in-situ vertical effective stress, the overconsolidation ratio, and the plasticity index of the clay. During axial pile loading, the mode of shearing along the pile shaft resembles the Direct Simple Shear (DSS) mode of failure. Thus, Karlsrud (2012) chose to use s_{ud} as a reference strength in his study. Figure 6.1 compare the stress conditions around a pile to the DSS test.

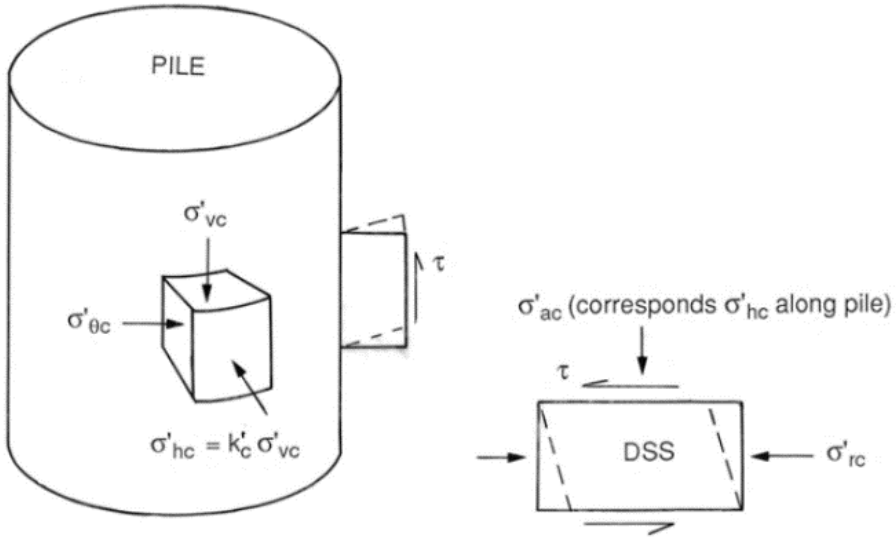

Figure 6.1: Stress conditions around a pile compared to that in DSS test (Karlsrud and Nadim, 1990)

For the primary α-method, the ultimate shaft friction is given by

$$\tau_{us} = \alpha \cdot s_{ud} \tag{6.1}$$

The α-value is determined on the basis of the normalized undrained strength, s_{ud}/σ'_{vo}, and the plasticity index, I_p , of the clay (Figure 6.2). The ultimate shaft friction is lower than the in-situ undrained strength due to the impact of the severe disturbance caused by pile installation on the stress-strain and strength properties of the soil (Karlsrud, 2012).

Figure 6.2 shows that the plasticity index has a significant effect on the ultimate shaft friction. This effect is further demonstrated by Figure 6.3, showing α-values from pile tests for normally consolidated to moderately overconsolidated clays with $s_{ud}/\sigma'_{v0}<0.4$. For low-plastic normally consolidated clays the minimum recommended α-value is as low as 0.2.

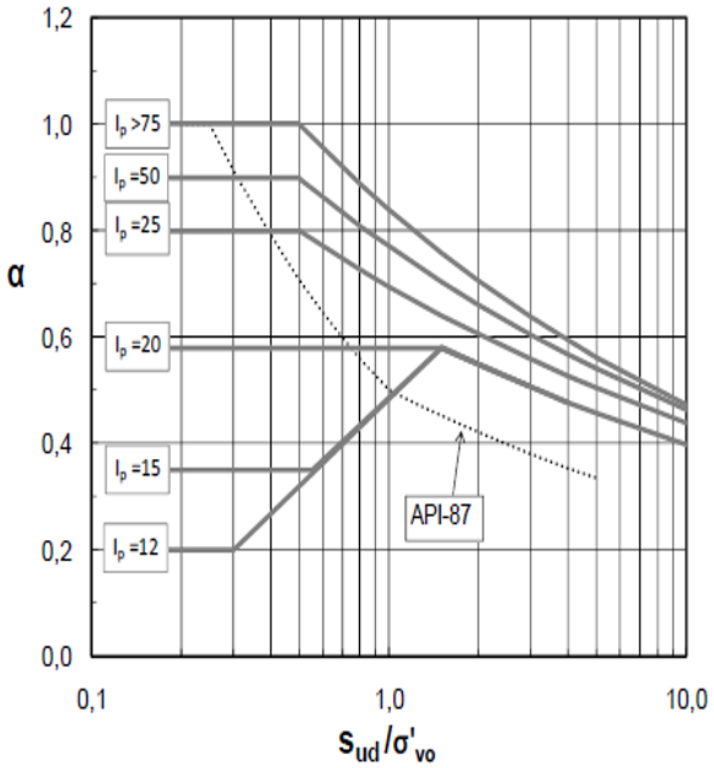

Figure 6.2: Proposed chart for determination of α-values (Karlsrud, 2012)

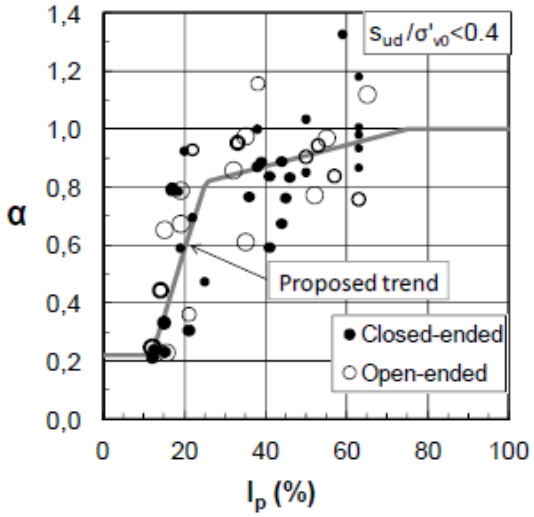

Figure 6.3: Effect of plasticity index on α-value for pile tests in clays with $s_{ud}/\sigma'_{v0}<0.4$ (Karlsrud, 2012)

The proposed α-method can be seen as a modification to the NGI-05 method and it also has some resemblance to the API-1987 method. However, these methods use the unconsolidated undrained (UU) strength as a reference. Karlsrud (2012) argues that it is important to move away from the use of the UU strength as reference strength. The UU strength is far more affected by sample quality and disturbance, than the s_{ud} strength.

In the alternative β-method, the β-value is determined from the overconsolidation ratio and plasticity index (Figure 6.4). The ultimate shaft friction is given by

$$\tau_s = \beta \cdot \sigma'_{v0} \tag{6.2}$$

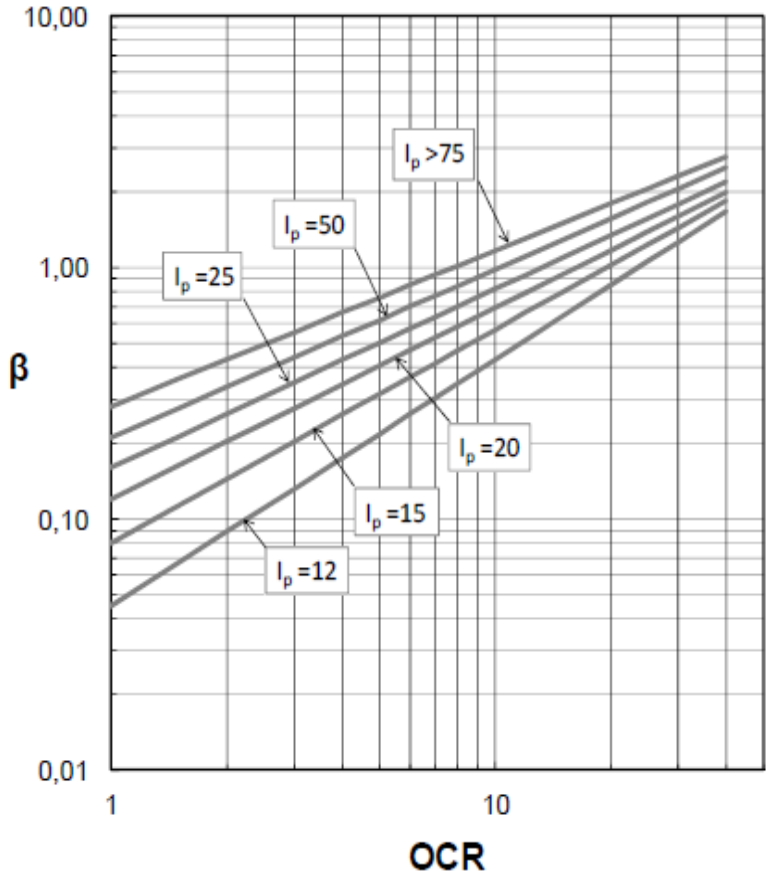

Figure 6.4: Proposed chart for determination of β-values (Karlsrud, 2012)

Figure 6.4 shows the proposed β-method. The β-values varies from 0.045 for low-plastic normally consolidated clays to about 2.0 for very stiff clays with OCR of 40.

Although the α- and β-method are two separate methods, they are to some extent correlated through the classical relationship between normalized undrained strength and the overconsolidation ratio.

No clear evidence is found by Karlsrud (2012) regarding any difference in the ultimate shaft friction for closed-ended and open-ended piles. Nor is any difference in resistance found between loading in compression or tension. This is in agreement with most other research carried out in the past. The pile dimensions, including pile length or flexibility, is also found to not affect the local ultimate shaft friction by Karlsrud (2012). However, the length or pile flexibility has a significant effect in several other proposed design methods.

6.1 Ultimate Shaft Friction Related to Radial Effective Stress

Figure 6.5 compares measured ultimate shaft friction, τ_{us}, to the measured radial (horizontal) effective stress at the pile shaft, $\sigma'_{hc} = \sigma'_{rc}$. As expected, it exist a clear correlation between ultimate shaft friction and measured radial effective stress against the pile. Most of the results fall in the range $\tau_{us} = (0.2 - 0.4) \cdot \sigma'_{hc}$.

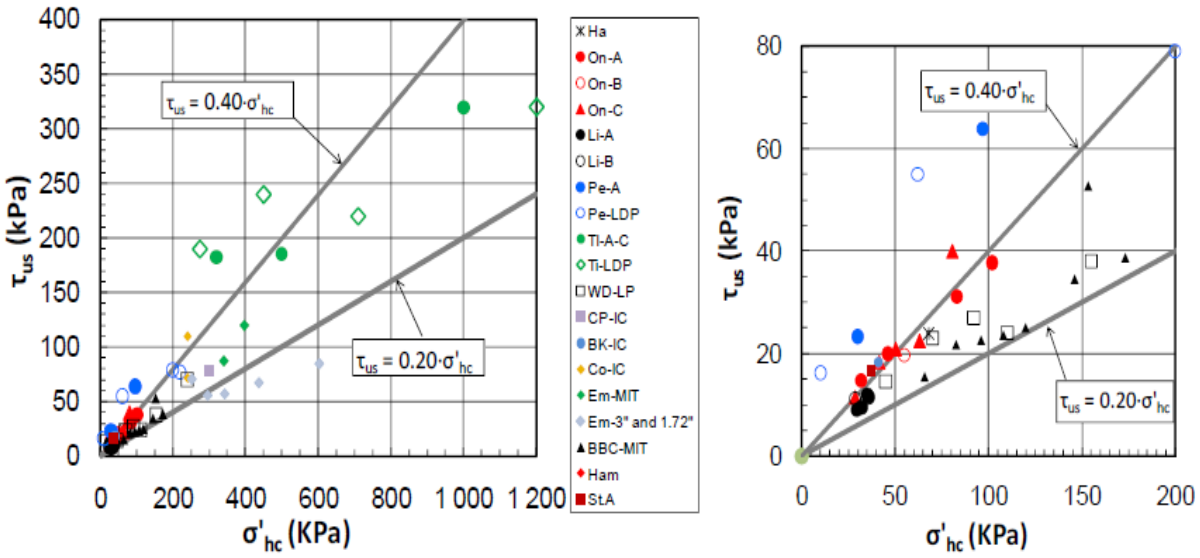

Figure 6.5: Measured ultimate shaft friction versus measured radial effective stress (Karlsrud, 2012)

Figure 6.6 presents τ_{us}/σ'_{hc} against OCR and I_p. It looks as though OCR and I_p has little impact on the ratio between the ultimate shaft friction and the radial effective stress. This is in contrast to the large impact OCR and I_p has on the α- and β-values (see Figure 6.2 and Figure 6.4). Thus, the impact of OCR and I_p on the ultimate shaft friction is mainly coming through its impact on the radial effective stress.

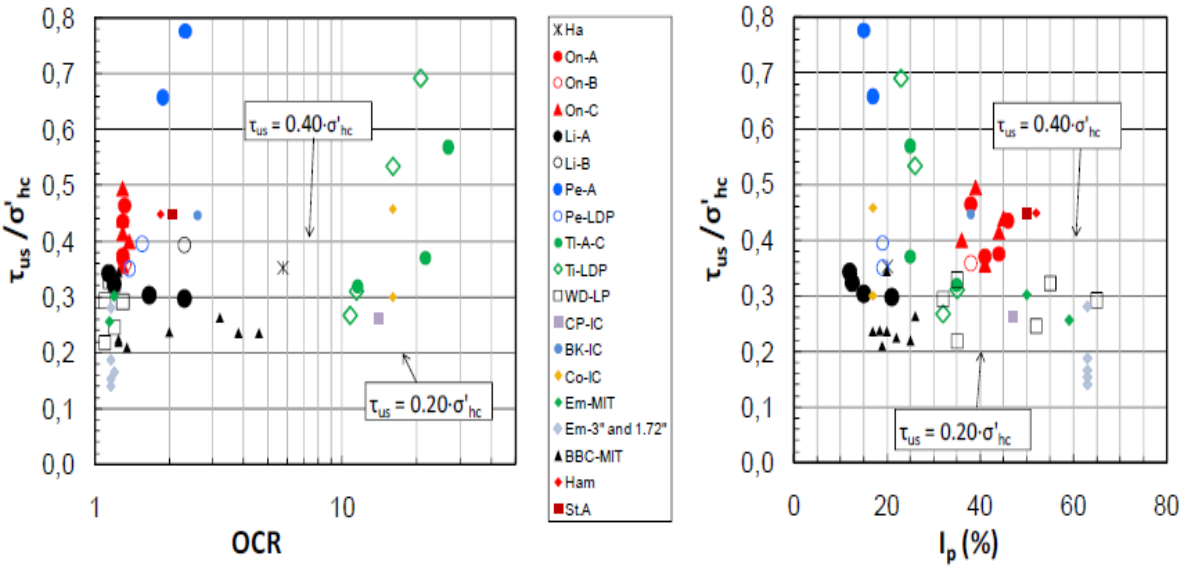

Figure 6.6: Measured ultimate shaft friction normalized with measured radial effective stress, in relation to OCR and I_p (Karlsrud, 2012)

7 Normal and Overconsolidated Clay with Low and High Plasticity

The plasticity index (I_p) is a measure of soil plasticity. Soils with high I_p tend to be clay or clayey soils, and soils with lower I_p tend to be silt. Non-plastic soils ($I_p = 0$), normally have little or no clay or silt. I_P is defined as the numerical difference between the liquid limit and the plastic limit ($I_p = w_L - w_p$). The liquid limit is the water content at which a soil changes from a liquid to a plastic state, while the plastic limit is the lowest water content at which the soil is plastic. The water content is expressed in terms of percentage as the ratio of the weight of water to the weight of solids. Procedures for determining the Atterberg limits are described in the standard (ISO/TS) 17892-12:2004. Determination of the Atterberg limits are subject to the judgement of the operator, thus some variability in results are expected.

Overconsolidation ratio (OCR) is the ratio by which the current vertical effective stress was exceeded in the past by the apparent preconsolidation pressure. The use of "apparent" is because OCR is not only dependent on overloading from physical larger overburden pressure or lower pore pressures in the past. The OCR will normally always be greater than 1.0 due to ageing, chemical weathering, or cementation effects. In this study there is not made any distinctions between the reasons for the apparent overconsolidation ratio.

7.1 Cases Studied

The main task of this thesis was to carry out numerical analysis of pile installation and reconsolidation phase. For the analysis, a low plasticity clay with $I_p = 15$ % and a high plasticity clay with $I_p = 40$ %, will be compared. Soils with different degree of plasticity is chosen to quantitatively study the effect of the plasticity on soil behaviour. Furthermore, the effect of overconsolidation ratio will be investigated. It is chosen to study a normally consolidated soil with OCR of 1.0, and a highly overconsolidated soil with OCR of 8.0. As discussed earlier, natural soils will normally have OCR > 1.0. Still, an OCR of 1.0 is chosen in order to study a true normally consolidated clay. An OCR of 8.0 is selected as an arbitrary overconsolidated case.

To summarize, the following four cases are studied:

a) $I_p = 15$ % and OCR = 1

b) I_p = 15 % and OCR = 8
c) I_p = 40 % and OCR = 1
d) I_p = 40 % and OCR = 8

7.2 Representative Soil Parameters

The plasticity index is not a direct input property in any constitutive soil model. Thus, the effect of plasticity index has to be represented by other soil parameters. For the numerical analysis, the Modified Cam-Clay (MCC) model is chosen as a constitutive model. Based on general correlations between the plasticity index and soil parameters that are input parameters in the MCC model, the effect of plasticity will be investigated.

Several attempts have been made to correlate the value of the compression index (C_c) of a soil with parameters such as liquid limit, natural water content, initial void ratio, plasticity index, and other properties of soil. Table 7.1 summarizes regression equations that direct or indirectly are related to I_p. As I_p is dependent on the liquid limit water content (w_L), and natural water content (w_n) tend to increase with increasing I_p, correlations with these properties are included.

Table 7.1: Compression index equations

Equation	Reference	Conditions of applicability
$C_c = 0.007(w_L - 10)$	Skempton (1944)	Remoulded clays
$C_c = 0.01404(w_n - 13.46)$	Nishida (1956)	Natural soils
$C_c = 0.0102(w_n - 9.15)$	Hough (1957)	Inorganic silty sand, silty clay
$C_c = 0.009(w_L - 10)$	Terzaghi and Peck (1967)	Normally consolidated clays
$C_c = 1.35Ip$	Schofield and Wroth (1968)	Remoulded clays
$C_c = 0.01(w_n - 5)$	Azzouz et al. (1976)	All clays
$C_c = 0.0046 + 0.0104Ip$	Nakase et al. (1988)	Clays with IP< 50%

It is clear from Table 7.1 that the compressibility of clays is found to increase with increasing w_L, w_n and I_p. The applicability of the different equations presented in Table 7.1 will depend on clay type and soil conditions. Still, the most comprehensive study was carried out by Azzouz et al. (1976). Regression equations presented by Azzouz et al. (1976) were based on experimental data from more than 700 consolidation tests on a large variety of undisturbed soils. It is chosen to use the correlations presented by Nakase et al. (1988) as they are based on

the plasticity index directly. In addition, Nakase et al. (1988) present correlations for both the compression index and swelling index. Nakase et al. (1988) performed a large testing program on twelve artificially prepared soils obtained from various coastal areas of Japan. The testing program consisted of triaxial compression, triaxial extension, and oedometer tests. These tests were performed to see if correlations between the plasticity index and parameters specifying a constitutive soil model could be determined. The plasticity index of the tested soils were ranging from 10 to 55. Nakase et al. (1988)presented parameters for the Cam-Clay model developed by (Schofield and Wroth, 1968). Figure 7.1 show that the compressibility of soils increases with increasing plasticity index.

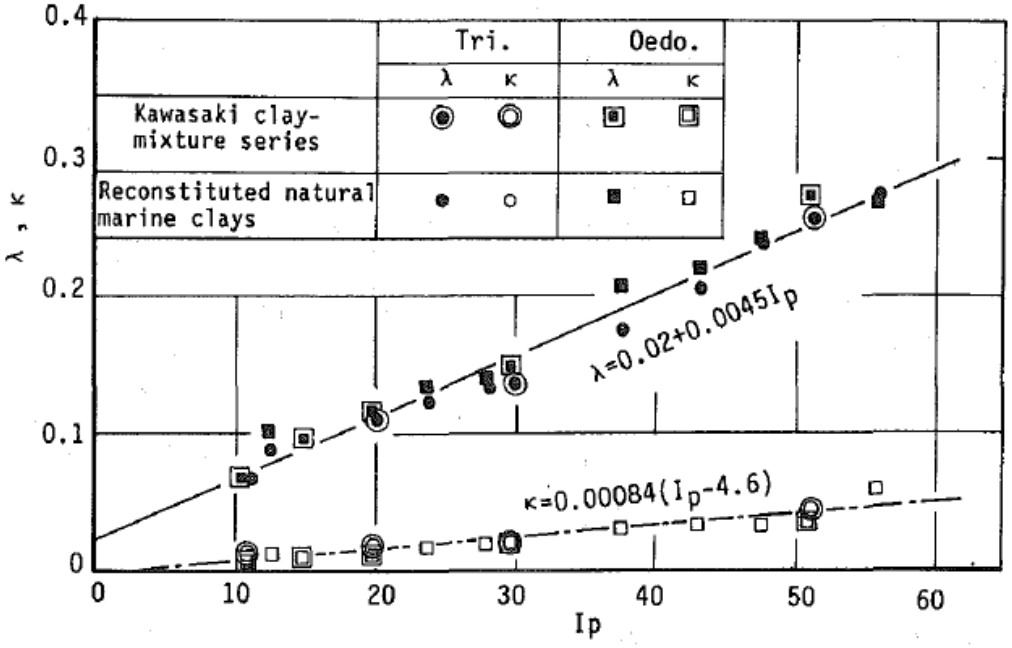

Figure 7.1: Correlation between Compressibility Index, Swelling Index, and Plasticity (Nakase et al., 1988)

Linear relationships for the compression index and swelling index based on the plasticity index are found by Nakase et al. (1988). Regression lines for linear correlations are given as

$$\lambda = 0.02 + 0.0045 I_p \tag{7.1}$$

$$\kappa = 0.00084(I_P - 4.6) \tag{7.2}$$

Schofield and Wroth (1968) predicted a relationship between the compressibility index and the plasticity index by using theory of critical state soil mechanics (CSSM), and found that:

$$\lambda = 0.00585 I_P \tag{7.3}$$

A comparison of the predictions with data collected by Mayne (1980) is shown in Figure 7.2. Mayne (1980) collected a large amount of data on experimental values of soil parameters required for the Cam-Clay model. The linear relationships with plasticity index captures well the trend of the collected data.

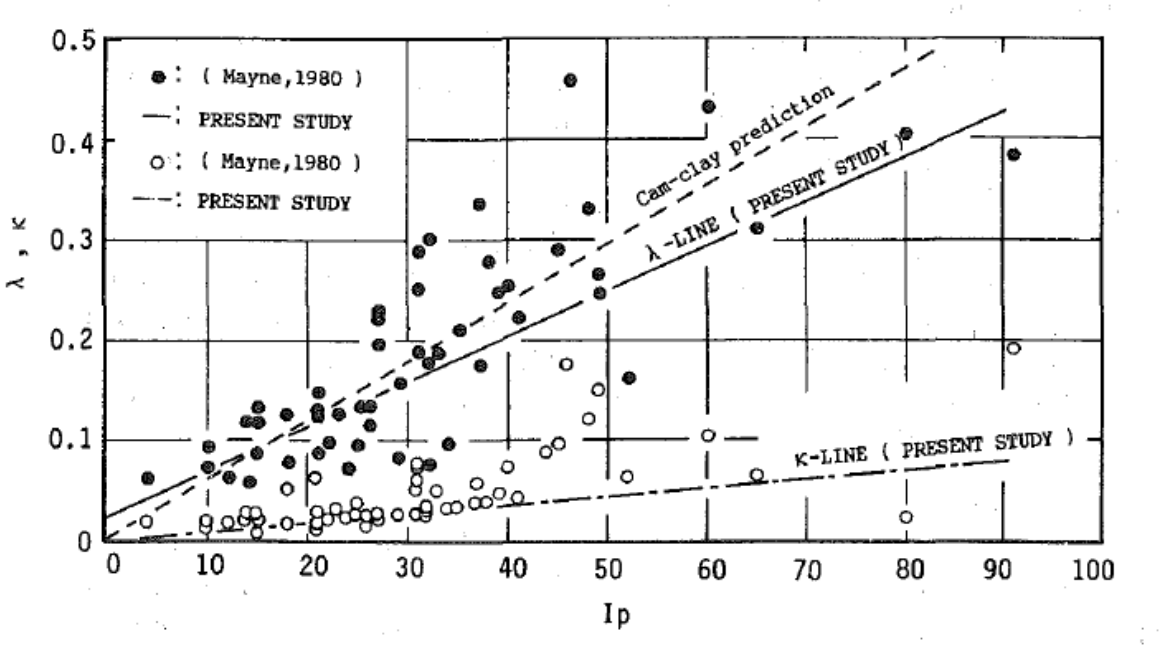

Figure 7.2: Comparison of Predictions by Nakase et al. (1988) (Present Study), Schofield and Wroth (1968) (Cam-clay prediction), and Data Collected by Mayne (1980)

From equation (7.1) and (7.2), the compression index and swelling index are estimated in Table 7.2 for the two cases of plasticity index being investigated.

Table 7.2: Compression Index and Swelling Index

Parameters		**I_p = 15 %**	**I_p = 40 %**
Compression index	λ	0.0875	0.2000
Swelling index	κ	0.0087	0.0297

Karlsrud and Hernandez-Martinez (2013) present results obtained on high-quality samples from 22 different sites in Norway and one in Britain (Bothkennar), using the Sherbrooke block

sampler. They compared deformation and strength parameters from individual tests against index data for the different clays tested. Karlsrud and Hernandez-Martinez (2013) chose the overconsolidation ratio (OCR), natural water content (w), and clay sensitivity (S_t) as key correlation parameters. Figure 7.3 show the maximum apparent friction angle, φ_{max}, from triaxial and DSS tests in relation to water content assuming zero attraction (Karlsrud and Hernandez-Martinez, 2013). φ_{max} is found by fitting a tangent Mohr–Coulomb line to the effective stress paths assuming zero attraction (a = 0). Figure 7.3 shows that φ_{max} tend to increase with water content. As discussed earlier, the plasticity index typically increase with water content.

Nakase et al. (1988) found no direct correlation between the slope of the critical state line, M, and I_P. In addition, the scatter in Figure 7.3 is rather large. It is decided to assume an equal strength for the four cases studied. An effective angle of friction of φ' = 30° is believed to be applicable. This corresponds to an inclination of the critical state line, M = 1.2, which is the same strength as used in the study by Randolph et al. (1979).

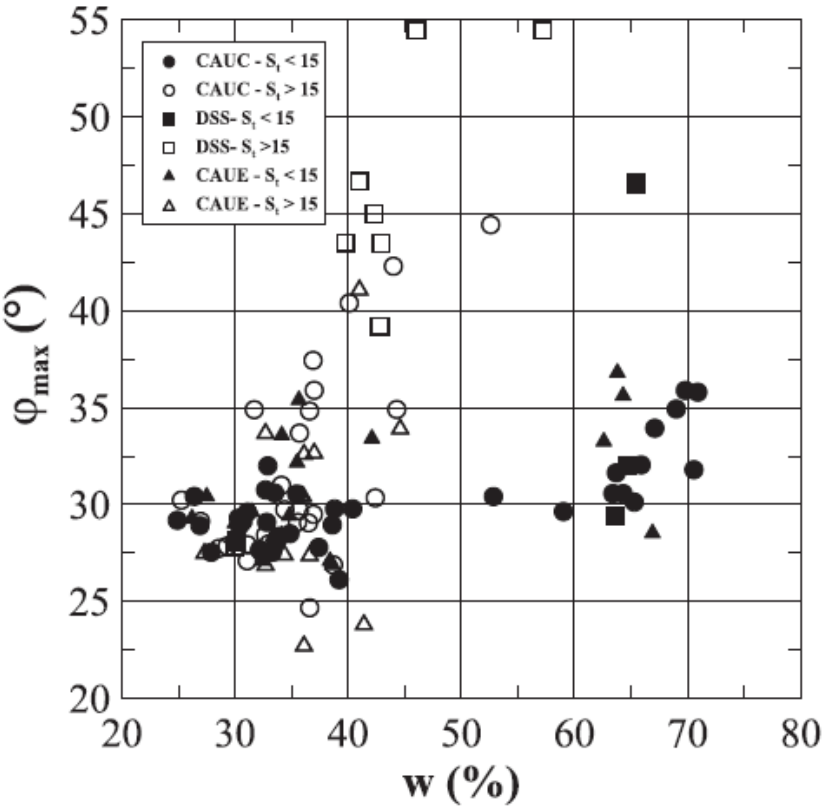

Figure 7.3: Maximum apparent friction angle assuming zero attraction intercept in relation to water content (Karlsrud and Hernandez-Martinez, 2013)

Tavenas et al. (1983) perform a comprehensive laboratory study on the permeability of intact soft clays from North America and Sweden. Although highly overconsolidated clays are excluded in the study, the clays tested are believed to represent a wide range of natural clay deposits. Tavenas et al. (1983) show that the in-situ permeability, k_0, is dependent of void ratio, clay fraction, plasticity and the fabric of the clay. However, the fabric is not easily assessed or quantified. Figure 7.4 show the *e* vs. lg *k* relationship according to an empirical parameter I_p + clay fraction (CF). The higher the I_p + CF parameter, the less pervious is the clay.

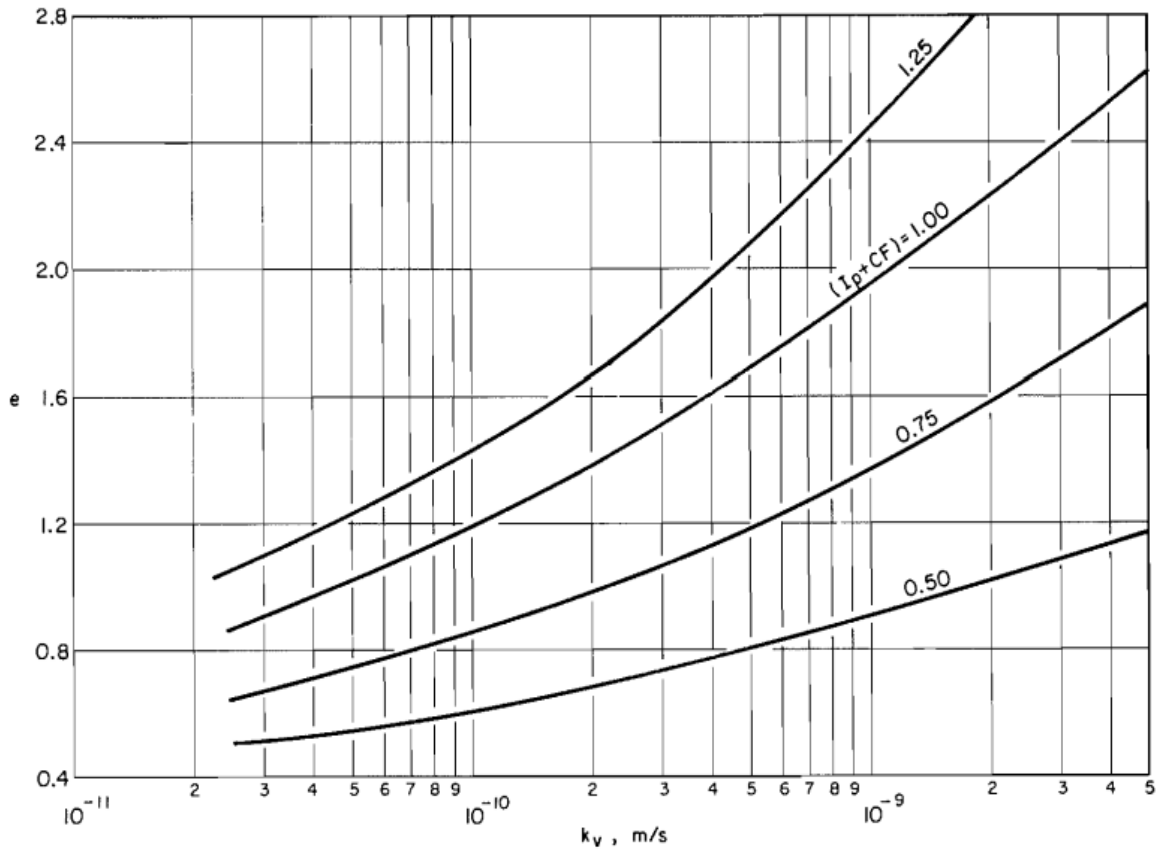

Figure 7.4: e vs. lg k. Relationships as a function of the empirical parameter I_p + CF (Tavenas et al., 1983)

By assuming a void ratio and clay fraction, the permeability can be estimated from the plasticity index in Figure 7.4. It should be emphasized that the plasticity of a clay is expected to increase with increasing clay content. However, a low plasticity (I_P = 15 %) and high plasticity (I_P = 40 %) clay with presumed similar clay fraction will be compared. This might be a simplification, but it captures the tendency of decreasing permeability with increasing plasticity index. For the numerical calculation, a void ratio of *e* = 1.2 and a clay fraction CF = 0.85, are assumed.

Meaning that (I_p + CF) = 1.00 for the low plasticity clay, and (I_p + CF) = 1.25 for the high plasticity clay. The estimated permeabilities are provided in Table 7.3.

Table 7.3: Permeability from Plasticity Index

Parameter		**I_p = 15 %**	**I_p = 40 %**
Permeability	k	$1*10^{-10}$ m/s = $8.64*10^{-6}$ m/day	$4*10^{-11}$ m/s = $3.46*10^{-6}$ m/day

It is believed that the correlations presented above are suitable to capture general trends in relation to the degree of plasticity. However, in practical design, such rude general correlations requires caution. The relationships should only be used as a rough estimation of parameters.

7.3 Predicted Ultimate Shaft Friction

To illustrate the effect of the plasticity index and overconsolidation ratio on the ultimate shaft friction, the shaft friction is calculated for the cases studied. When the α-approach by Karlsrud (2012) is used, the relationship between normalized undrained strength and the overconsolidation ratio need to be estimated. Ladd and Foott (1974) developed the principle called "Stress History And Normalized Soil Engineering Properties" (SHANSEP). The SHANSEP principle assumes that the normalized strength is closely related to the OCR through

$$\frac{s_u}{\sigma'_{v0}} = S(OCR)^m \tag{7.4}$$

Figure 7.5 presents the normalized strength versus OCR for DSS tests performed by Karlsrud and Hernandez-Martinez (2013). The figure shows the range of values of the constant, *S*, and power, *m*, that captures all the data. The average line is represented by

$$\frac{s_{uD}}{\sigma'_{v0}} = 0.22(OCR)^{0.8} \tag{7.5}$$

Using equation (7.5), the ultimate shaft friction can be predicted from the two procedures proposed by Karlsrud (2012). The effective overburden pressure at the investigated depth (10 m) is σ'_{v0} = 100 kPa. Table 7.4 summarizes the predicted shaft friction from the α-approach (Figure 6.2) and the β-approach (Figure 6.4). The shaft friction increases significantly with

increasing degree of plasticity and with increasing overconsolidation ratio based on the approach proposed by Karlsrud (2012).

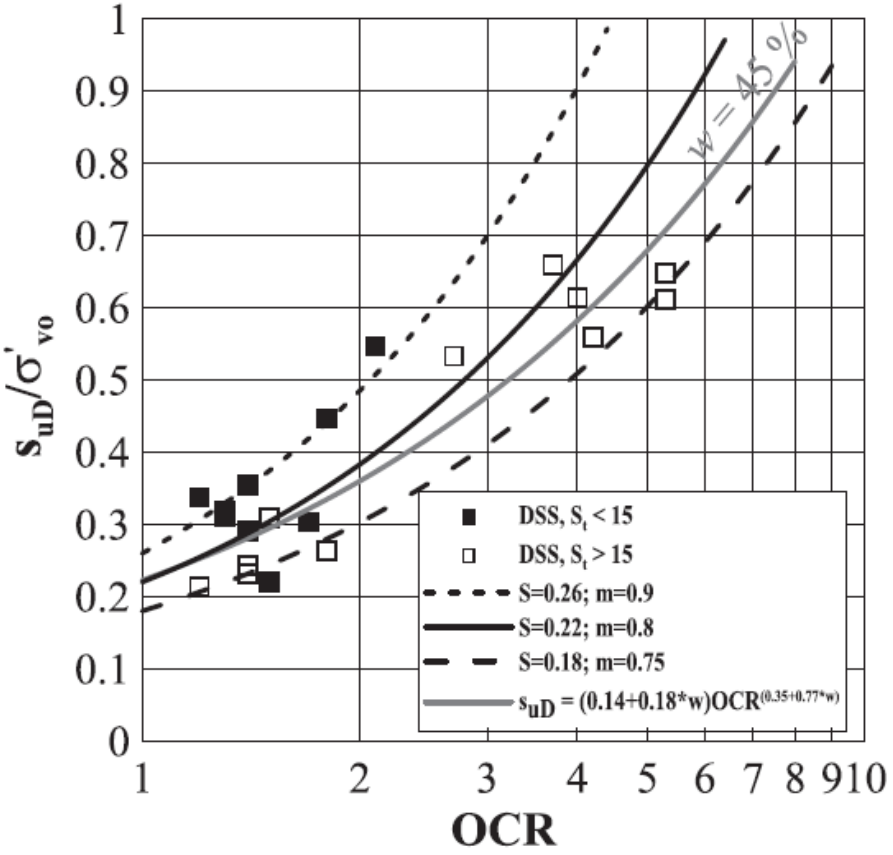

Figure 7.5: Normalized strength versus OCR (Karlsrud and Hernandez-Martinez, 2013)

Table 7.4: Predicted Ultimate Shaft Friction for the Different Cases

Case	$\frac{s_{ud}}{\sigma'_{v0}}$	**α**	**τ_{us} (α)**	**β**	**τ_{us} (β)**	**τ_{us} (average)**
a) I_P = 15 % and OCR = 1	0.22	0.35	0.35*22 = 8 kPa	0.08	0.08*100 = 8 kPa	**8 kPa**
b) I_P = 15 % and OCR = 8	1.16	0.50	0.50*116 = 58 kPa	0.45	0.45*100 = 45 kPa	**51.5 kPa**
c) I_P = 40 % and OCR = 1	0.22	0.87	0.87*22 = 19 kPa	0.20	0.20*100 = 20 kPa	**19.5 kPa**
d) I_P = 40 % and OCR = 8	1.16	0.75	0.75*116= 87	0.80	0.80*100 = 80 kPa	**83.5 kPa**

8 Numerical Analysis

The installation effects of a driven pile are investigated by performing numerical simulations using Plaxis 2D. Plaxis is a finite element program specifically designed for geotechnical applications.

8.1 Material Properties

The Modified Cam-Clay (MCC) model is used in the numerical simulations. Parameters for the four cases studied are summarized in Table 8.1.

Table 8.1: Material properties

Case		a)	b)	c)	d)
General					
Material model		Modified Cam-Clay	Modified Cam-Clay	Modified Cam-Clay	Modified Cam-Clay
Material behavior		Undrained (A)	Undrained (A)	Undrained (A)	Undrained (A)
Dry Unit Weight	γ_{unsat}	20 kN/m^3	20 kN/m^3	20 kN/m^3	20 kN/m^3
Saturated unit weight	γ_{sat}	20 kN/m^3	20 kN/m^3	20 kN/m^3	20 kN/m^3
Initial void ratio	e_0	1.2	1.2	1.2	1.2
Parameters					
Compression index	λ	0.0875	0.0875	0.2000	0.2000
Swelling index	κ	0.0087	0.0087	0.0297	0.0297
Poisson's ratio	ν	0.2	0.2	0.2	0.2
Strength (Inclination of CSL)	M	1.2	1.2	1.2	1.2
Flow parameters					
Vertical permeability	k'_v	$8.64*10^{-6}$ m/day	$8.64*10^{-6}$ m/day	$3.46*10^{-6}$ m/day	$3.46*10^{-6}$ m/day
Horizontal permeability	k'_h	$8.64*10^{-6}$ m/day	$8.64*10^{-6}$ m/day	$3.46*10^{-6}$ m/day	$3.46*10^{-6}$ m/day
Change in permeability	c_k	0.6	0.6	0.6	0.6
Initial					

Coefficient of lateral earth pressure	K_0	0.656	1.400	0.648	1.500
Overconsolidation ratio	OCR	1.0	8.0	1.0	8.0

The compressibility and permeability were determined in section 7.2 based on correlations with the plasticity index. Hydraulic conductivity of the clay is assumed isotropic, meaning that the horizontal permeability is assumed to equal the vertical permeability.

Brinkgreve et al. (2014) recommend that the initial void ratio, e_0, and the change in permeability, c_k, should be defined to enable the modelling of change in permeability due to compression of the soil. In radial drainage, the reduction in horizontal permeability with decreasing void ratio should be accounted for. A variation of permeability with void ratio was represented by Tavenas et al. (1983) in terms of a linear e vs. lg k relation. The relationship between these two parameters was introduced as: $e = e_0 + c_k \log(k_h/k_{h0})$. Tavenas et al. (1983) suggest that c_k may be calculated as $c_k = 0.5e_0$. A unique value of the initial void ratio of $e_0 = 1.2$ was assumed for the four cases studied for ease of comparison.

A typical unit weight of $\gamma = 20$ kN/m^3 is assumed. An equal strength is assumed for all cases, as the inclination of the critical state line is set to be $M = 1.2$. This strength corresponds to an effective angle of friction of $\varphi' = 30°$. The Poisson's ratio is a real elastic parameter, with a value usually in the range between 0.1 and 0.2 (Brinkgreve et al., 2014). A Poisson's ratio of $\nu_{ur} = 0.2$ is assumed.

For the MCC model in Plaxis, the coefficient of lateral earth pressure, K_0^{nc}, is automatically determined based on the M parameter. K_0^{nc} is the stress ratio in the normally consolidated state, and the K_0^{nc}-values proposed by Plaxis are realistic. For overconsolidated soils, Plaxis calculates K_0 by using the relationship suggested by Wroth (1978):

$$K_0 = OCR \cdot K_{0,nc} - \frac{\nu_{ur}}{1 - \nu_{ur}}(OCR - 1) \tag{8.1}$$

Plaxis suggests that $K_0 \approx 3.5$ for the overconsolidated case b) and case d). The proposed values of K_0 are unrealistically large. Thus, values for K_0 are determined manually. Relationships between s_u/σ'_{v0}, OCR, I_P and K_0 based on correlations by Andresen et al. (1979) and Brooker and Ireland (1965) are presented in Figure 8.1. The in-situ K_0 for the cases with OCR of 8 was

estimated using the correlation to OCR and plasticity index in Figure 8.1. From this relation, $K_0 = 1.4$ for case b), and $K_0 = 1.5$ for case d).

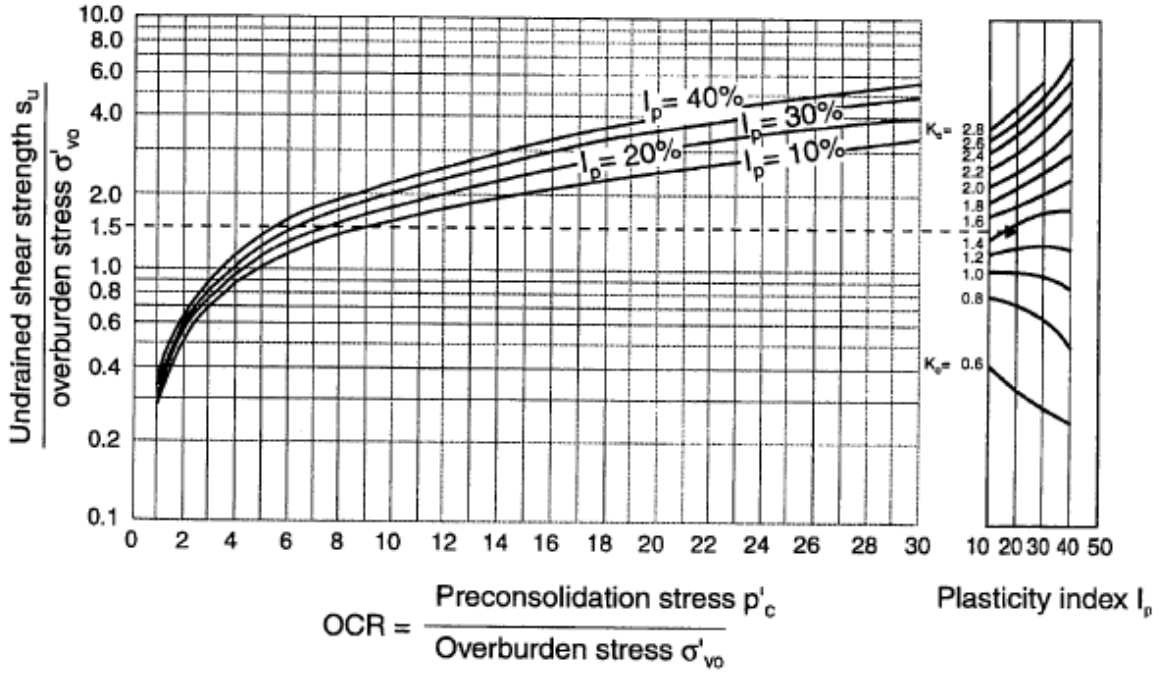

Figure 8.1: Relationships between s_u/σ'_{v0}, OCR, I_P and K_0 based on correlations by Andresen et al. (1979) and Brooker and Ireland (1965) (Lunne et al., 1997)

8.2 Modelling

Modelling of the installation process of a single pile is carried out in Plaxis 2D by performing an axisymmetric analysis. For axisymmetric problems, the x-coordinate represents the radius, the y-axis represents to the axial line of symmetry, and the z-coordinate corresponds to the circumferential direction. In an axisymmetric model, deformation and stresses are assumed identical in any radial direction. By default, Plaxis 2D have standard fixities that fix the bottom in all directions and the vertical boundaries in the horizontal directions. A sufficiently large model is created so that any influence of the boundaries are avoided. The soil is modelled by 15-noded triangular elements. The 15-node triangle is the default element in Plaxis 2D, and it is particularly recommended to be used in axisymmetric analysis.

In the analysis, a pile length of 10 m is assumed. The pile tip is not modelled, as it is the installation effect along the pile shaft that is of interest. In addition, modelling the tip of the pile may cause numerical problems. A closed-ended pile with diameter of 101 mm is studied. This

corresponds to the pile diameter of the "IC-pile" developed at Imperial College. The IC-pile is used in several sites (Pentre, Bothkennar, Cowden and Cannons P.) in the data collected by Karlsrud (2012). The pile diameter is in the midrange of the pile sizes in the collected data.

Pile installation is modelled in the finite element program by the expansion of a cylindrical cavity (CEM). Carter et al. (1979) explain that in plane strain, the solution for expansion from a finite radius will ultimately furnish the solution to the expansion from an initial radius of zero. A doubling of the cavity size produce sufficiently good results for both the elastic, perfectly plastic model and the modified Cam-clay model (Carter et al., 1979). The accuracy gained of further expansion of the cavity is negligible.

Assuming a pile diameter of 101 mm, the initial cavity radius in the numerical model is

$$a_0 = r_0/\sqrt{3} = 50.5/\sqrt{3} = 29 \text{ mm} \tag{8.2}$$

From an initial radius (a_0), a prescribed displacement to a final radius (a_f) is performed. From equation (8.2), a_0 = 29 mm, and thus a_f = 58 mm. The cavity expansion is assumed to occur undrained, since piles installation normally only takes a short period of time. Figure 8.2 show the geometry of the model and the finite element mesh. Note that the figure is not in scale as the initial radius and prescribed displacement are heavily enlarged to be visible. The ground water table is at the ground surface. The model is 10 m high and 10 m wide. A very fine mesh is applied close to the "pile", i.e. the cylindrical cavity. Accuracy of the mesh is confirmed by checking the effect of mesh refinements.

As the cavity expansion generates large strains, it is necessary to account for large displacements by using the "updated mesh" option in Plaxis. The influence of changes in the mesh geometry on the equilibrium is normally neglected in finite element analysis. This approximation is convenient as deformations typically are relatively small in engineering problems. However, if large soil deformations occur, it is necessary to take geometry changes in the mesh into account. Plaxis allows for large displacement calculations by the "updated mesh" option. Brinkgreve et al. (2014) mention three special features that need to be included in a large displacement calculation. Firstly, additional terms in the structure stiffness matrix has to be included to model the effects of large structural distortions on the finite element equations. Secondly, the stress changes that occur during rotation of finite material need to be modelled. To accomplish this, the co-rotational rate of Kirchhoff stress is adopted as a definition of stress rate in Plaxis. This stress rate is expected to give good results as long as the shear strains are

not too large. The third important feature of large deformation theory is that the finite element mesh has to be updated as the calculation proceeds. The updated Lagrangian formulation is utilized for this purpose. An updated mesh analysis is less robust and more time consuming than a normal calculation in Plaxis (Brinkgreve et al., 2014).

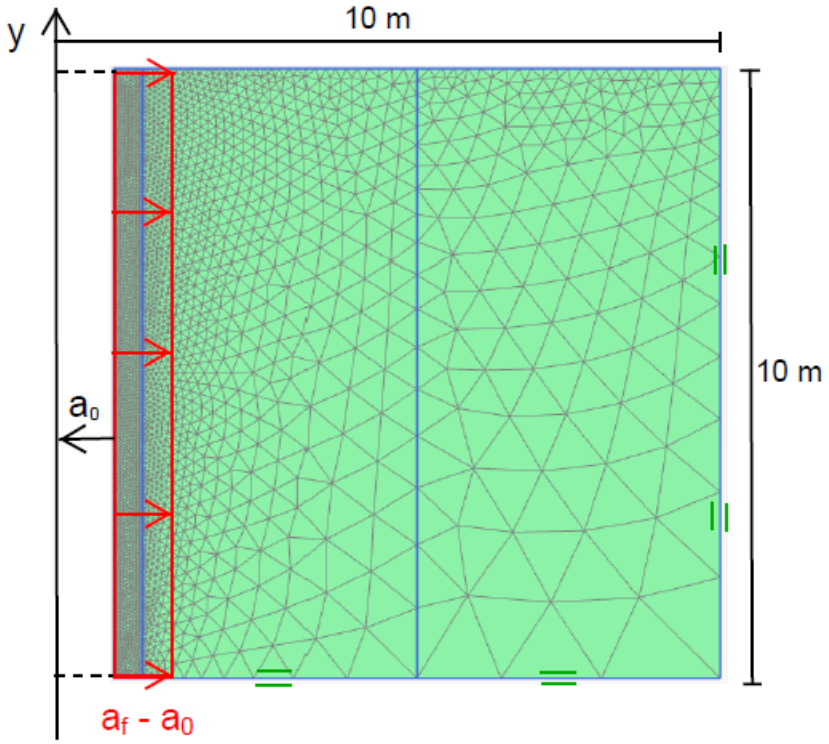

Figure 8.2: Model geometry and mesh in Plaxis 2D

After generating the initial stresses in the *Initial phase* in Plaxis 2D, the expansion of a cavity in undrained conditions is performed in the second phase. By applying a *prescribed displacement* in Plaxis, the cavity is expanded from a_0 = 29 mm to a_f = 58 mm. Subsequently, the reconsolidation process is carried out in the third phase. The excess pore pressures induced by pile installation are assumed to dissipate radially outwards from the pile. The consolidation process is set to last until all excess pore pressures have decreased below 1 kPa. Since the focus of this analysis is on the soil behaviour, there is no need to model the pile material. The cavity is set as impermeable for the reconsolidation phase.

8.3 Results

In the presentation of the results, the distance to the pile axis, *r*, is normalized by the outer pile radius, r_0. Results out to a distance $r/r_0 = 100$ are included, i.e. out to 5 m from the pile axis. The pile installation has no influence on the stress state further from the pile. A logarithmic scale is used to amplify the area close to the pile. The stresses acting on the pile surface corresponds to the stresses at $r/r_0 = 1$. The stresses and pore pressures at the pile surface are estimated by extrapolating.

The resulting stresses from the CEM-MCC model are normalized by the undrained shear strength from direct simple shear, s_{ud}. The computed s_{ud} are found using the Soil Test feature in Plaxis (Appendix A). Normalizing by the undrained shear strength allows for direct comparison between different depths. It is decided to investigate the stresses at 10 m depth, corresponding to an effective overburden pressure of $\sigma'_{v0} = 100$ kPa.

8.3.1 Stress Distributions in the Soil Immediately After Pile Driving

Figure 8.3 to Figure 8.6 show the stress distribution after cavity expansion, normalized by the undrained shear strength. For all cases a) to d), the radial effective stress acting on the pile shaft is about $2.5 \cdot s_{ud}$. The vertical and circumferential stresses also change near the pile. At the pile shaft, the circumferential effectives stress is about $0.5 \cdot s_{ud}$, and the vertical effective stress is about $1.5 \cdot s_{ud}$ for all cases. This is a result of the chosen strength parameter *M* in the MCC model, as defined in equation (4.29) to (4.31).

A plastic zone is developed around the pile where the soil has reached critical state. In the plastic zone, the mobilized shear stress exceeds the undrained shear strength of the soil. The maximum stress difference is uniformly $2 \cdot s_{ud}$ in the region of failure. The plasticized radius coincides with the zone close to the pile where there is no change in effective stresses. For case a), the extension of the plastic zone is approximately $r_p = 7 \cdot r_0$. For case b), the extension of the plastic zone is approximately $r_p = 5 \cdot r_0$. For case c) and case d), the extension of the plastic zone is approximately $4 \cdot r_0$ and $3 \cdot r_0$, respectively. The size of the plastic zones are confirmed by viewing plastic points in the Plaxis output program. At larger radii than r_p, the soil is either hardening or it is very close to the in-situ state.

A zone of negative (tensile) circumferential stress is observed for the cases with OCR = 8 (Figure 8.4 and Figure 8.6). Tensile stresses are observed for radii between 9 to 11 times r_0 for

case b), and from 5 to 7 times r_0 for case d). Cracks radiating from the pile axis may occur in reality, and will be self-healing close to the pile during the reconsolidation phase (Randolph et al., 1979). The main effect of cracks further from the pile will be accelerating of the dissipation process due to an increase in radial permeability.

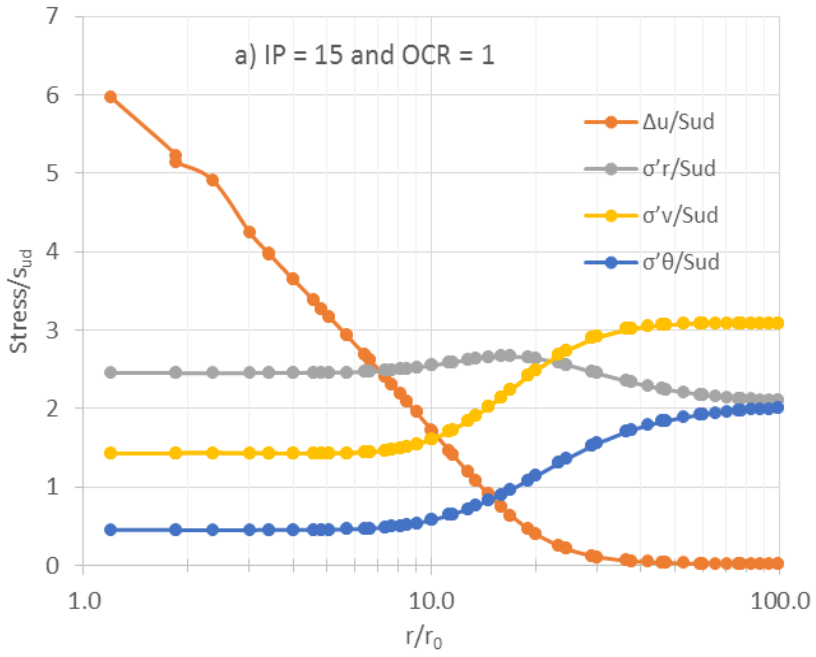

Figure 8.3: Stress distributions in the soil after cavity expansion, case a)

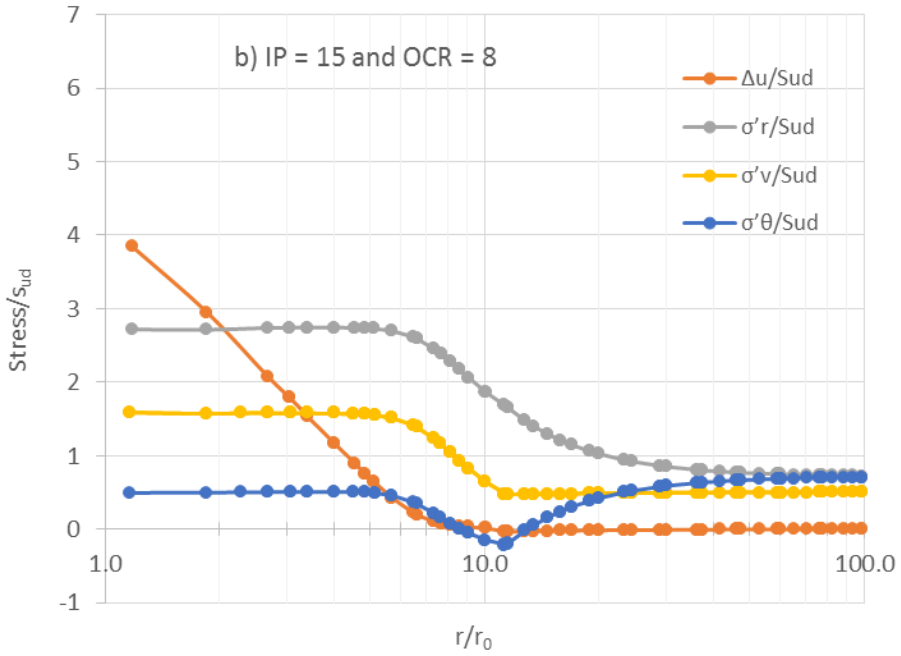

Figure 8.4: Stress distributions in the soil after cavity expansion, case b)

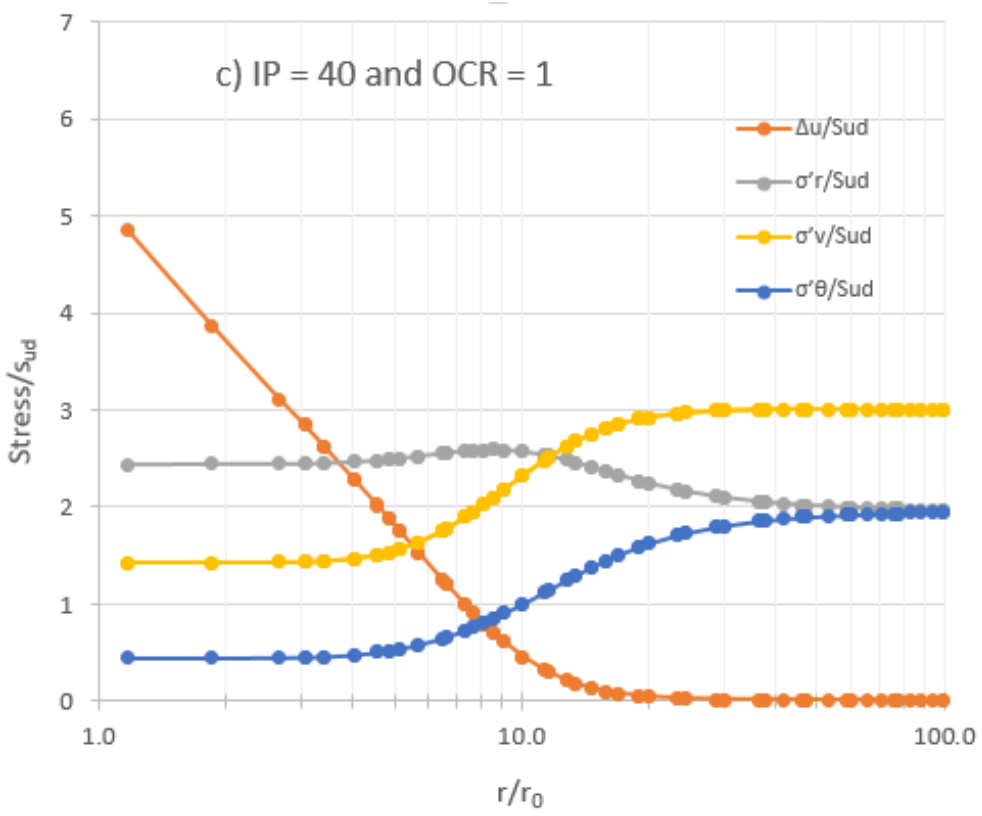

Figure 8.5: Stress distributions in the soil after cavity expansion, case c)

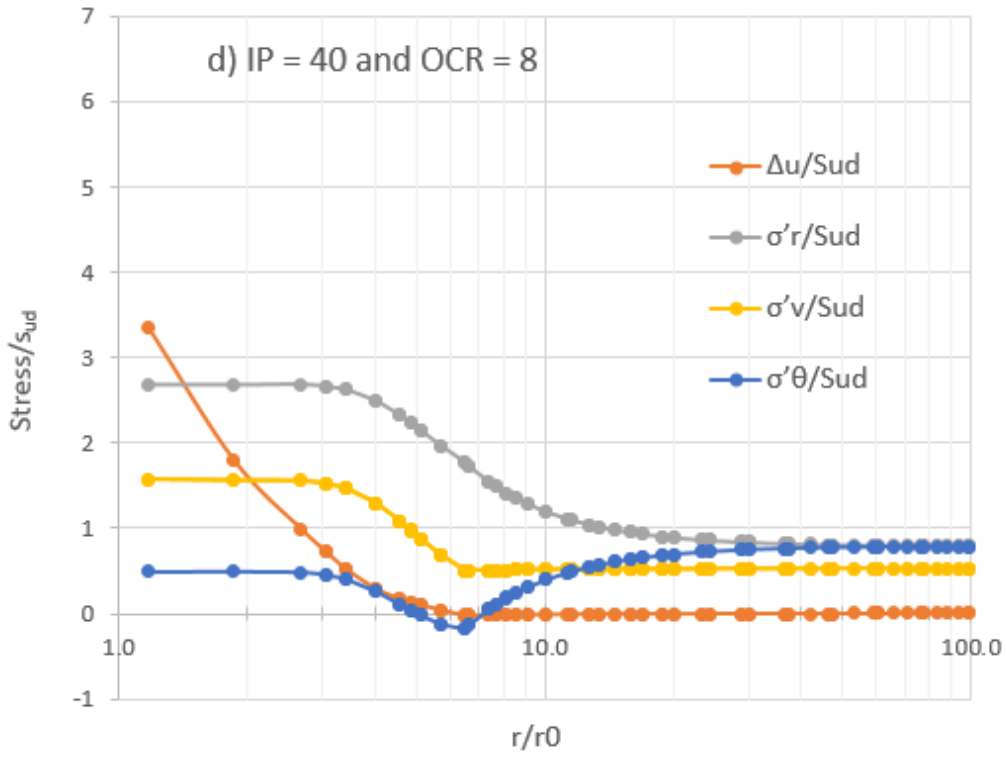

Figure 8.6: Stress distributions in the soil after cavity expansion, case d)

8.3.2 Stress Distributions in the Soil after Reconsolidation

Stress distributions in the soil at the end of reconsolidation are plotted in Figure 8.7 to Figure 8.10. Pile driving has significantly altered the stresses in the soil out to about $30 \cdot r_0$. At the pile shaft, the generated stress normalized by s_{ud} is quite similar for all four cases. The radial effective stress acting on the pile has a value of about $4.5 \cdot s_{ud}$. The vertical and circumferential effective stresses at the pile are also virtually equal in all cases; $\sigma'_v \approx \sigma'_\theta \approx 2.75 \cdot s_{ud}$.

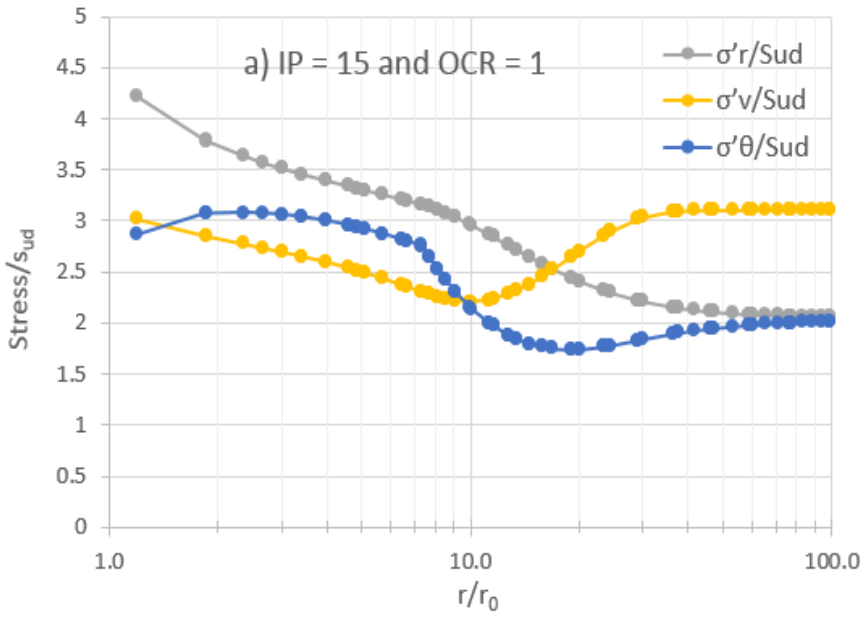

Figure 8.7: Stress distributions in the soil after reconsolidation, case a)

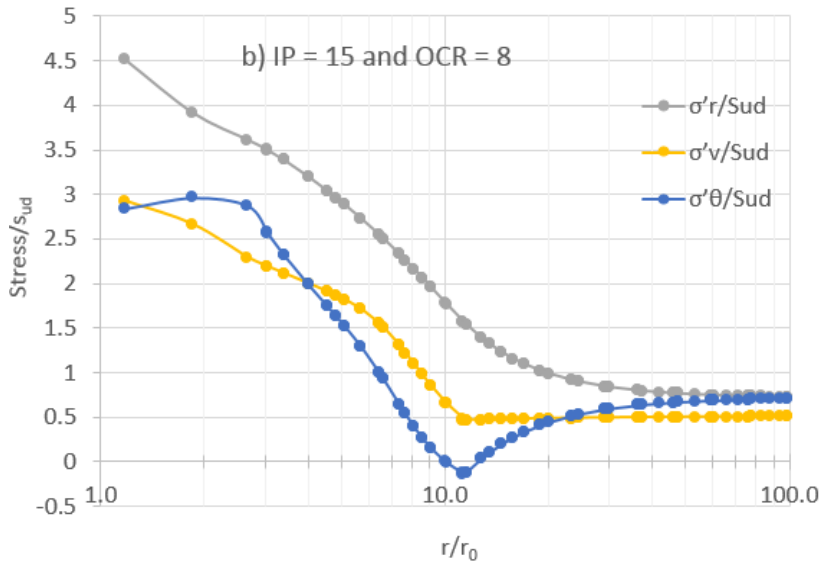

Figure 8.8 Stress distributions in the soil after reconsolidation, case b)

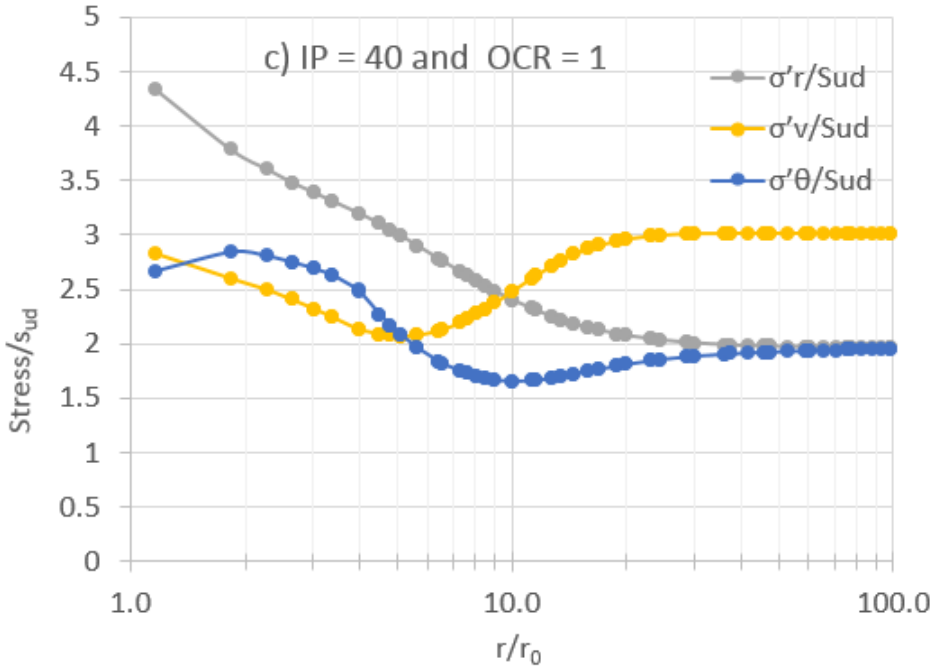

Figure 8.9: Stress distributions in the soil after reconsolidation, case c)

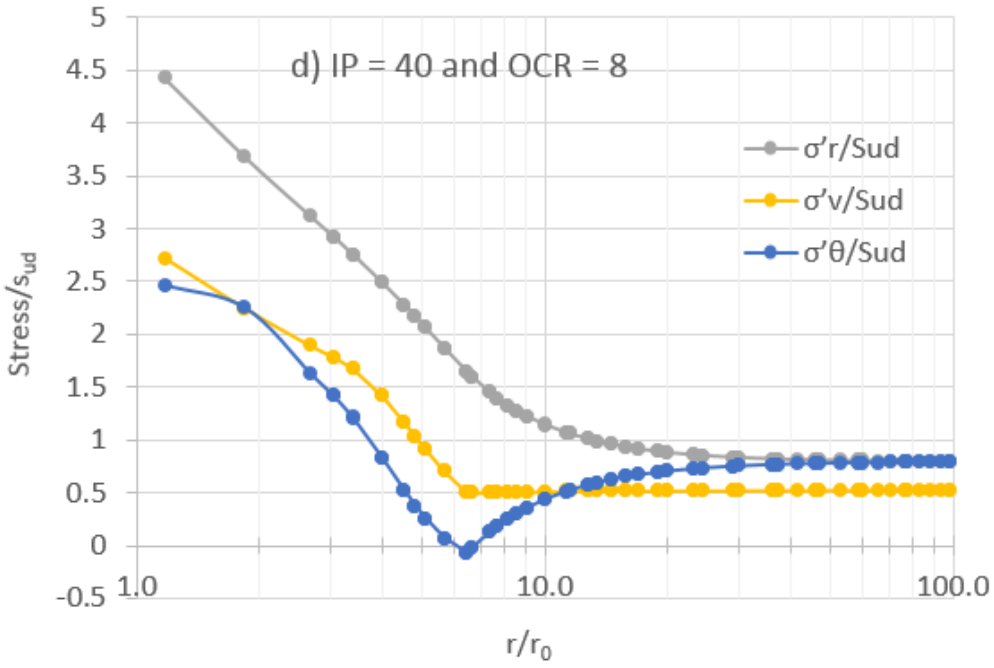

Figure 8.10: Stress distributions in the soil after reconsolidation, case d)

In Figure 8.11 to Figure 8.14, the effective stresses in the soil after reconsolidation are normalized by the effective overburden stress prior to driving. In other words, all cases are normalized by σ'_{v0} = 100 kPa. The largest effective stresses are generated in the soils with OCR of 8. For the cases with OCR = 8, the radial effective stress at the pile shaft is about $9 \cdot \sigma'_{v0}$,

while $\sigma'_v \approx \sigma'_\theta \approx 5.5 \cdot \sigma'_{v0}$. For the cases with OCR = 1, the radial effective stress at the pile shaft is about $1.5 \cdot \sigma'_{v0}$, while $\sigma'_v \approx \sigma'_\theta \approx 0.9 \cdot \sigma'_{v0}$. No evident impact from the plasticity index is found.

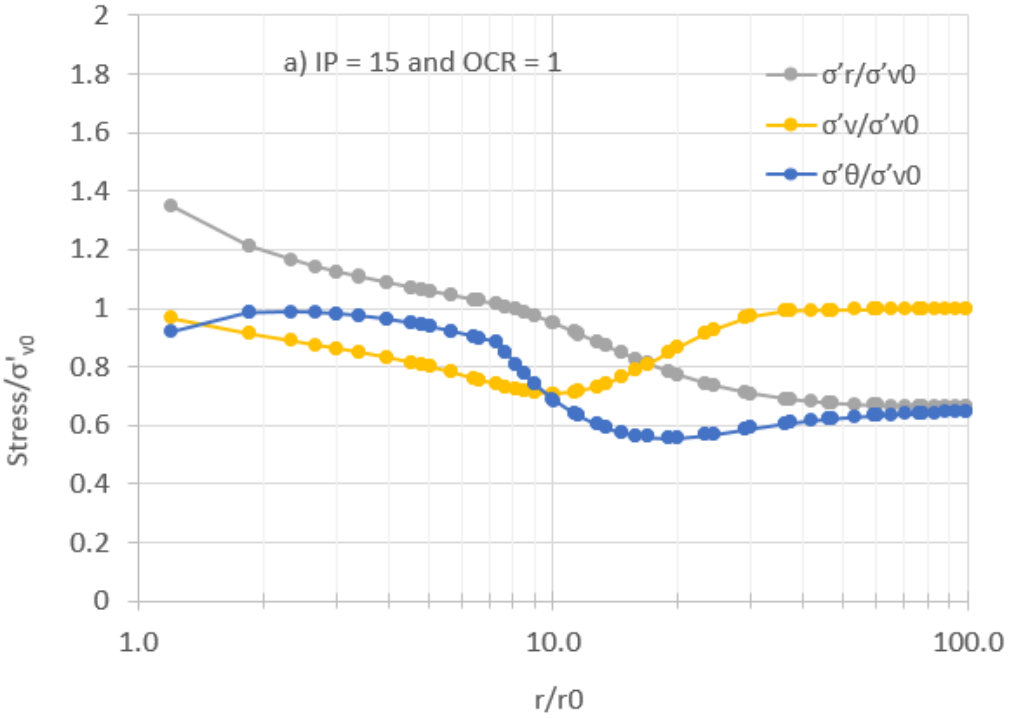

Figure 8.11: Stresses normalized by effective oberburden pressure, case a)

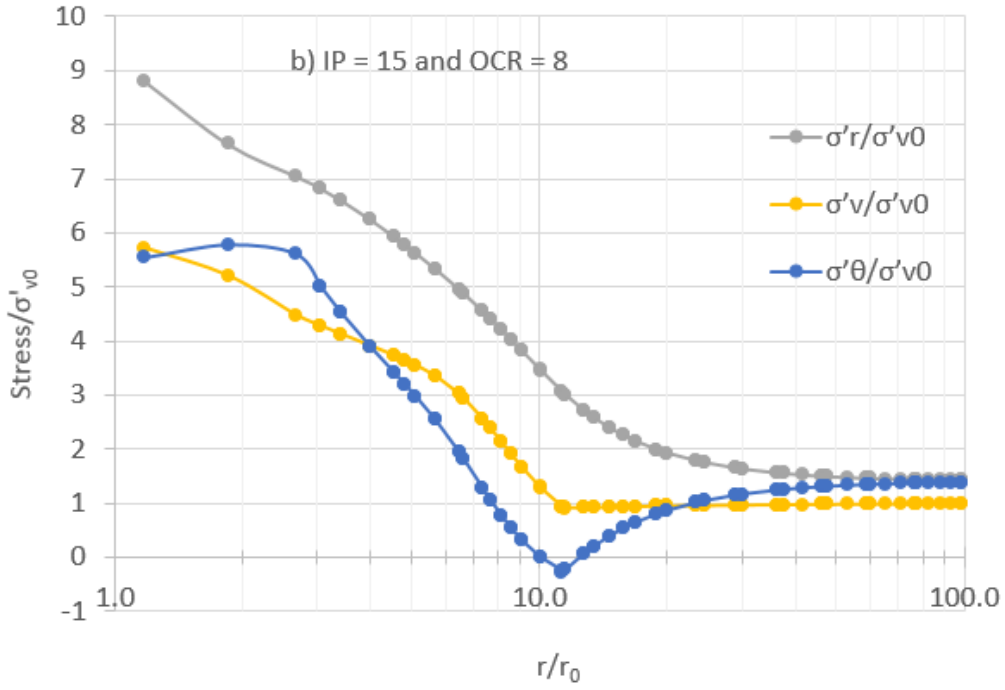

Figure 8.12: Stresses normalized by effective oberburden pressure, case b)

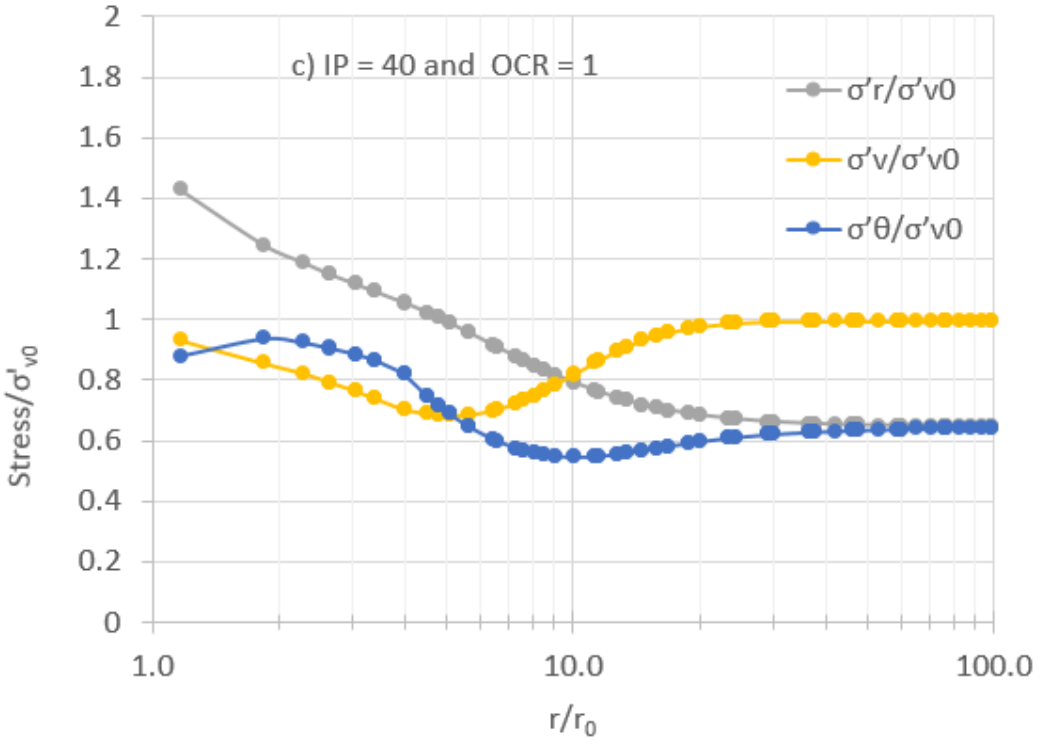

Figure 8.13: Stresses normalized by effective oberburden pressure, case c)

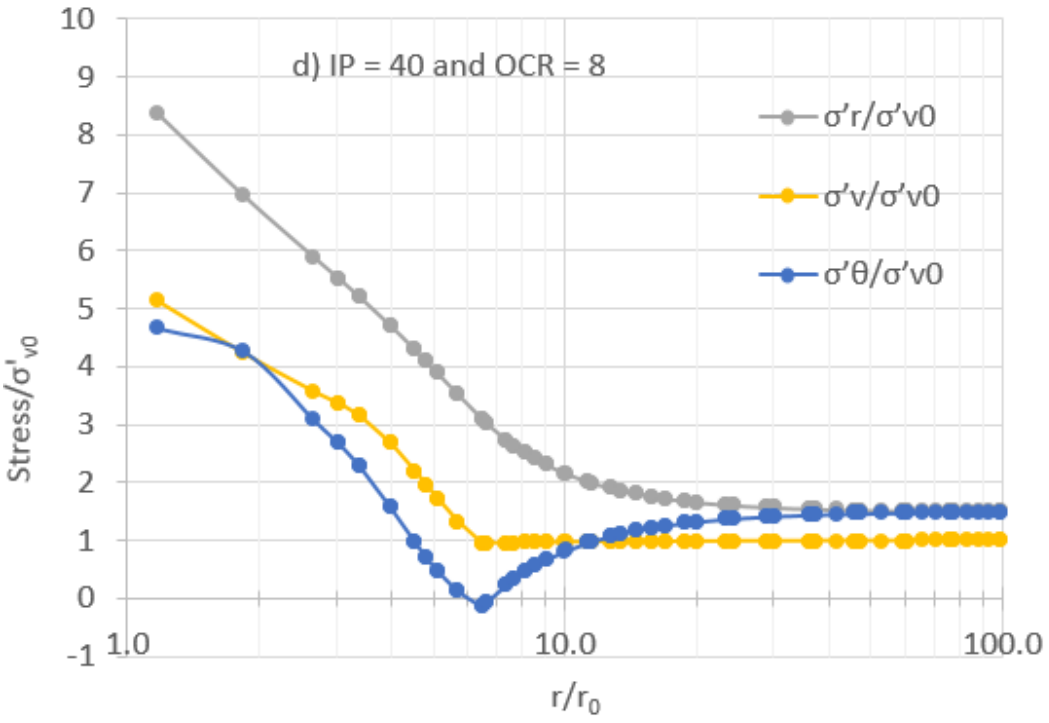

Figure 8.14: Stresses normalized by effective oberburden pressure, case d)

8.3.3 Mean Effective Stress in the Soil after Reconsolidation

During the reconsolidation phase, the effective mean stress, p', increase as the pore pressure dissipates. Figure 8.15 compares the effective mean pressures for the four cases studied when the reconsolidation phase is complete. The in-situ mean effective pressure, p'_0, which the soil experienced before pile driving, normalizes the mean effective pressure in Figure 8.15.

There is a much larger increase in the mean effective stress around the pile for the cases with OCR of 8. For these cases, p' is approximately 5 times p'_0 at the pile surface. In addition, the mean effective stress is a bit larger for case b) than case d). For the cases with OCR of 1, p' is approximately 1.5 times p'_0 at the pile shaft. The plasticity index show no clear trend on the size of the mean effective stress acting on the pile shaft. In each case, the effective mean pressure decrease with distance from the pile, but it reaches the in situ p'_0 at different pile radii. The extension of the influenced area is approximately $7 \cdot r_0$ for the cases with I_p = 40 %, and approximately $11 \cdot r_0$ for the cases with I_p = 15 %. Outside this area, changes in mean effective stress is zero.

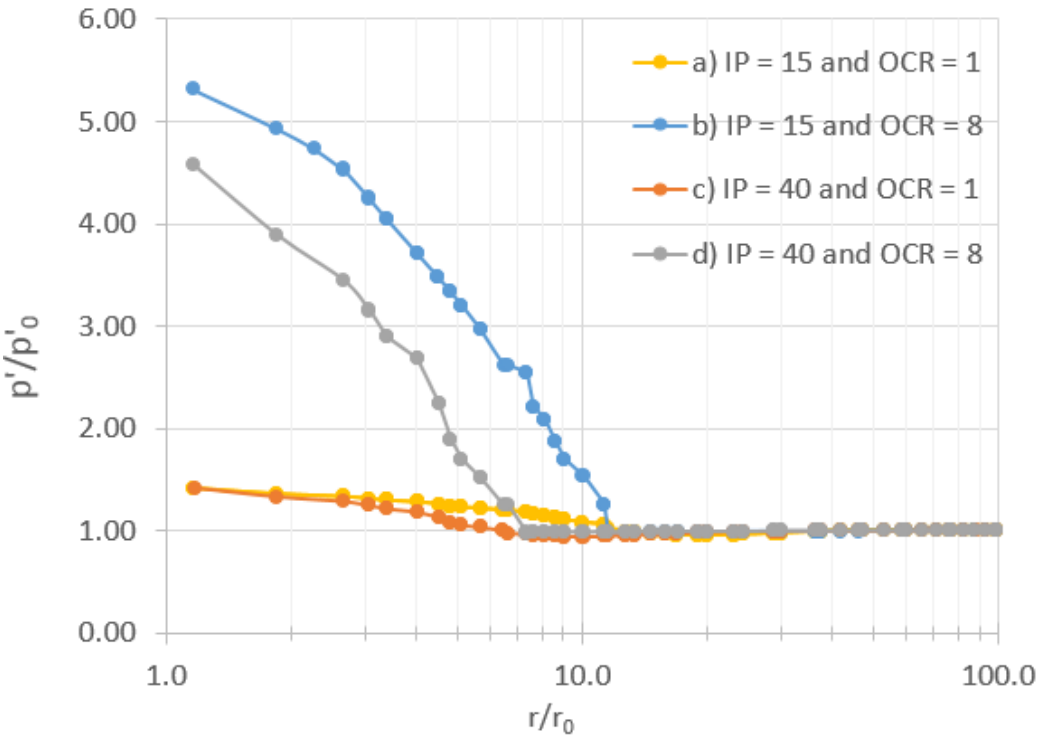

Figure 8.15: Effective mean pressure after reconsolidation

8.3.4 Isotropic OCR

During reconsolidation, the soil close to the pile will experience primary loading. This is due to increase in shear strain as the rigid pile prevents inward movement of the soil. However, further from the pile, the soil will experience unloading/reloading during reconsolidation. To investigate the extension of these zones, Figure 8.16 to Figure 8.19 show the isotropic overconsolidation ratio in the soil after reconsolidation. The isotropic OCR is different from the conventional OCR, which is in terms of effective vertical stress. Isotropic OCR is the ratio between the isotropic mean preconsolidation stress, p'_c, and the current equivalent mean effective stress, p'_{eq}.

For case a), the soil undergo primary loading out to about $7 \cdot r_0$. From 7 to 30 times r_0, the soil is unloading. Case b) experience primary loading out to about $3 \cdot r_0$. Case c) and case d) experience primary loading out to $4 \cdot r_0$ and $2 \cdot r_0$, respectively. The results are summarized in Table 8.2. The extension of the disturbed zone is approximately 30 times r_0 for all cases.

Table 8.2: Extension of inner zone that undergoes primary loading

Case	a)	b)	c)	d)
r	$7 \cdot r_0$	$3 \cdot r_0$	$4 \cdot r_0$	$2 \cdot r_0$

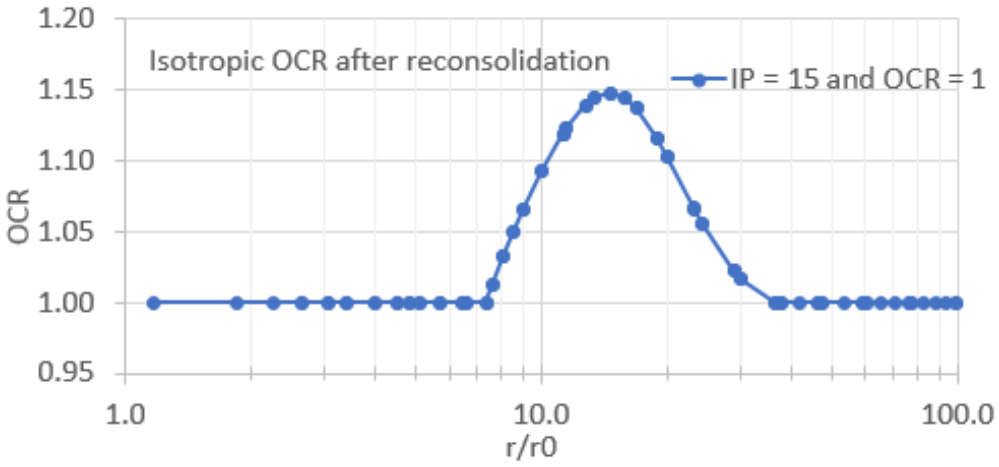

Figure 8.16: Overconsolidation ratio after the end of reconsolidation, case a)

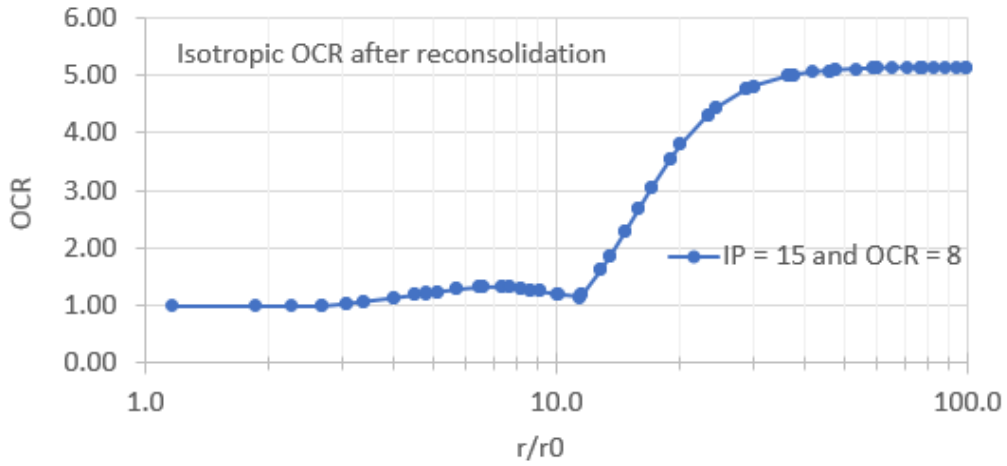

Figure 8.17: Overconsolidation ratio after the end of reconsolidation, case b)

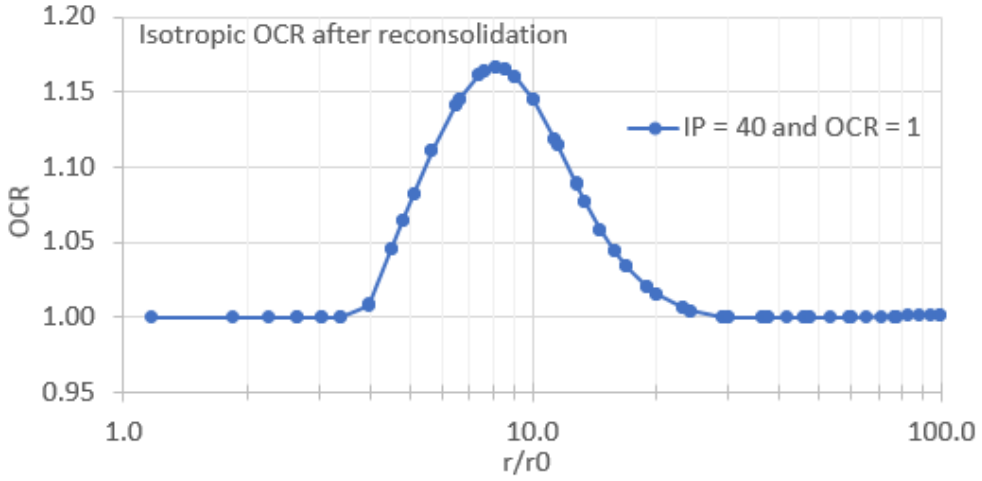

Figure 8.18: Overconsolidation ratio after the end of reconsolidation, case c)

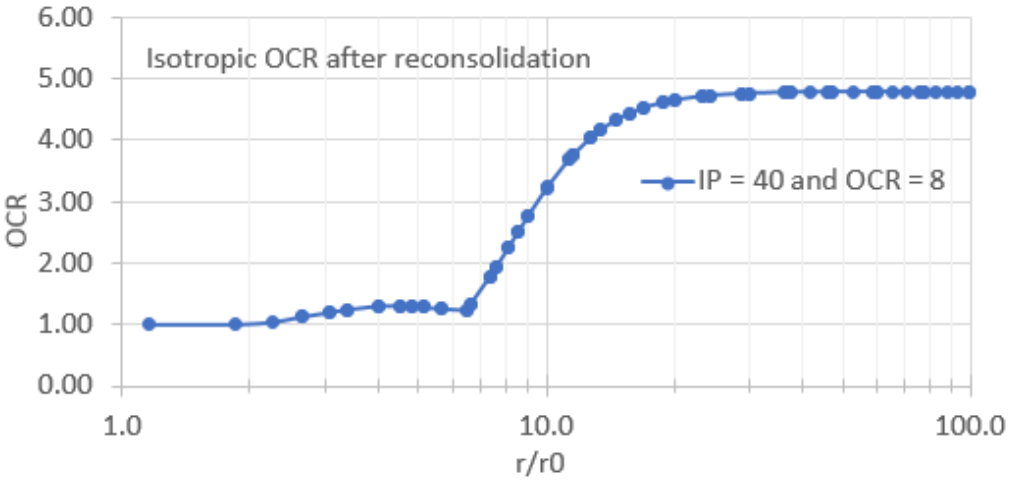

Figure 8.19: Overconsolidation ratio after the end of reconsolidation, case d)

8.4 Comparison between measured response and model predictions

In the following section, results from the Plaxis analysis are compared with measured field response found in literature. The measured data is mainly obtained from Karlsrud (2012). The numerical model in the Plaxis analysis is referred as the CEM-MCC model.

8.4.1 Radial Effective Stress at the End of Installation

Measured Response Against the Pile Shaft

Figure 8.20 show the radial effective stress after installation normalized by the initial vertical effective stress, $K_i = \sigma'_{ri}/\sigma'_{v0}$ (Karlsrud, 2012). Measuring the effective stress against the pile shaft during installation is challenging, as the generated total radial earth pressure and pore pressure are very large. Thus, a small error in either total earth pressure or pore pressure could have a considerable impact on the effective stress. The large scatter observed in Figure 8.20 confirms this, and the negative values of K_i are of course incorrect. Still, the data suggest that K_i is increasing with increasing OCR. A typical trend line for the assumed in-situ K_0-values at the different sites are also shown in Figure 8.20. It appears that K_i is lower than the assumed K_0 for most cases.

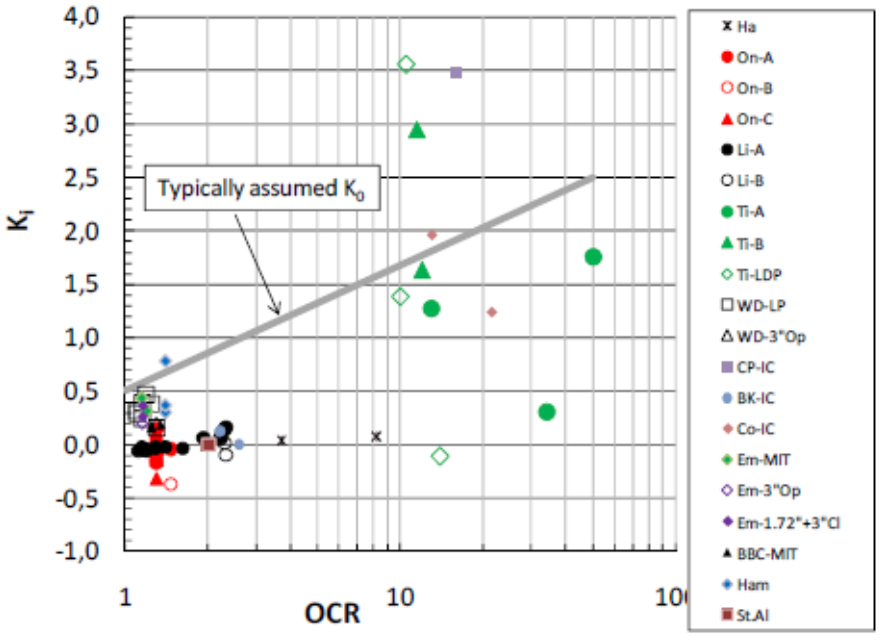

Figure 8.20: Normalized effective stress ratio, $K_i = \sigma'_{ri} / \sigma'_{vo}$, acting on the pile at end of installation (Karlsrud, 2012)

Results for the CEM-MCC Model

The normalized radial effective stress ratio for the CEM-MCC model are presented in Figure 8.21. Figure 8.21 display $\sigma'_{ri}/\sigma'_{vo}$ with distance from the pile, while Figure 8.20 display K_i at the pile surface. Table 8.3 provide the predicted K_i by extrapolating $\sigma'_{ri}/\sigma'_{vo}$ to $r/r_0 = 1$. Clearly, the CEM-MCC model overpredicts the radial effective stress at the pile surface compared to the data in Figure 8.20. However, the relatively low measured radial effective stress in Figure 8.20 is to some degree due to inaccuracies in measurements.

Table 8.3: K_i predicted from Plaxis simulation

Case	a)	b)	c)	d)
K_i	0.8	5.3	0.8	5.1

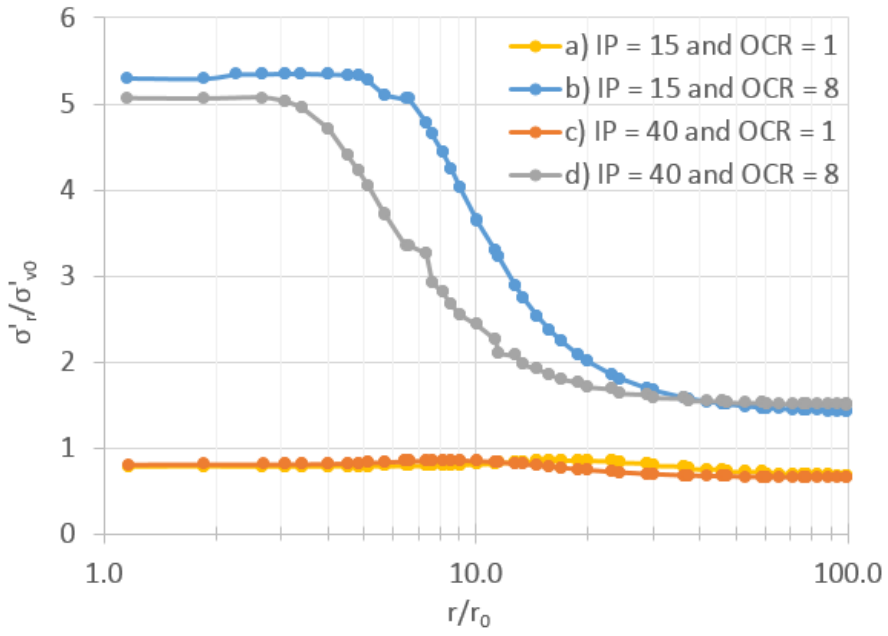

Figure 8.21: $\sigma'_{ri} / \sigma'_{vo}$ at end of installation. Results from Plaxis simulation.

8.4.2 Excess Pore Pressure at the End of Installation

Measured Response Against the Pile Shaft

Figure 8.22 shows normalized excess pore pressures, $\Delta u_i / s_{ud}$, acting on the pile shaft in relation to OCR for all the instrumented piles presented by Karlsrud (2012). The excess pore pressures predicted with the CEM-EP model based on G_{50}/s_{uc} from Figure 4.4 are also included. Solid

symbols are for closed-ended piles and open symbols for open-ended. The largest size symbols represent the largest piles and the smallest symbols is for model piles. Only measurements made longer than four pile diameters from the pile tip or from the ground surface are included to avoid possible geometry effects. Though the scatter is rather large, a clear trend of decreasing $\Delta u_i/s_{ud}$ with increasing OCR can be seen in Figure 8.22. It also appears that the closed-ended piles typically give higher excess pore pressures than the open-ended piles. However, for high OCR, there is no apparent difference between open-ended and closed-ended piles. For the closed-ended CEM-EP model, it appears the excess pore pressures are underpredicted for low OCR clays and overpredicted for high OCR clays.

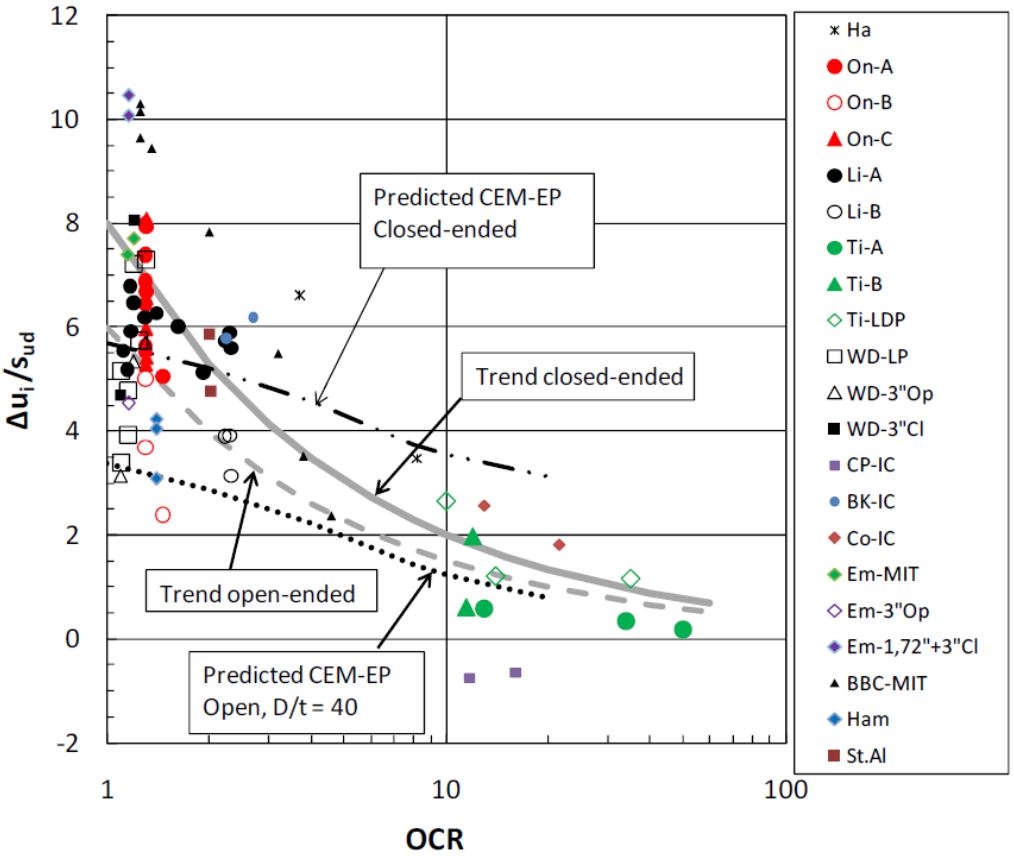

Figure 8.22: Measured normalized excess pore pressure against the pile shaft, $\Delta u_i/s_{ud}$, versus OCR (Karlsrud, 2012)

Differences in pile size and execution of pile installation, may have contributed to the large scatter in Figure 8.22. In addition, there is possible inaccuracy associated with the various instrumentation systems used. The accuracy expresses the closeness of the measurement to the actual value of the quantity being measured. Piezometer filters has to be de-aired and fully saturated when they enter into the ground to avoid entrapped air and ensure sufficient accuracy

in measurements. In the high OCR clays however, negative pore pressures can be generated and cause cavitation and desaturation even if the piezometer filters initially were well saturated. In these instances, the pore pressures measured shortly after pile installation may be too low. Karlsrud (2012) believes that very little of the scatter in the data are due to uncertainties in the assessed values of s_{ud} and OCR.

Figure 8.23 compares the normalized excess pore pressure with the plasticity index for clays with OCR less than 2. The data may suggest some tendency for increasing pore pressure with increasing I_p, the scatter is however large. An increase in $\Delta u_i / s_{ud}$ with I_p is contrary to what is expected from Figure 4.4 assuming that G_{50}/s_u decrease with increasing I_p.

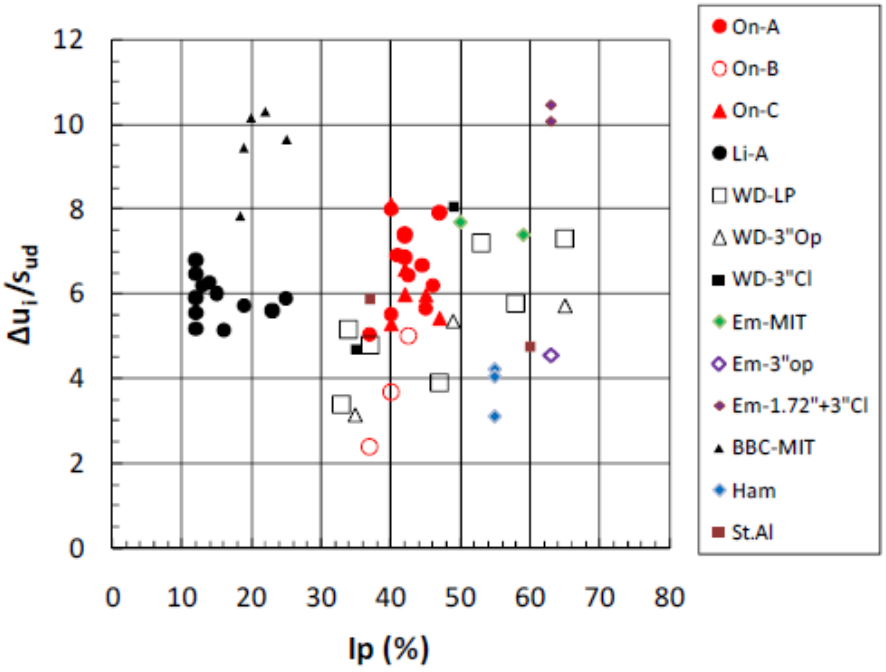

Figure 8.23: Measured normalized excess pore pressure against the pile shaft, $\Delta ui / s_{ud}$, versus I_p for OCR<2 (Karlsrud, 2012)

Some collected data of measured excess pore pressure around a driven pile are shown in Figure 8.24. The excess pore pressure at the pile wall is observed to be close to or greater than the effective vertical stress. Lo and Stermac (1965) found that the excess pore pressure induced in a normally consolidated clay can exceed the effective vertical stress by 30 %. Koizumi and Ito (1967) showed measurements of excess pore pressure larger than two times the effective overburden pressure. The excess pore pressure vanished about two or three weeks after pile driving. Bjerrum and Johannessen (1961) reported measurements of considerable excess pore pressure in a clay soil up to three to four months after pile installation. The radial extent of the

excess pore pressure is $r/r_o \approx 12$ for the two upper cases and $r/r_o \approx 30$ for the bottom case. As indicated by the trend lines, it appears the excess pore pressures decrease approximately linearly with the logarithm of the radius from the pile axis. However, the scatter in the field measurements is quite large.

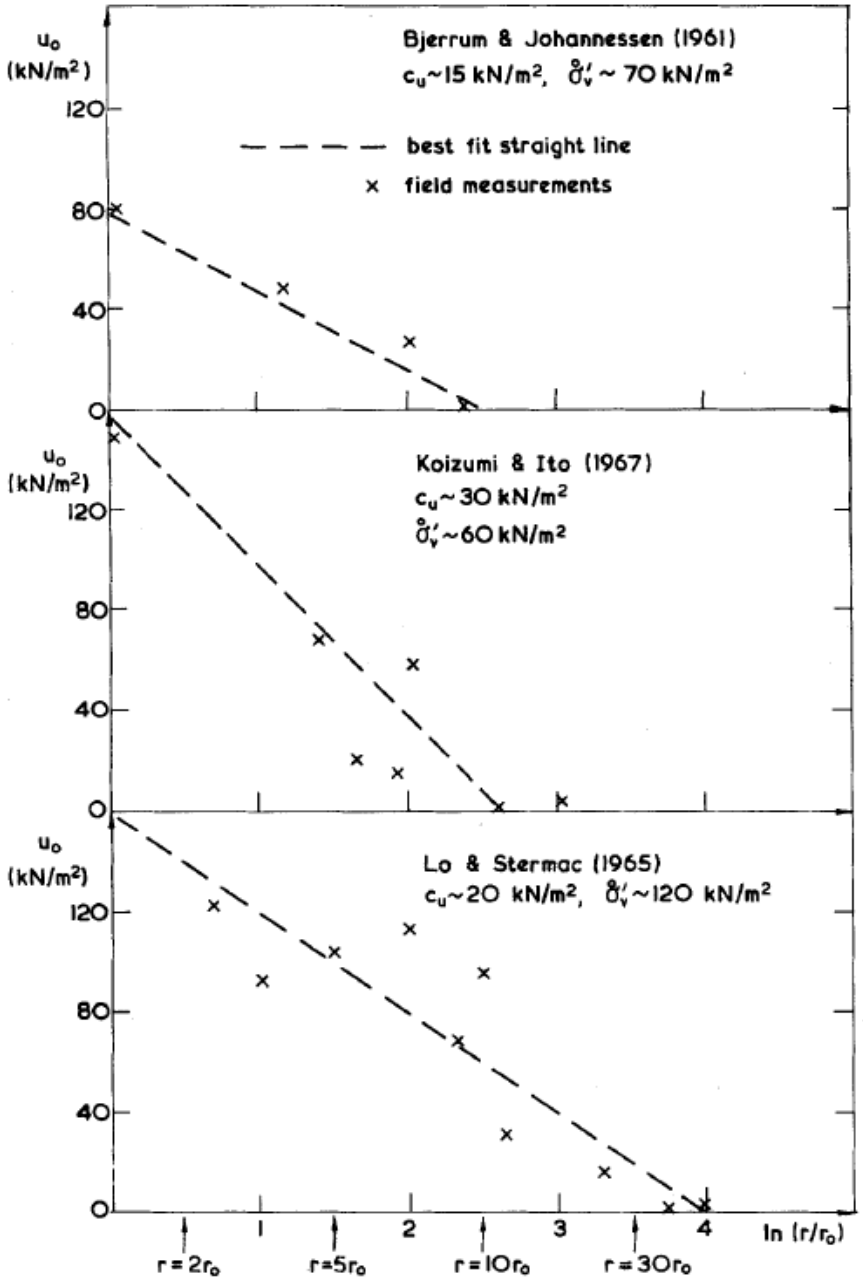

Figure 8.24: Field measurements of excess pore pressures induced by pile driving (Randolph and Wroth, 1979)

Results for the CEM-MCC Model

The excess pore pressure normalized by s_{ud} are lowest for the highly overconsolidated soils (OCR = 8), as shown in Figure 8.25. The extrapolated excess pore pressures at the pile shaft are from $4 \cdot s_{ud}$ for case d), to $6.5 \cdot s_{ud}$ for case a). The excess pore pressure is about $2 \cdot s_{ud}$ higher for the cases with OCR of 1 than for the cases with OCR of 8, given similar I_p. A clear trend of decreasing $\Delta u_i/s_{ud}$ with increasing OCR is also found in field measurements by Karlsrud (2012) (Figure 8.23). Some tendency of increasing $\Delta u_i/s_{ud}$ with I_p is found in the data by Karlsrud (2012). However, the Plaxis results show a tendency for the opposite.

The radial extent of the generated excess pore pressure varies from $r/r_o \approx 7$ for case d), to $r/r_o \approx 30$ for case a). The shapes of the curves present a linear decrease of the excess pore pressure with the logarithm of the radius from the pile axis. This agrees with the field measurements in Figure 8.24.

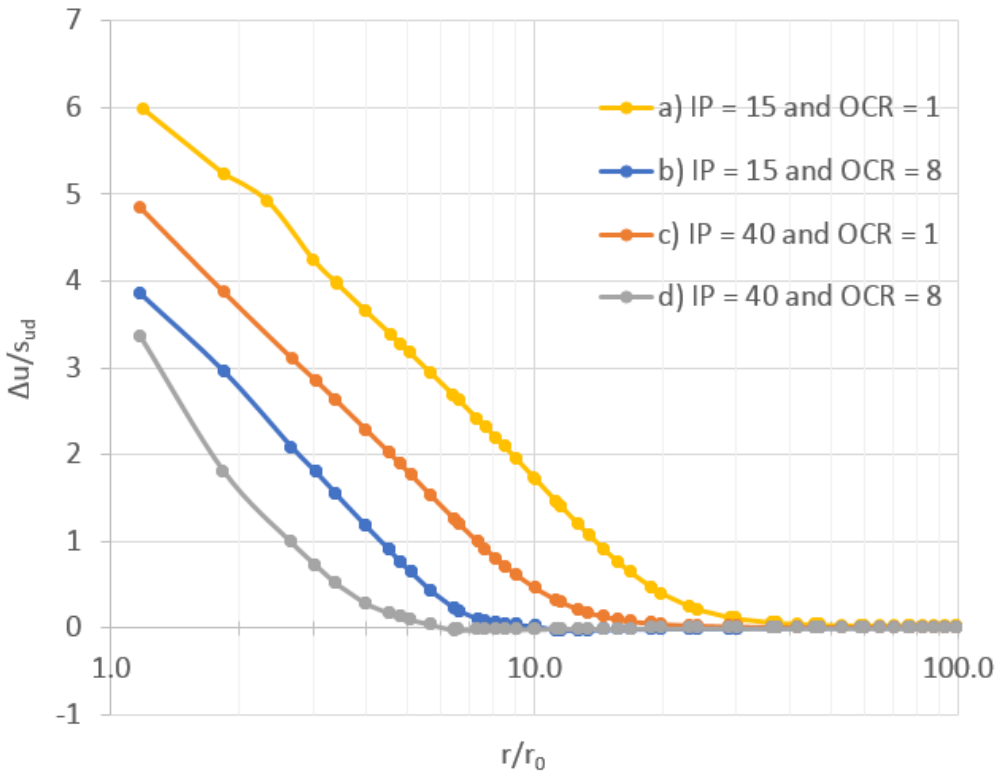

Figure 8.25: Excess pore pressure normalized by undrained shear strength

In Figure 8.26, the excess pore pressures are normalized by the effective overburden stress prior to driving. In other words, all cases are normalized by $\sigma'_{v0} = 100$ kPa. This plot show largest values of $\Delta u/\sigma'_{v0}$ near the pile for cases with OCR of 8. The cases with OCR of 8 also show the steepest decrease in excess pore pressure with distance from the pile. In fact, outside $4\text{-}6 \cdot r_0$, Δu

is largest for the cases with OCR = 1. A bit higher excess pore pressure is predicted for the cases with I_p of 15 %.

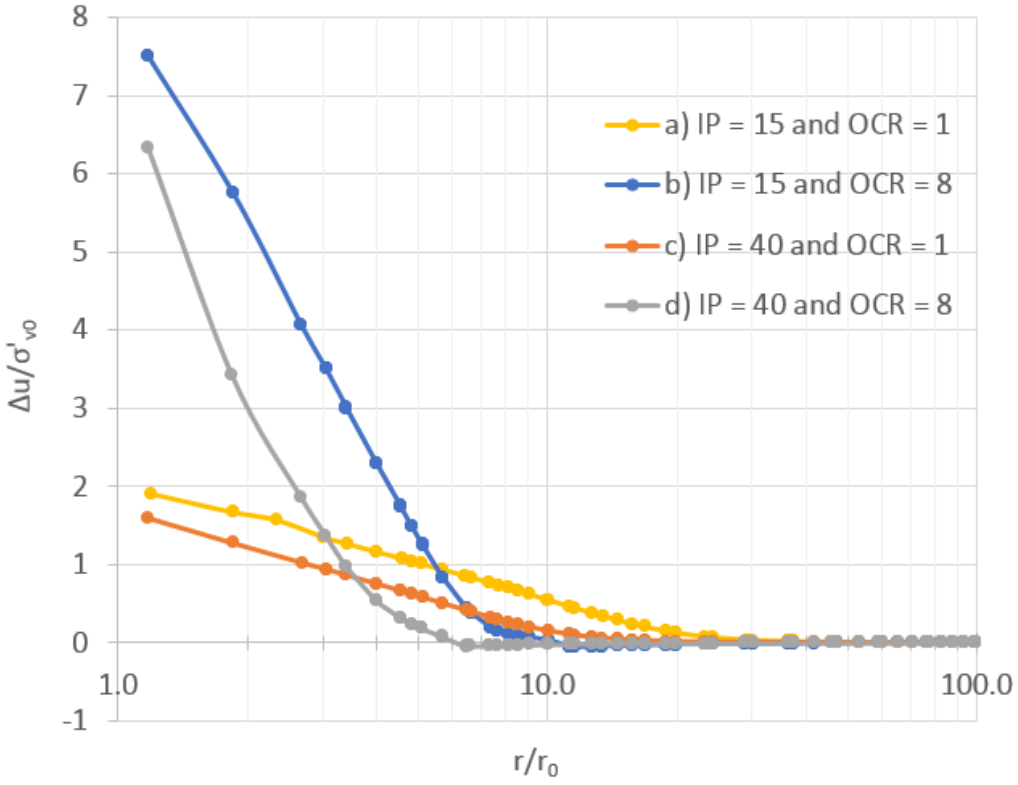

Figure 8.26: Excess pore pressure normalized by initial effective vertical stress

8.4.3 Consolidation Time

The predicted consolidation times for the four cases studied are summarized in Table 8.4. It appears that the value of OCR has a large effect on the time for consolidation. Significant shorter consolidation times are observed for the cases with OCR of 8. The extent to which excess pore pressures are generated are shorter for the cases with OCR of 8. Consequently, as the gradient of the excess pore pressure distribution is steeper, the time for consolidation will be reduced. Figure 8.27 show the excess pore pressure over time at the pile wall, normalized by the excess pore pressure just after pile installation. Note that the pore pressure falls off rapidly initially for the cases with OCR of 8. The cases with OCR of 1 display a more delayed response.

It is noted that the predicted consolidation times to reach 100 % consolidation are very long. 100 % consolidation is assumed to be reached when all excess pore pressure in the soil has decreased below 1 kPa. Typically, the time it takes for a pile to reach full bearing capacity may vary from 2-3 weeks for a stiff overconsolidated clay, to more than half a year for a soft clay.

70-80 % of the bearing capacity will normally be reached after two-three months in a soft clay (Vegdirektoratet, 2014). The times for 90 % dissipation of excess pore pressure at the pile shaft (t_{90}) compare well with observations. As seen in Table 8.4, t_{90} varies from about 1 day for case b) to approximately 90 days for case c). By extrapolating from the dissipation curves in Figure 8.27, the times to reach a certain degree of pore pressure dissipation may be estimated.

Table 8.4: Consolidation times

Case	a) I_p = 15 % and OCR = 1	b) I_p = 15 % and OCR = 8	c) I_p = 40 % and OCR = 1	d) I_p = 40 % and OCR = 8
Time to reach 100 % consolidation	1090 days	85 days	2330 days	290 days
Time to reach 90 % consolidation, t_{90}	35 days	1 day	90 days	10 days

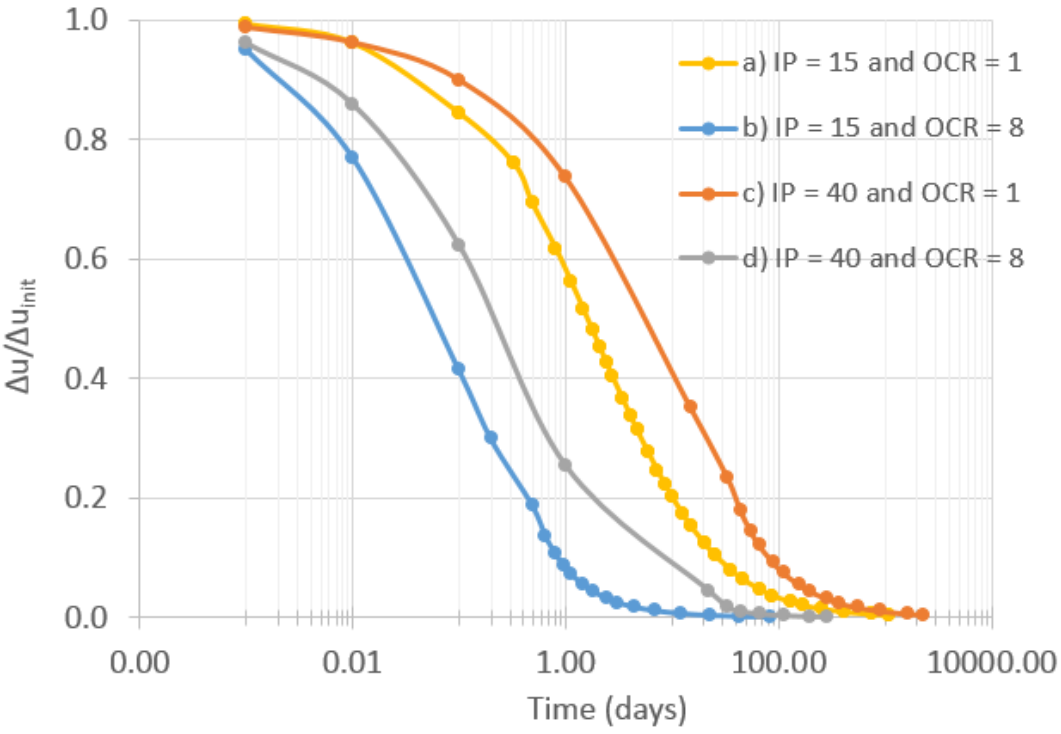

Figure 8.27: Normalized excess pore pressure at the pile shaft over time

8.4.4 Radial Effective Stress at the End of Reconsolidation

Measured Response Against the Pile Shaft

The change in radial effective stress generated from pile installation clearly influence the piles shaft friction. The radial effective stress gives the amount of lateral support of the pile and it influences the soil yielding. A convenient state parameter to study is therefore the final radial effective stress ratio, $K_c = \sigma'_r/\sigma'_{v0}$. Karlsrud (2012) summarizes measured values of radial effective stress at the pile shaft in Figure 8.28. The data in Figure 8.28 suggest that there is no scale effect on the measured values of K_c, and no clear difference between open-ended and closed-ended piles. This is quite surprising, considering the large differences in strains caused by pile installation. Although the data show large scatter, there is a clear trend for K_c to increase with OCR. In addition, there is a clear trend of low K_c-values for low-plastic clays. The K_c-values in low plastic clays are actually below the in-situ K_0-values, as indicated by the trend line for I_p = 12 %. K_0 in Figure 8.28 has been calculated in the same manner as in the case study. The trend lines in Figure 8.28 indicate that K_c is around 0.2 for case a), and around 0.6 for case c). Further, the trend lines indicate that K_c should be in the order of 1.5-2 for case b) and case d). At OCR = 8, the two trend lines have converged.

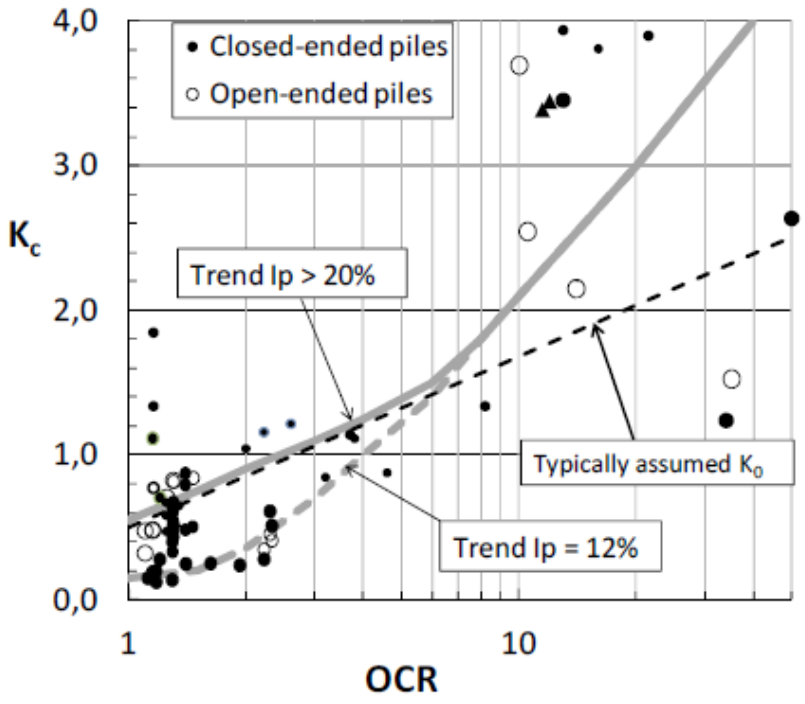

Figure 8.28: Measured values of horizontal effective stress ratio, K_c, at the end of reconsolidation (Karlsrud, 2012)

The total earth pressures acting on the pile are measured to decrease significantly during the re-consolidation process in the data from Karlsrud (2012). This effect is most apparent for piles in low to moderately overconsolidated clays. Karlsrud (2012) concludes that no unique correlation to OCR and plasticity index can be made due to the large scatter in the measured values of K_c. This is one of the reasons why Karlsrud (2012) did not recommend any method to predict the ultimate shaft friction based on the measured values of K_c.

When piles are pulled out of the ground after testing in low OCR clays, it has been observed that a layer of clay normally sticks to the pile. Karlsrud (2012) argues that for clays with OCR less than approximately 4, the critical shear plane is likely to be at some distance from the pile surface. However, the radial (horizontal) effective stress is measured at the pile shaft. This also makes correlations between measured ultimate shaft friction and measured radial effective stress less attainable.

Results for the CEM-MCC Model

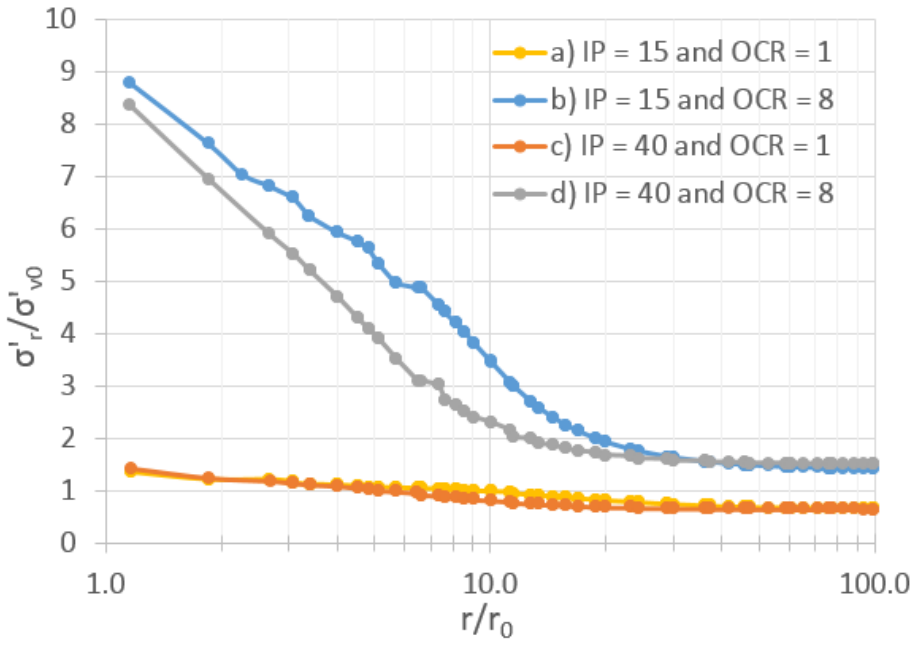

Figure 8.29: Distribution of final radial effective stress ratio, σ'_r/σ'_{v0}.

Figure 8.29 compare the final radial effective stress ratio around the pile for the cases studied. No difference in the radial effective stress is predicted between the two plasticity indexes with OCR = 1. With some distance from the pile, lower radial effective stresses are predicted for case d) than case b). However, no apparent difference is found when extrapolating the stresses

to the pile shaft. At the pile surface, $K_c \approx 9$ for the cases with OCR = 8 and $K_c \approx 1.5$ for the cases with OCR = 1.

The soil parameters in the numerical analysis carried out are based on general correlations and not site specific values for the data in Figure 8.28. Still, the result must be said to fit field measurements poorly. However, the scatter in the field measurements in Figure 8.28 is substantial. It is also worth mentioning that the undrained failure of a soil element depend on the complete effective stress state, and not only the radial effective stress.

Table 8.5 compare the predicted radial effective stresses at the pile shaft, with the estimated ultimate shaft friction in section 7.3. From Figure 6.5 and Figure 6.6, the τ_{us}/σ'_r ratio typically lies between 0.2 and 0.4 based on Karlsrud's data. The size difference in the estimated ultimate shaft friction in Table 7.4 should ideally be reflected in the predicted radial effective stress for the different cases. Results from the numerical analysis show that the CEM-MCC model largely overpredicts the measured horizontal effective stresses. The radial effective stress is in particular overpredicted for the cases with $I_p = 15$ %. However, the *relative* increase in radial effective stress due to increased OCR is somewhat reflected in the numerical model.

Table 8.5: Radial effective stress from the numerical analysis compared with the ultimate shaft friction from Karlsrud's approach

Case	**K_c (σ'_{v0} = 100 kPa)**	**σ'_r (CEM-MCC)**	**τ_{us} (Karlsrud)**	**$\frac{\tau_{us}}{\sigma'_r}$**
a) I_p = 15 % and OCR = 1	1.5	150 kPa	8 kPa	**0.05**
b) I_p = 15 % and OCR = 8	9.0	900 kPa	51.5 kPa	**0.06**
c) I_p = 40 % and OCR = 1	1.5	150 kPa	19.5 kPa	**0.13**
d) I_p = 40 % and OCR = 8	9.0	900 kPa	83.5 kPa	**0.09**

8.5 Parametric Study

In this section, a sensitivity analysis on the flexibility parameters, λ and κ, is carried out. The background for performing the sensitivity analysis is given in section 8.5.1. Subsequently, a numerical analysis with hypothetical changes in the flexibility parameters is carried out in section 8.5.2. The effects of the parameter variation on the radial effective stress have been looked at.

8.5.1 Theory

Andersen and Jostad (2002) present consolidation analysis of cylindrical suction caissons using a finite element method program. Suction anchors has a very large radius and a relatively small wall thickness. Andersen and Jostad (2002) distinguish between volumetric compressibility of a thin remoulded zone close to the skirt wall experiencing virgin compression, and a undisturbed zone further out experiencing unloading/reloading. The excess pore pressure in the remoulded zone was assumed to be equal to the octahedral effective stress prior to installation of the caissons. Just after pile installation, zero effective stress is assumed in the remoulded zone. Zero effective stress is to some degree in agreement with the very low effective stress measured at the pile shaft in normally consolidated clays after pile driving (Figure 8.20 and Figure 8.24). Figure 8.30 show the octahedral normal effective stress, σ'_{oct}, in the remoulded zone after 90 % pore pressure dissipation. The octahedral effective stress is normalized by the in situ stress prior to suction anchor installation, $\sigma'_{oct,0}$. The analysis were performed with K_0 = 0.55, and a remoulded zone with thickness equal to the skirt wall thickness. σ'_{oct} decreases with increasing ratio between the moduli in the intact clay and the moduli in the remoulded zone.

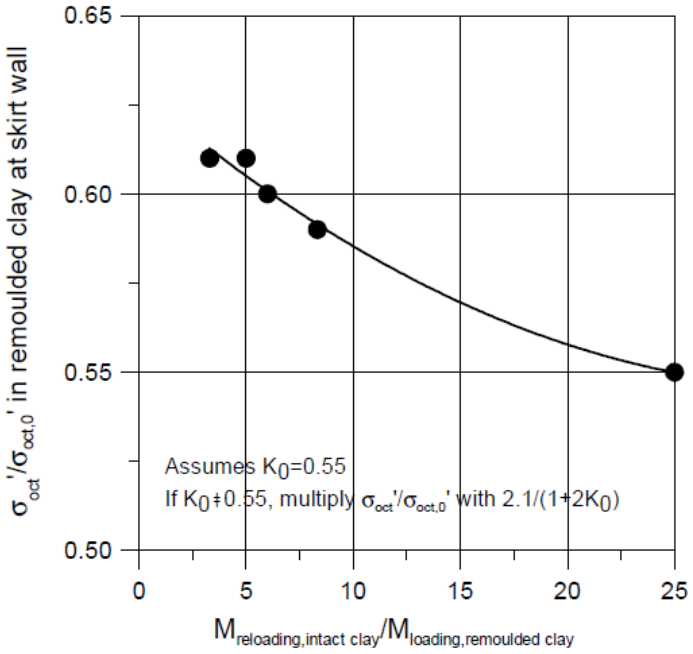

Figure 8.30: Octahedral effective stress after 90 % pore pressure dissipation at skirt wall of suction anchor (Andersen and Jostad, 2002)

Andersen and Jostad (2002) argue that the reduction in σ'_{oct} is linked to the increased compressibility of the clay in the remoulded zone. The effective stress did not return to the original effective stress because of the increased volumetric compressibility of the clay in the

remoulded zone. The difference in compressibility will lead to an arching effect around the remoulded zone when the excess pore pressure dissipates. Similar mechanisms of arching effects are well recognized for pile driving in sand. Chow et al. (1998) explain the circumferential arching mechanism around pile shafts during installation in sand. Augustesen (2006) reproduce this explanation in Figure 8.31. Immediately after driving, a remoulded zone of soil exists near the pile surface (Figure 8.31 a). During pile driving, a large degree of sand compaction at the pile tip can create a zone of loose sand around the pile shaft. The relative density in the remoulded zone is very low and the radial effective stresses acting at the pile shaft are also low. Between the remoulded zone and the intact soil, the relative density of the sand is very large. In this "transition zone", large circumferential stresses are present due to arching (Figure 8.31 b). Karlsrud et al. (1993) suggest that arching effects also occur in low plasticity deposits.

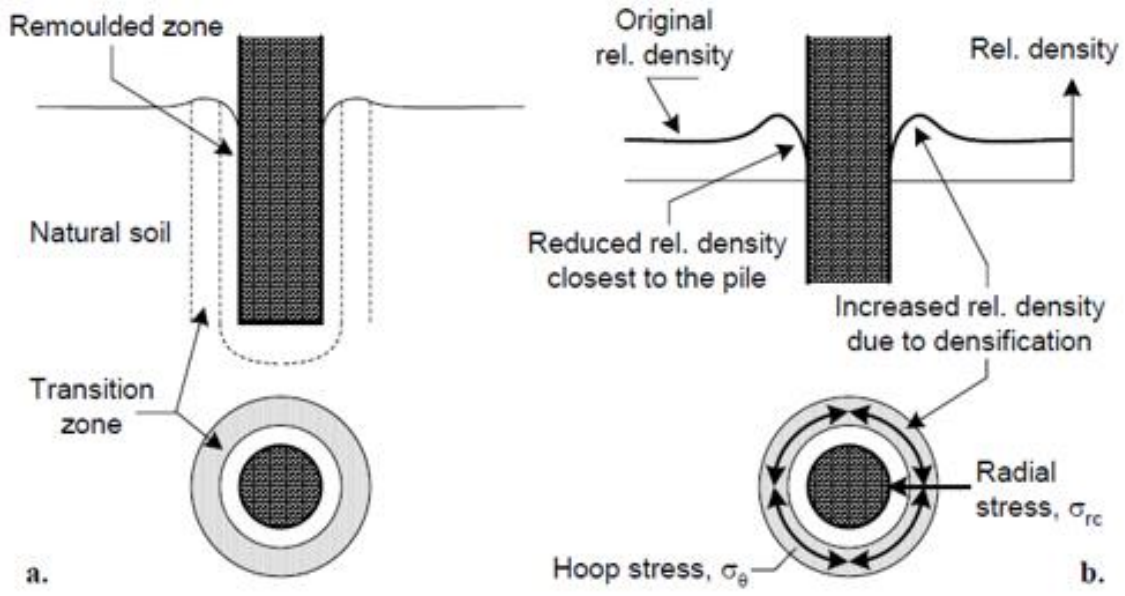

Figure 8.31: a) Zones created during pile driving; b) Relative density in the soil and arching mechanisms around the pile shaft due to pile driving (Augustesen, 2006)

Swelling Index

The unloading and reloading stiffness of clays are non-linear and generally show dependence of loading history. Figure 8.32 show how significantly the tangent unloading modulus may reduce with effective stress. The figure is based on oedometer tests on a clay from Bjørvika in Oslo (typical w = 45 % and I_p = 25 %). The clay sample has been preconsolidated to 100 kPa

(Karlsrud, 2012). It is also illustrated how the tangent reloading modulus depends on the level at which unloading stopped. The reloading modulus is approximately constant up until a stress level about 25 % below the preconsolidation pressure, and then tend to decrease linearly until it meets the modulus line for normally consolidated clay. In addition, the reloading modulus is initially stiffer than the unloading modulus.

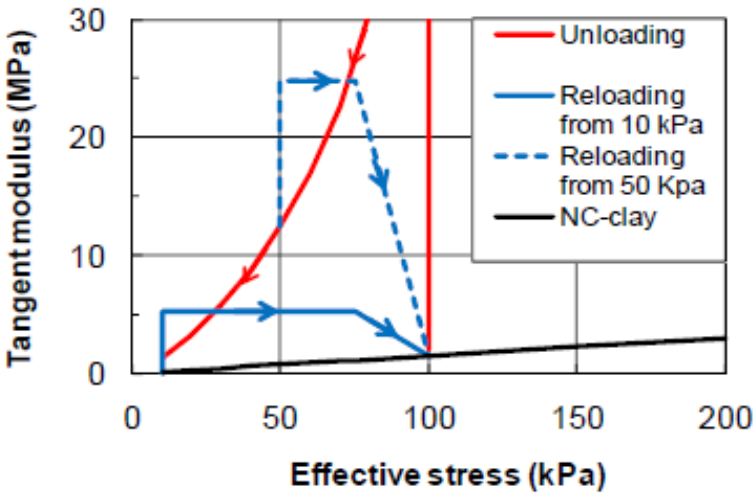

Figure 8.32: Example of tangent unloading and reloading modulus for Bjørvika clay (Karlsrud, 2012)

Compression Index

Modelling of the soil response during the consolidation process after pile installation (reconsolidation) is challenging since the volumetric compressibility of the soil depends on the effective stress level and stress changes that occur during the process. The large shear strains and disturbance in the zone close to the pile wall will also significantly affect the compressibility characteristics. Figure 8.33 compares the results of oedometer tests on intact clay (IC) and remoulded reconsolidated (RR) clay on soil samples from Onsøy. RR clay is the remoulded inner zone near the pile. The original fabric is completely erased in this zone. As a result of the reconsolidation, the clay in this zone has undergone a reduction in water content and a corresponding volume change. The effect of the severe remoulding is an increase in the volumetric strain at in-situ stress level by 8 to 12 %. Similar effect was observed at Haga clay. In addition, the virgin compression index is observed to be lower for RR clay than for IC clay.

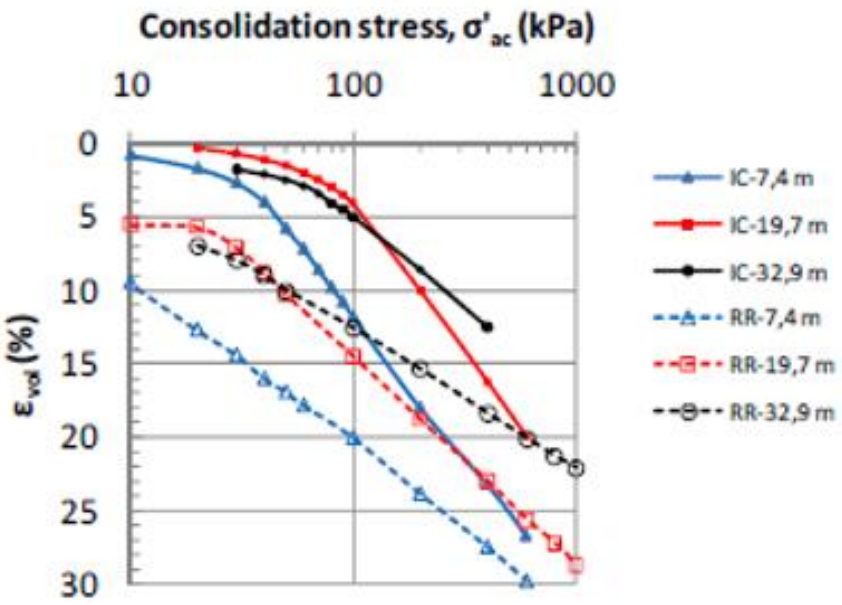

Figure 8.33: Comparison between oedometer tests in intact and remoulded reconsolidated clay from Onsøy (Karlsrud, 2012)

8.5.2 Numerical Analysis with Adjusted Parameters

Increased Swelling Index

Figure 8.32 illustrate how the tangent reloading modulus depends on the level at which unloading stopped. The reloading modulus decrease with increasing overconsolidation ratio. In other words, for reloading, κ increase with increasing OCR. As a sensitivity study, κ is increased by a factor of five for the cases with OCR of 8. A factor of five is arbitrary selected to investigate the sensitivity.

It is in the following assumed that the soils with OCR of 8 has a selling index that is five times the swelling index for the cases with OCR of 1. For case b), the swelling index is increased from 0.0087 to 0.0435. For case d), the swelling index is increased from 0.0297 to 0.1485. Material properties are otherwise kept as in Table 8.1.

The resulting radial effective stress from the numerical analysis with adjusted swelling index, are presented in Figure 8.34 and Figure 8.35. The radial effective stresses are normalized by the undrained shear strength, and is compared to the results from the initial analysis in section 8.3. The grey coloured plots are the results from the original analysis (section 8.3.2). Close to the pile, out to about 3-4 times the pile radii, the radial effective stress increase due to the increased swelling index. The larger κ during the dissipation process leads to larger radial

effective stress acting on the pile shaft. For both cases, the radial effective stress acting on the pile shaft increase with approximately $1 \cdot s_{ud}$.

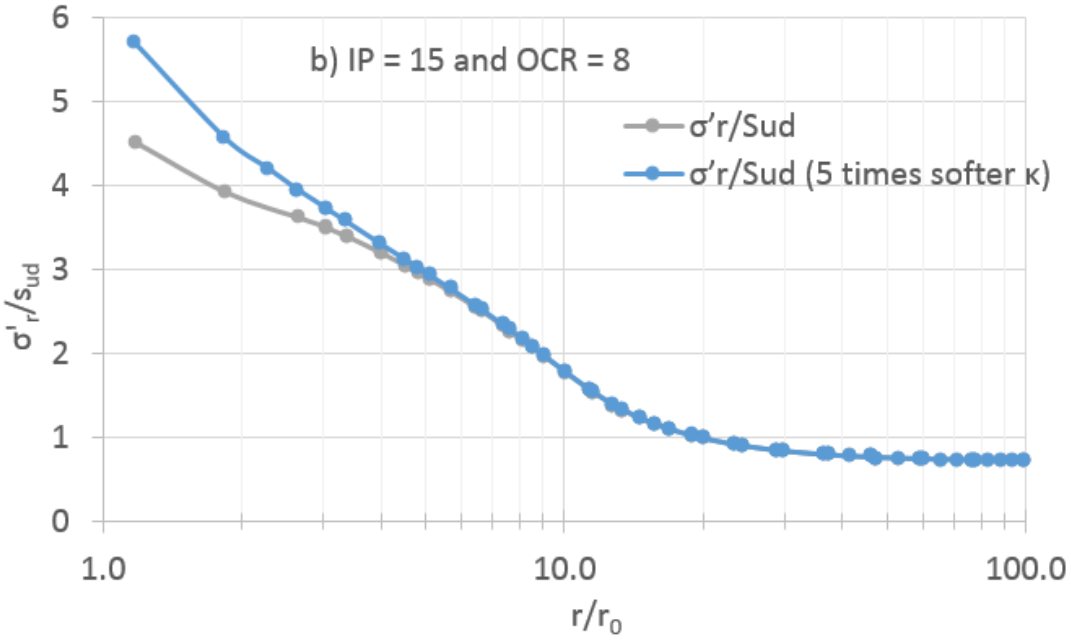

Figure 8.34: Radial effective stress normalized by undrained shear strength, case b)

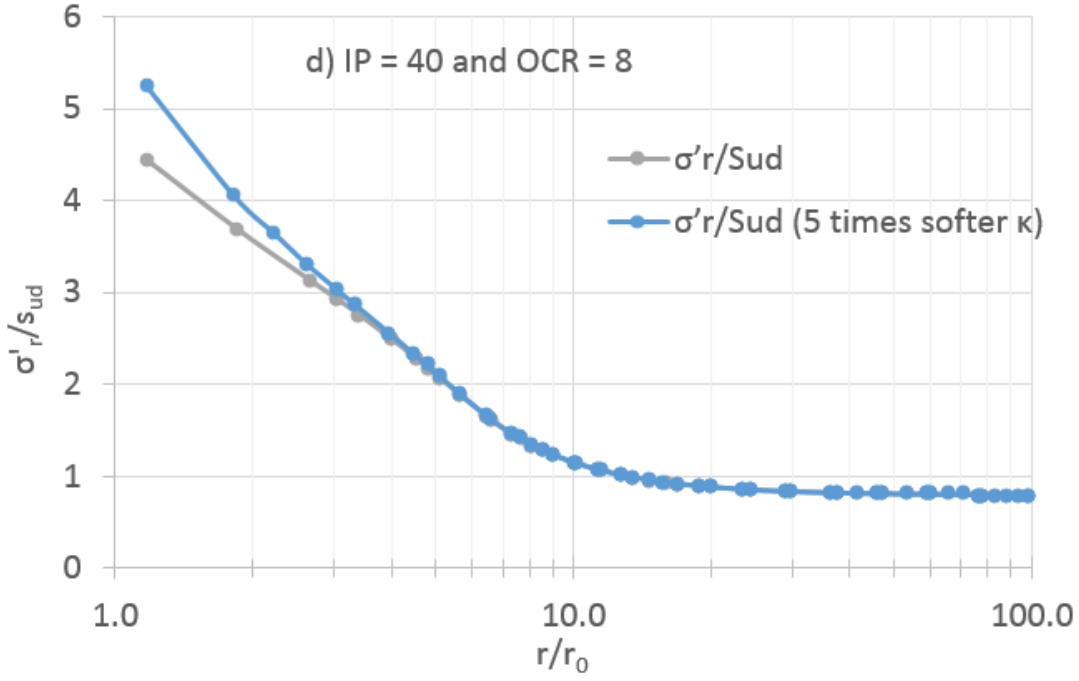

Figure 8.35: Radial effective stress normalized by undrained shear strength, case d)

Decreased Compression Index

As discussed earlier, the soil close to the pile will experience primary loading during the reconsolidation. The zone that undergoes primary loading consists of severely remoulded clay close to the pile, and disturbed clay subjected to more measureable shear strains. Figure 8.33 illustrate that the virgin compression index is observed to be lower for a remoulded reconsolidated sample, compared to an undisturbed sample. For the sake of comparison, a numerical analysis with decreasing λ by a factor of five is carried out. For case a) and b), the compression index is reduced from 0.0875 to 0.0175. For case c) and d), the compression index is reduced from 0.2000 to 0.0400.

Figure 8.36 to Figure 8.39 compare the computed radial effective stresses with the stresses from the initial analysis (section 8.3.2). The predicted circumferential and vertical effective stress changes are given in Appendix C. The following observations are made from the results:

- The results in Figure 8.37 and Figure 8.39 are virtually identical with the results in Figure 8.34 and Figure 8.35, respectively. In other words, increasing κ by a factor of five, produce the same results as decreasing λ by a factor of five.
- A larger increase in the radial effective stress is observed for the cases with OCR of 1, compared to the cases with OCR of 8. The extension of the zone around the pile that has an increase in radial effective stress is also larger for the cases with OCR of 1.
- For case a), the vertical effective stress increase around the pile as a result of the decreased compression index. The circumferential effective stress is unaffected by the adjusted compression index (Appendix C.1).
- For case b), case c) and case d), the circumferential effective stress decrease around the pile as a result of the decreased compression index. The vertical effective stress has a slight increase near the pile surface for case b) and case c). For case d), the vertical effective stress is unaffected by the adjusted compression index (Appendix C.2 – C.4).

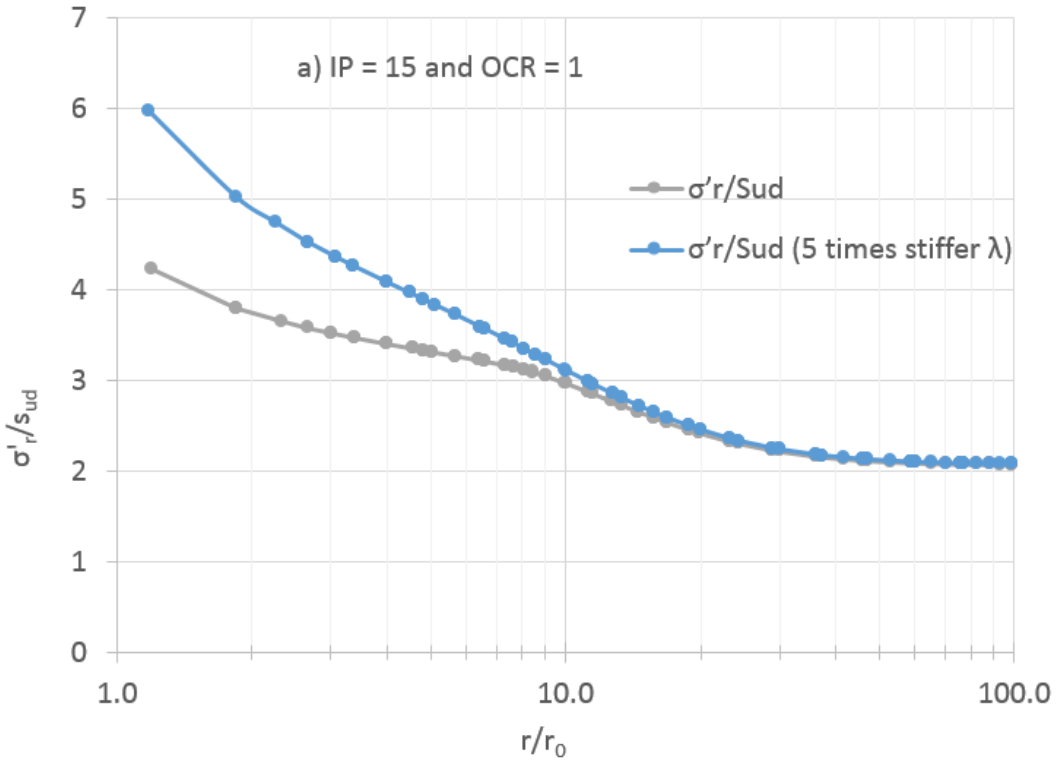

Figure 8.36: Radial effective stress normalized by undrained shear strength, case a)

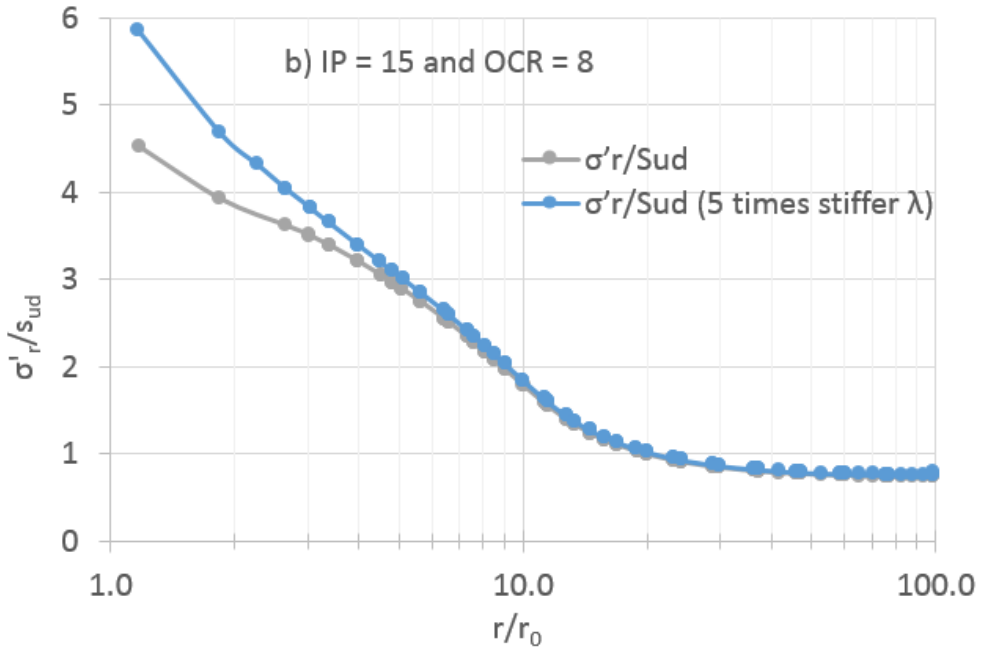

Figure 8.37: Radial effective stress normalized by undrained shear strength, case b)

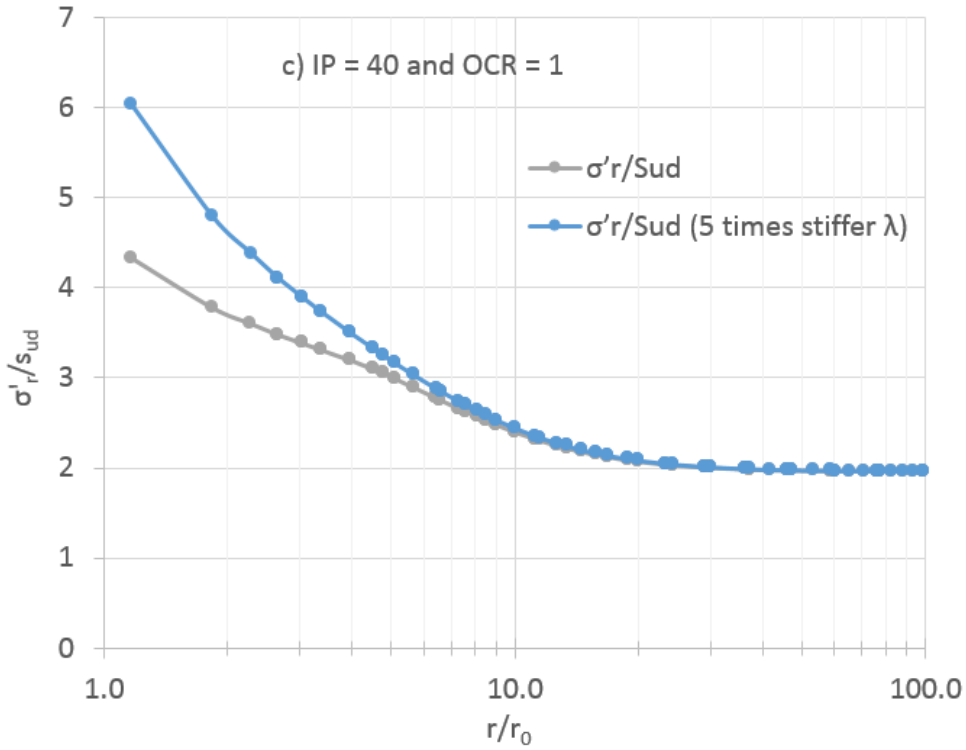

Figure 8.38: Radial effective stress normalized by undrained shear strength, case c)

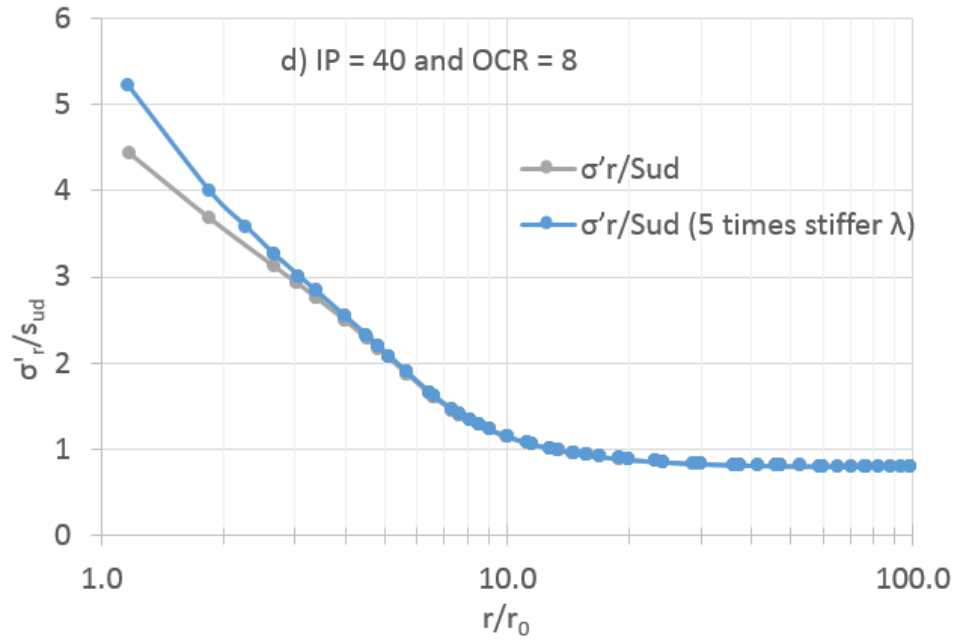

Figure 8.39: Radial effective stress normalized by undrained shear strength, case d)

9 Summary of Results and Discussion

The installation and reconsolidation phases have been analysed by fully coupled finite element analysis in Plaxis 2D. The results here are close to the results from the uncoupled CEM-MCC predictions by Randolph et al. (1979). Predictions the final effective stress at the pile shaft, normalized by s_{ud}, are slightly lower than what is predicted by Randolph et al. (1979). Clearly, the results presented in this study are not directly comparable with the results from Randolph et al. (1979) as different soil parameters are used. Still, some of the difference is believed to be due to differences in modelling. In the numerical analysis carried out in this study, vertical strains are allowed as the model realistically include the ground surface. The analysis by Randolph et al. (1979) is in perfect plane strain conditions.

Representative soil parameters for the different degrees of plasticity are determined in section 7.2. The flexibility parameters are found to generally increase with I_p. In addition, the permeability generally decrease with increasing I_p. No clear correlations between soil strength and I_p has been found in literature. A similar strength, *M*, is assumed for the four cases studied. If a larger *M* is used, the final radial effective stress ratio, K_c, is expected to increase.

Table 9.1 summarize the most important results from the case study. The extension of the plastic zone is linked to the size of the shear modulus, *G*, which in turn is linked to the bulk modulus, *K*, in the MCC model. From equation (3.7) and (3.8), *G* increase with increasing OCR, and decrease with increasing I_p. Thus, the plasticized radius increase with increasing OCR, and decrease with increasing I_p. Further, the computed excess pore pressure is linked to the size of the plastic zone. Greater excess pore pressure is generated with increasing size of the plasticized radius, as defined in equation (4.27). During shearing, the mean effective stress changes for the MCC model. For clays with OCR values larger than 2, negative excess pore pressure is developed as the clays tend to dilate on shearing. A decrease in the excess pore pressure, normalized by s_{ud}, is therefore observed for increasing values of OCR.

As the extent of the generated excess pore pressure is shorter for the cases with OCR of 8, shorter consolidation times are predicted for these cases. Further, the consolidation time is shorter for the cases with I_p = 15 % than the cases with I_p = 40 %, given similar OCR. This is due to the relatively higher permeability assumed for the cases with I_p = 15 %. The times for 90 % dissipation of excess pore pressure (t_{90}) compares well with trends from field observations. Pile set-up tend to occur rapidly for stiff overconsolidated clays, and slower for normally consolidated soft clays.

In general, the numerical model seem to overpredict the radial effective stress observed at the pile wall. The relatively large measured reduction in total radial stress during pore pressure dissipation partially explain why the effective stress end up much lower than what is predicted in the numerical analysis. The total stress also reduce during the reconsolidation phase in Plaxis, but not to the same extent. In addition, soil sensitivity has not been accounted for in the numerical analysis. Normal or lightly overconsolidated clay tend to have higher sensitivity than heavily overconsolidated clay (Randolph et al., 1979). Destructuration of soil structure will lead to lower radial effective stress acting on the pile surface. Low plasticity clays with high silt content are likely to demonstrate shorter consolidation times than higher plasticity clays. Rapid initial pore pressure dissipation during pile installation, will cause greater damage to the soil and less "set-up" following installation (Randolph, 2003). This may contribute to the low radial effective stress and shaft friction reported in low plasticity clays.

Table 9.1: Summary of results

Case	a) I_p = 15 % and OCR = 1	b) I_p = 15 % and OCR = 8	c) I_p = 40 % and OCR = 1	d) I_p = 40 % and OCR = 8
Installation				
Plasticized radius, r_p	$7 \cdot r_0$	$5 \cdot r_0$	$4 \cdot r_0$	$3 \cdot r_0$
$K_i = \sigma'_{ri}/\sigma'_{v0}$	0.8	5.3	0.8	5.1
$\Delta u_i/s_{ud}$	6.5	4.5	5	4
Extent of excess pore pressure field	$30 \cdot r_0$	$10 \cdot r_0$	$20 \cdot r_0$	$7 \cdot r_0$
Reconsolidation				
t_{90}	35 days	1 day	90 days	10 days
Extent of inner zone experiencing primary loading	$7 \cdot r_0$	$3 \cdot r_0$	$4 \cdot r_0$	$2 \cdot r_0$
$K_c = \sigma'_{ri}/\sigma'_{v0}$	1.5	9.0	1.5	9.0

In this study, the focus is on changes in effective stresses due to pile installation and subsequent dissipation of excess pore pressures. However, after the end of reconsolidation, pile capacity may still increase due to thixotropy and/or creep effects. According to Karlsrud (2012), this may be most relevant for clays with low plasticity and low OCR, where very low radial effective stresses are observed at the end of the reconsolidation phase. In contrast, Figure 2.2 suggests that the thixotropy strength ratio increase with I_p. In addition, Figure 2.3 by Nakase et al. (1988) suggests that the coefficient of secondary compression increase with increasing I_p. This might indicate that these processes occurs differently in the clay surrounding a pile, than in the laboratory work leading to Figure 2.2 and Figure 2.3.

Figure 9.1 shows the radial effective stress near the pile shaft as a function of the λ/κ ratio, for all the cases studied. In order to compare the results, the stresses in the figure are taken at r/r_0 = 1.15. This is done to avoid approximate results from extrapolating to the pile shaft (r/r_0 = 1.0). Clearly, the radial effective stress near the pile is dependent on the ratio between the compression index and the swelling index. The radial effective stress decrease with increasing λ/κ ratio. For the low λ/κ ratios, the radial effective stress is largest for the cases with OCR = 1. However, for larger λ/κ ratios, the radial effective stress is largest for the cases with OCR = 8. Based on these results, the radial effective stress near the pile is somewhat more sensitive to the λ/κ ratio for the cases with OCR of 1.

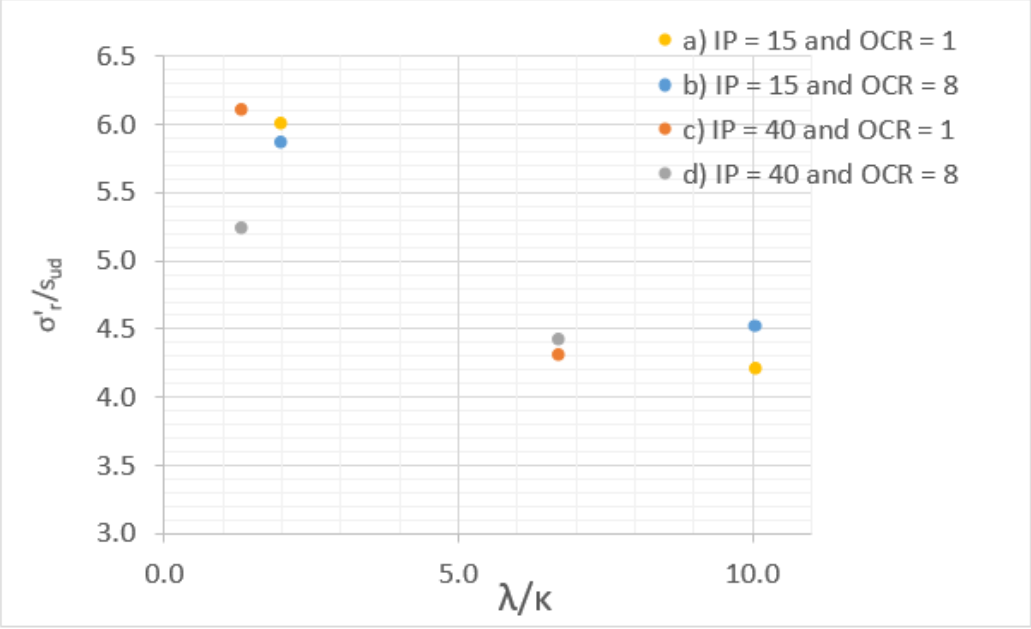

Figure 9.1: Radial effective stress at r/r_0=1.15 as a function of the λ /κ ratio

Chow et al. (1998) explain that the arching mechanism around piles installed in sand, comes from sand compaction at the pile tip which creates a zone of loose sand around the pile shaft. The arching effect observed in the numerical analysis has different causes. The numerical model only consider the effect of cavity expansion. Shearing and disturbance of the soil from penetration of the tip of the pile is not included.

Karlsrud et al. (1993) suggest that ”cylindrical arching” and “silo” effects occur in low plasticity deposits. The cylindrical arching effect comes from large circumferential stresses sustained by arching. The vertical silo effect involves relief of vertical effective stresses due to friction on silo walls. A large ratio between the compression index in the inner zone and the swelling index in the surrounding clay, may enable arching and silo effects during the reconsolidation phase. For case a), a vertical silo effect appears valid from the parametric study (section 8.5.2). The radial and vertical effective stress at the pile shaft decrease, as the λ/κ ratio increase. For case b), case c) and case d), a circumferential arching effect seem to be governing. A reduction in the arching effect allow the radial effective stress to increase close to the pile, as the λ/κ ratio decrease. If this gives a correct picture of soil behaviour, differences in unloading/reloading stiffness might explain some of the increase in shaft friction with increasing OCR.

Perhaps the low stresses observed in low plasticity clays partly can be due to a large λ/κ ratio? An unsuccessful attempt has been made to find data on the virgin compression index from reconstituted remoulded clay samples, compared to the swelling index from undisturbed samples. The found correlations with I_p are based either solely on remoulded samples, or solely on intact samples. In section 10.2, the author recommends that future work on this subject could be to investigate the correlation between soil disturbance, compressibility and I_p.

10 Conclusions and Recommendations for Further Work

10.1 Conclusion

The two most widely applied methods for modelling of the stress and strain changes due to pile installation are the Cavity Expansion Method (CEM) and the Strain Path Method (SPM). A literature survey on these theories are carried out, with particular focus on the CEM coupled with the EP and MCC soil models.

In this study, the CEM is coupled with the MCC model to study pile installation in a FEM program. Plaxis 2D is used to calculate the stress distribution around the pile, the initial pore pressure field, the dissipation of the excess pore pressures with time, and the corresponding effective stress changes for four different cases. Table 9.1 summarize the most important results from the case study. Material properties for the different cases are provided in Table 8.1.

During pile driving, a plastic zone is developed around the pile where the mobilized shear stress exceeds the undrained shear strength of the soil. The plasticized radius decrease with increasing I_p and OCR.

The excess pore pressure, normalized by s_{ud}, is lowest for the overconsolidated high plasticity case, and highest for the normally consolidated case with low plasticity. A trend of decreasing $\Delta u_i/s_{ud}$ with increasing OCR is also observed in field measurements (Karlsrud, 2012). The excess pore pressure at the pile shaft is somewhat underpredicted for the cases with OCR of 1, and overpredicted for the cases with OCR of 8. In contrast to the numerical predictions, the data from Karlsrud (2012) suggest a tendency of increasing $\Delta u_i/s_{ud}$ with increasing I_p. The generated excess pore pressure curves present a linear decrease with the logarithm of the radius from the pile axis. The shortest consolidation time is predicted for the overconsolidated low-plastic case, and the longest consolidation time is predicted for the normally consolidated case with high plasticity.

The impact of OCR and I_p on the ultimate shaft friction is mainly coming through its impact on the radial effective stress. The CEM-MCC model largely overpredicts the measured radial effective stress. There is no distinction in the magnitude of the predicted radial effective stress for different I_p. However, greater stress is predicted for the cases with OCR of 8.

At the pile shaft, the generated stress normalized by s_{ud} is quite similar for the four cases studied. After pile installation, $\sigma'_r/s_{ud} = 2.5$, $\sigma'_v/s_{ud} = 1.5$ and $\sigma'_\theta/s_{ud} = 0.5$. After dissipation of excess pore

pressure, $\sigma'_r/s_{ud} = 4.5$, and $\sigma'_v \approx \sigma'_\theta \approx 2.75 \cdot s_{ud}$. Based on the numerical analysis, pile driving has significantly altered the stresses in the soil out to about $30 \cdot r_0$.

During the reconsolidation process, soil particles will move inwards towards the pile and most of the soil will be unloading in shear. However, in the inner zone close to the pile, the soil undergoes further increase in shear strain as the pile prevents inward movement of the soil. The extension of this inner zone decrease with increasing I_p and OCR.

A sensitivity analysis on the flexibility parameters, λ and κ, is carried out. An increased κ during the dissipation process leads to larger radial effective stress acting on the pile shaft. The radial effective stress at the pile shaft increase if λ is decreased for the reconsolidation phase. Figure 9.1 shows the radial effective stress near the pile shaft as a function of the λ/κ ratio. A large ratio between the compression index in the inner zone and the swelling index in the surrounding clay, causes lower radial effective stress at the pile.

10.2 Recommendations for Further Work

Laboratory tests on clays subjected to various degrees of shear straining could be carried out to investigate the correlation between soil disturbance and compressibility. Low to high plasticity clays should be included in the testing program. The compressibility of the severely strained clay close to the pile, which experience primary loading, can then be compared to the compressibility of the clay further out which experience unloading/reloading.

The Strain Path Method could be used to perform a similar investigation as conducted in this study. The Modified Cam-Clay model could be used for comparison reasons. Numerical analysis with constitutive models that include aspects such as destructuration and creep might also be interesting.

References

ANDERSEN, K. H. & JOSTAD, H. P. Shear strength along outside wall of suction anchors in clay after installation. Proceedings of the Twelfth International Offshore and Polar Engineering Conference. Kitakyushu, Japan, 2002.

ANDRESEN, A., BERRE, T., KLEVEN, A. & LUNNE, T. 1979. Procedures used to obtain soil parameters for foundation engineering in the North Sea. *Marine Georesources & Geotechnology,* 3**,** 201-266.

AUGUSTESEN, A. H. 2006. *The effects of time on soil behaviour and pile capacity.* Aalborg University, Department of Civil Engineering.

AZZOUZ, A. S., KRIZEK, R. J. & COROTIS, R. B. 1976. Regression analysis of soil compressibility. *土質工学会論文報告集,* 16**,** 19-29.

BALIGH, M. M. 1975. Theory of deep site static cone penetration resistance. *Massachusetts Inst. of Tech. Report,* 1.

BALIGH, M. M. 1985. Strain path method. *Journal of Geotechnical Engineering,* 111**,** 1108-1136.

BJERRUM, L. & JOHANNESSEN, I. 1961. *Pore pressures resulting from driving piles in soft clay,* Norwegian Geotechnical Institute.

BRINKGREVE, R., KUMARSWAMY, S. & SWOLFS, W. 2014. PLAXIS 2D Manual. *Delft University of Technology and PLAXIS bv The Netherlands*.

BROOKER, E. W. & IRELAND, H. O. 1965. Earth pressures at rest related to stress history. *Canadian geotechnical journal,* 2**,** 1-15.

BUDHU, M. 2008. *Foundations and Earth Retaining Structures*.

CARTER, J. P., RANDOLPH, M. & WROTH, C. 1979. Stress and pore pressure changes in clay during and after the expansion of a cylindrical cavity. *International Journal for Numerical and Analytical Methods in Geomechanics,* 3**,** 305-322.

CARTER, J. P., RANDOLPH, M. F. & WROTH, P. 1978. *Some Aspects of the Performance of Open and Closed-Ended Piles,* University of Cambridge, Department of Engineering.

CASTRO, J. & KARSTUNEN, M. 2010. Numerical simulations of stone column installation. *Canadian Geotechnical Journal,* 47**,** 1127-1138.

CHOW, F., JARDINE, R., BRUCY, F. & NAUROY, J. 1998. Effects of time on capacity of pipe piles in dense marine sand. *Journal of Geotechnical and Geoenvironmental Engineering,* 124**,** 254-264.

GIBSON, R. & ANDERSON, W. 1961. In situ measurement of soil properties with the pressuremeter. *Civil engineering and public works review,* 56**,** 615-618.

HILL, R. 1950. The mathematical theory of plasticity.

HOUGH, B. K. 1957. Basic soils engineering.

ISO/TS, C. TS 17892-12: 2004. *Geotechnical investigation and testing—laboratory testing of soil—part,* 12**,** 17892-12.

KARLSRUD, K. 2012. *Prediction of load-displacement behavior and capacity of axially-loaded piles in clay based on analyses and interpretation of pile load test results.* PhD Dissertation, Norwegian University of Science and Technology, Trondheim.

KARLSRUD, K. & HERNANDEZ-MARTINEZ, F. G. 2013. Strength and deformation properties of Norwegian clays from laboratory tests on high-quality block samples 1. *Canadian Geotechnical Journal,* 50**,** 1273-1293.

KARLSRUD, K., KALSNES, B. & NOWACKI, F. 1993. Response of piles in soft clay and silt deposits to static and cyclic axial loading based on recent instrumented pile load tests. *Offshore Site Investigation and Foundation Behaviour.* Springer.

KARLSRUD, K. & NADIM, F. Axial capacity of offshore piles in clay. Offshore Technology Conference, 1990. Offshore Technology Conference.

KARSTUNEN, M., KRENN, H., WHEELER, S. J., KOSKINEN, M. & ZENTAR, R. 2005. Effect of anisotropy and destructuration on the behavior of Murro test embankment. *International Journal of Geomechanics,* 5**,** 87-97.

KOIZUMI, Y. & ITO, K. 1967. Field tests with regard to pile driving and bearing capacity of piled foundations. *Soils and Foundations,* 7**,** 30-53.

LADANYI, B. 1963. Expansion of a cavity in a saturated clay medium. *J. Soil Mech. and Found. Div., ASCE,* 89**,** 127-161.

LADD, C. C. & FOOTT, R. 1974. New design procedure for stability of soft clays. *Journal of the Geotechnical Engineering Division,* 100**,** 763-786.

LEROUEIL, S., KABBAJ, M., TAVENAS, F. & BOUCHARD, R. 1985. Stress–strain–strain rate relation for the compressibility of sensitive natural clays. *Géotechnique,* 35**,** 159-180.

LEROUEIL, S. & VAUGHAN, P. 1990. The general and congruent effects of structure in natural soils and weak rocks. *Géotechnique,* 40**,** 467-488.

LO, K. & STERMAC, A. Induced pore pressures during pile-driving operations. Soil Mech & Fdn Eng Conf Proc/Canada/, 1965.

LUNNE, T., ROBERTSON, P. & POWELL, J. 1997. Cone penetration testing. *Geotechnical Practice*.

MAYNE, P. 1980. CAM-CLAYS PREDICTIONS OF UNDRAINED STRENGTH. *Journal of Geotechnical and Geoenvironmental Engineering*, 106.

MESRI, G. 1973. CEOFFICIENT OF SECONDARY COMPRESSION *Journal of Soil Mechanics & Foundations Div*, 99.

MITCHELL, J. K. 1961. Fundamental aspects of thixotropy in soils. *Transactions of the American Society of Civil Engineers,* 126**,** 1586-1620.

NAKASE, A., KAMEI, T. & KUSAKABE, O. 1988. Constitutive parameters estimated by plasticity index. *Journal of Geotechnical Engineering,* 114**,** 844-858.

NISHIDA, Y. 1956. A brief note on compression index of soil. *Journal of Soil Mechanics and Foundation Engineering, ASCE,* 82**,** 1-14.

RANDOLPH, M. 2003. Science and empiricism in pile foundation design. *Geotechnique,* 53**,** 847-875.

RANDOLPH, M. F., CARTER, J. & WROTH, C. 1979. Driven piles in clay—the effects of installation and subsequent consolidation. *Geotechnique,* 29**,** 361-393.

RANDOLPH, M. F. & WROTH, C. 1979. An analytical solution for the consolidation around a driven pile. *International Journal for Numerical and Analytical Methods in Geomechanics,* 3**,** 217-229.

ROSCOE, K. H. & BURLAND, J. 1968. On the generalized stress-strain behaviour of wet clay.

ROSCOE, K. H., SCHOFIELD, A. & WROTH, C. 1958. On the yielding of soils. *Geotechnique,* 8**,** 22-53.

ROY, M., MICHAUD, D., TAVENAS, F., LEROUEIL, S. & LA ROCHELLE, P. The interpretation of static cone penetration tests in sensitive clays. Proc. Eur. Symp. Penetration Testing, Stockholm 2.1, 323, 1975.

SCHOFIELD, A. & WROTH, P. 1968. Critical state soil mechanics.

SKEMPTON, A. & NORTHEY, R. 1952. The sensitivity of clays. *Geotechnique,* 3**,** 30-53.

SKEMPTON, A. W. 1944. Notes on the compressibility of clays. *Quarterly Journal of the Geological Society,* 100**,** 119-135.

SODERBERG, L. O. 1962. Consolidation theory applied to foundation pile time effects. *Geotechnique,* 12**,** 217-225.

TAVENAS, F., JEAN, P., LEBLOND, P. & LEROUEIL, S. 1983. The permeability of natural soft clays. Part II: Permeability characteristics. *Canadian Geotechnical Journal,* 20**,** 645-660.

TERZAGHI, K. 1943. *Theoretical soil mechanics*, Wiley New York.

TERZAGHI, K. & PECK, R. 1967. Soil mechanics in engineering practice. John Wiley & Sons, Inc., New York.

VEGDIREKTORATET 2014. Håndbok V220 Geoteknikk i vegbygging. *In:* VEGVESEN, S. (ed.) *Veiledning.* http://www.vegvesen.no/Fag/Publikasjoner/Handboker.

WHEELER, S. J., NÄÄTÄNEN, A., KARSTUNEN, M. & LOJANDER, M. 2003. An anisotropic elastoplastic model for soft clays. *Canadian Geotechnical Journal,* 40**,** 403-418.

WHITTLE, A. J. 1987. *A constitutive model for overconsolidated clays with application to the cyclic loading of friction piles.* Massachusetts Institute of Technology.

WHITTLE, A. J. 1993. *Assessment of an effective stress analysis for predicting the performance of driven piles in clays*, Springer.

WHITTLE, A. J. & SUTABUTR, T. 1999. Prediction of pile setup in clay. *Transportation Research Record: Journal of the Transportation Research Board,* 1663**,** 33-40.

WROTH, C. In situ measurement of initial stresses and deformation characteristics: Proc Conference on In-situ Measurements of Soil Properties, Raleigh, NC, 1–4 June 1975, V2, P181–230, disc P231–277. International Journal of Rock Mechanics and Mining Sciences & Geomechanics Abstracts, 1978. Pergamon, 67.

List of Symbols and Abbreviations

ENGLISH

c_v = Vertical coefficient of consolidation

c_h = Horizontal coefficient of consolidation

C_c = Compression index

c_k = Change in permeability due to compression of the soil

e = Void ratio

e_0 = Initial void ratio

E = Young's modulus

E_{50} = Secant modulus at 50% of maximum stress

G = Shear modulus

G_{50} = The secant shear modulus at 50 % mobilization of shear strength

I_p = Plasticity index

k = Coefficient of permeability, hydraulic conductivity

k_0 = Coeficient of peremeability at zero volume change

k_h = Horizontal permeability

k_v = Vertical permeability

K_0 = Coefficient of earth pressure at rest = $\sigma`_{h0}/ \sigma`_{v0}$

K_c = Horizontal (radial) effective stress ratio after full reconsolidation

K_i = Horizontal (radial) effective stress ratio at end of pile installation

m = Power in SHANSEP equation

m = Dimensionless deformation modulus number

M = Oedometer modulus

r = Radial distance from center of pile

r_i = Inner pile radius

r_o = Outer pile radius

r_p = Radius of plastic zone

s_u = Undrained shear strength

s_{ur} = Remoulded undrained shear strength

s_{uc} = Undrained shear strength from triaxial compression test

s_{ue} = Undrained shear strength from triaxial extension test

s_{ud} = Undrained shear strength from direct simple shear test

S = Normalized undrained strength for OCR=1 (SHANSEP)

S_t = Sensitivity

T = Time factor

T* = Modified time factor

t = Time

u = Pore water pressure

u_o = *In situ* pore pressure

Δu = Excess pore pressure

U = Normalized excess pore pressure (degree of dissipation)

w = Water content

w_L = Liquid limit

w_p = Plastic limit

GREEK

α = Ultimate shaft friction normalized to undrained strength

β = Ultimate shaft friction normalized to vertical effective stress

γ = Shear strain

γ' = Effective unit weight

γ_w = Unit weight of water

φ' = Effective friction angle

ε = Strain

ε_v = Volumetric strain

σ'_a = Axial effective stress in a DSS-test

σ'_c = Effective consolidation stress in a DSS-test

σ_r, σ'_r = Radial stress (total, effective)

σ_θ, σ'_θ = Circumferential stress (total, effective)

σ_v, σ'_v = Vertical stress (total, effective)

σ_1, σ'_1 = Major principal stress (total, effective)

σ_2, σ'_2 = Intermediate principal stress (total, effective)

σ_3 , σ'_3 = Minor principal stress (total, effective)

τ = Shear stress

τ_0 = Initial shear stress a sample is consolidated under

τ_s = Shear stress on pile surface (shaft friction)

τ_{us} = Ultimate shaft friction on pile surface at failure

ABBREVIATIONS

ASCE = American Society of Civil Engineers

CAUC = Anisotropic Consolidated Undrained Triaxial Test Sheared in Compression

CAUE = Anisotropic Consolidated Undrained Triaxial Test Sheared in Extension

CEM = Cavity Expansion Method

CSSM = Critical State Soil Mechanics

DSS = Direct Simple Shear

EP = Linear Elastic, perfectly Plastic soil model

GWT = Ground Water Table

IC = Imperial College

MCC = Modified Cambridge Clay model

MIT = Massachusetts Institute of Technology

MITE1-3 = Effective stress based clay models developed at MIT

NC = Normally Consolidated

NGI = Norwegian Geotechnical Institute

OCR = Overconsolidation ratio

SPM = Strain Path Method

UU = Undrained, unconsolidated triaxial test

Appendices

Appendix A – DSS Soil Test in Plaxis 2D

A.1 s_{ud} for case a)

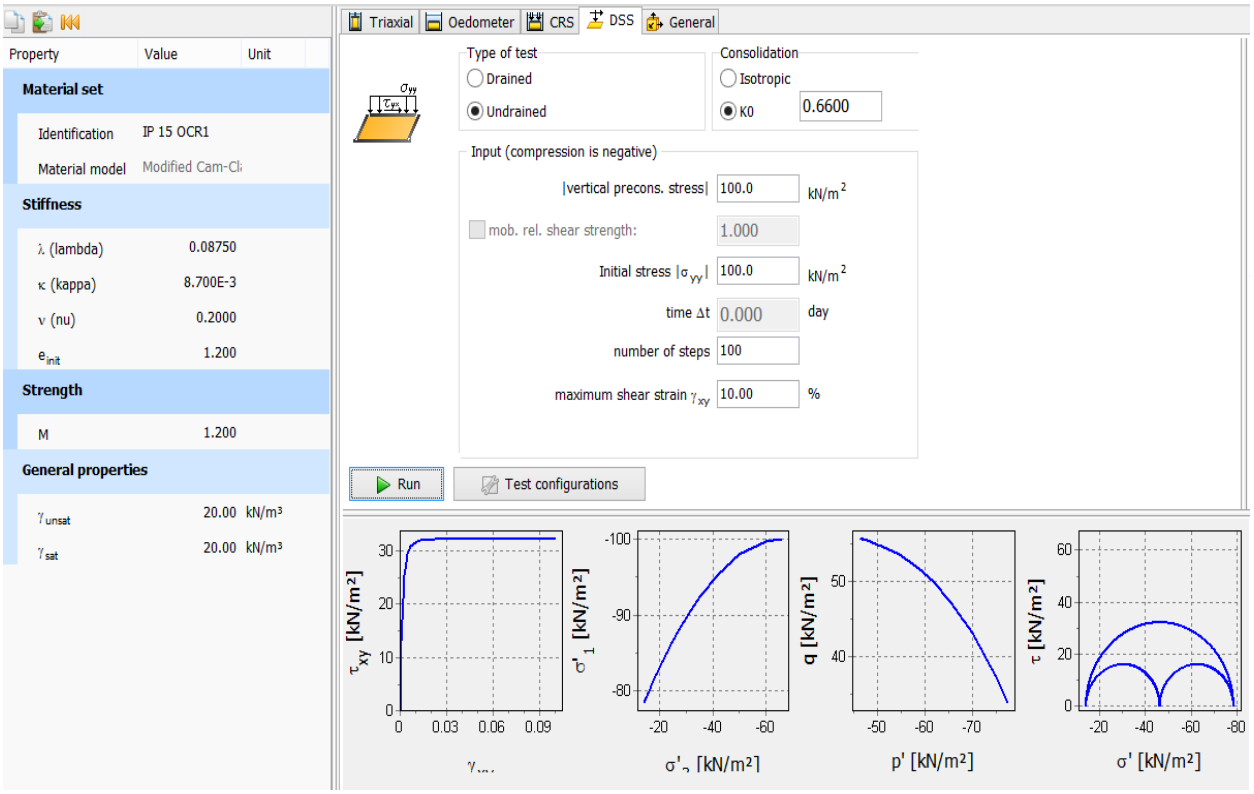

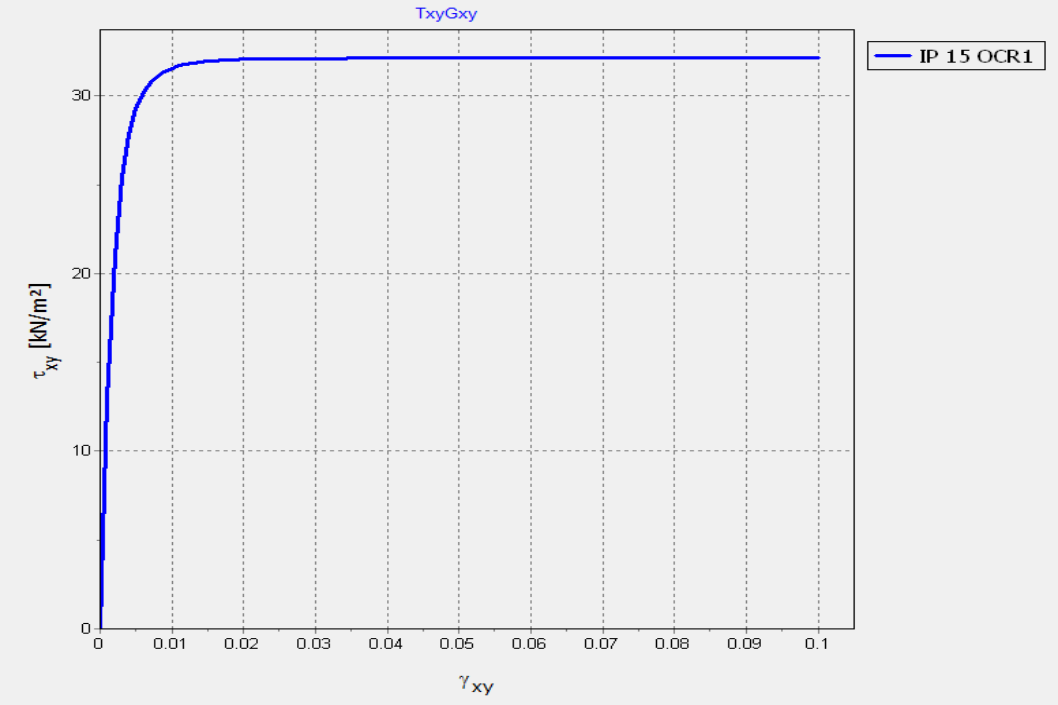

Figure A.1: Direct Simple Shear Test for case a)

Case a): s_{ud} = 32 kPa

A.2 s_{ud} for case b)

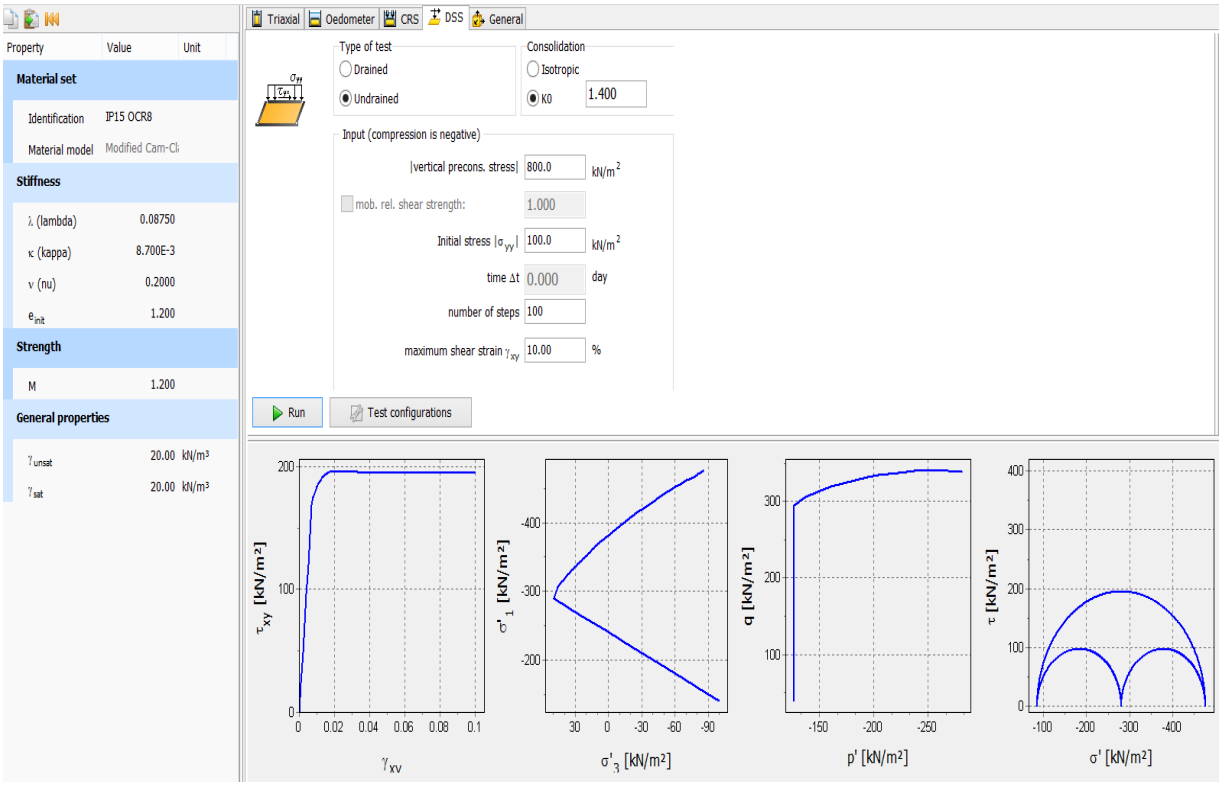

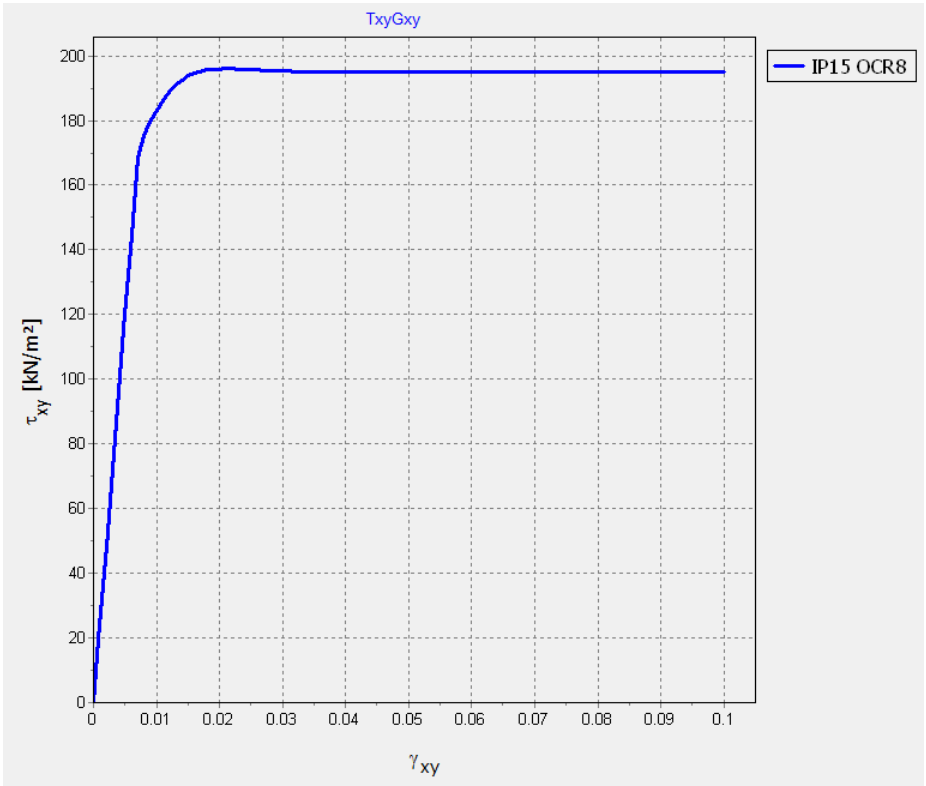

Figure A.2: Direct Simple Shear Test for case b)

Case b): s_{ud} = 195 kPa

A.3 s_{ud} for case c)

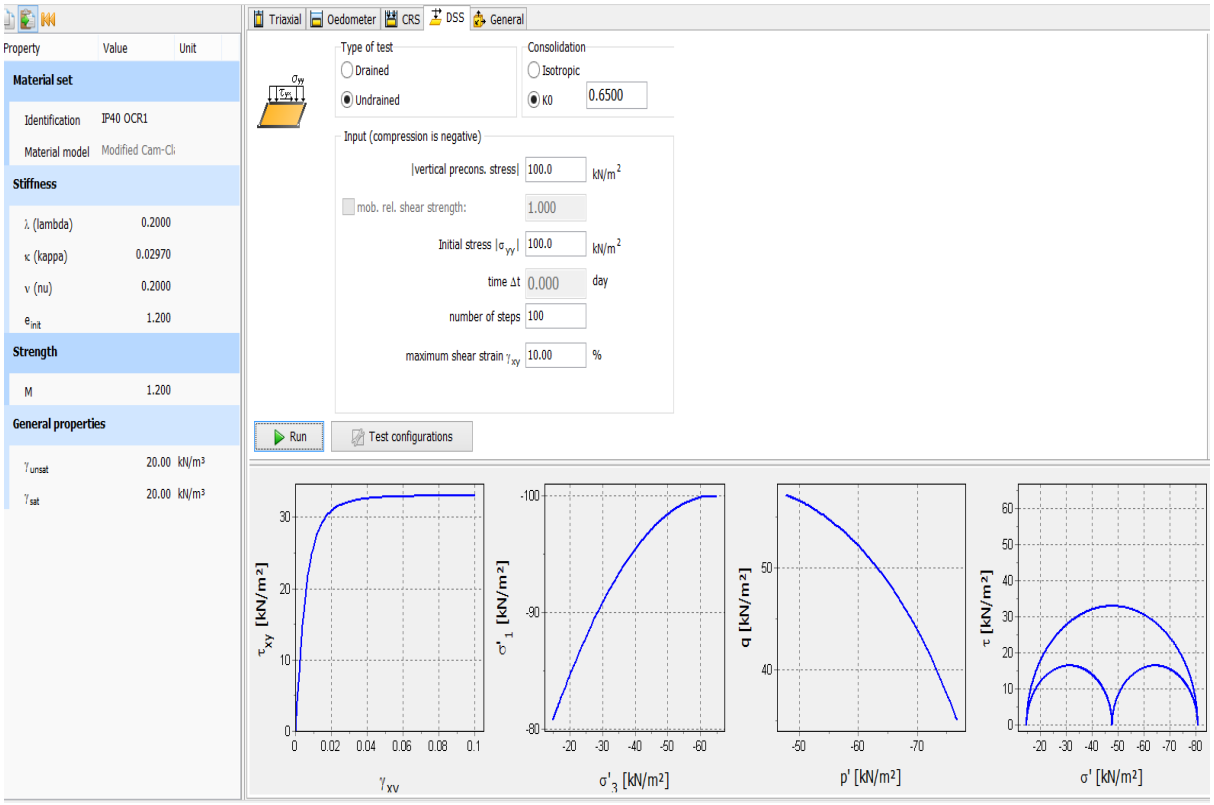

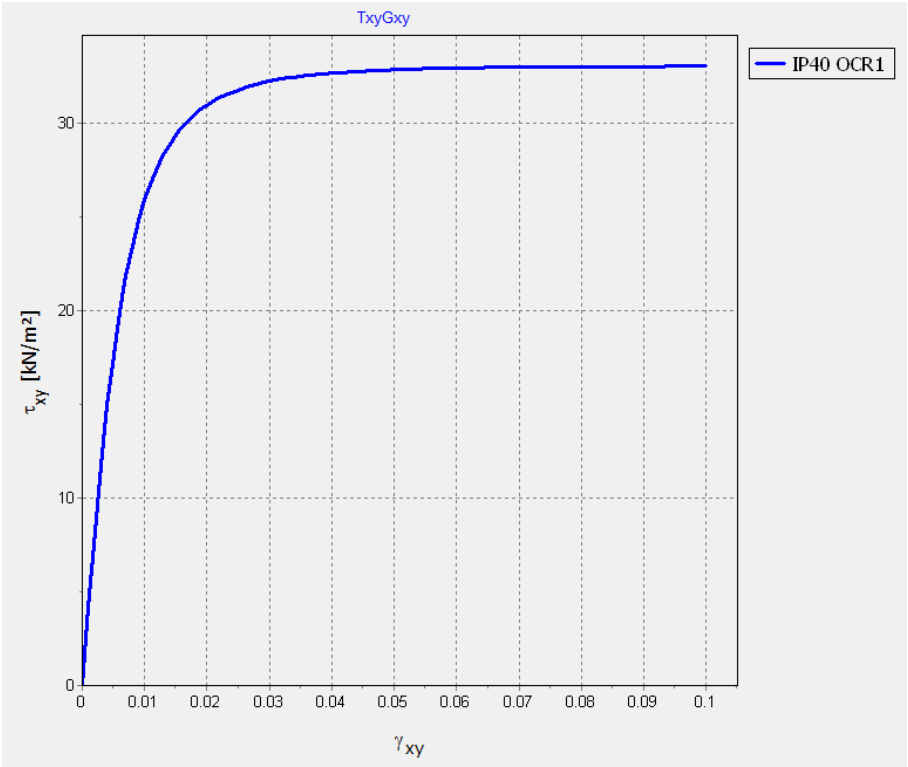

Figure A.3: Direct Simple Shear Test for case c)

Case c): s_{ud} = 33 kPa

A.4 s_{ud} for case d)

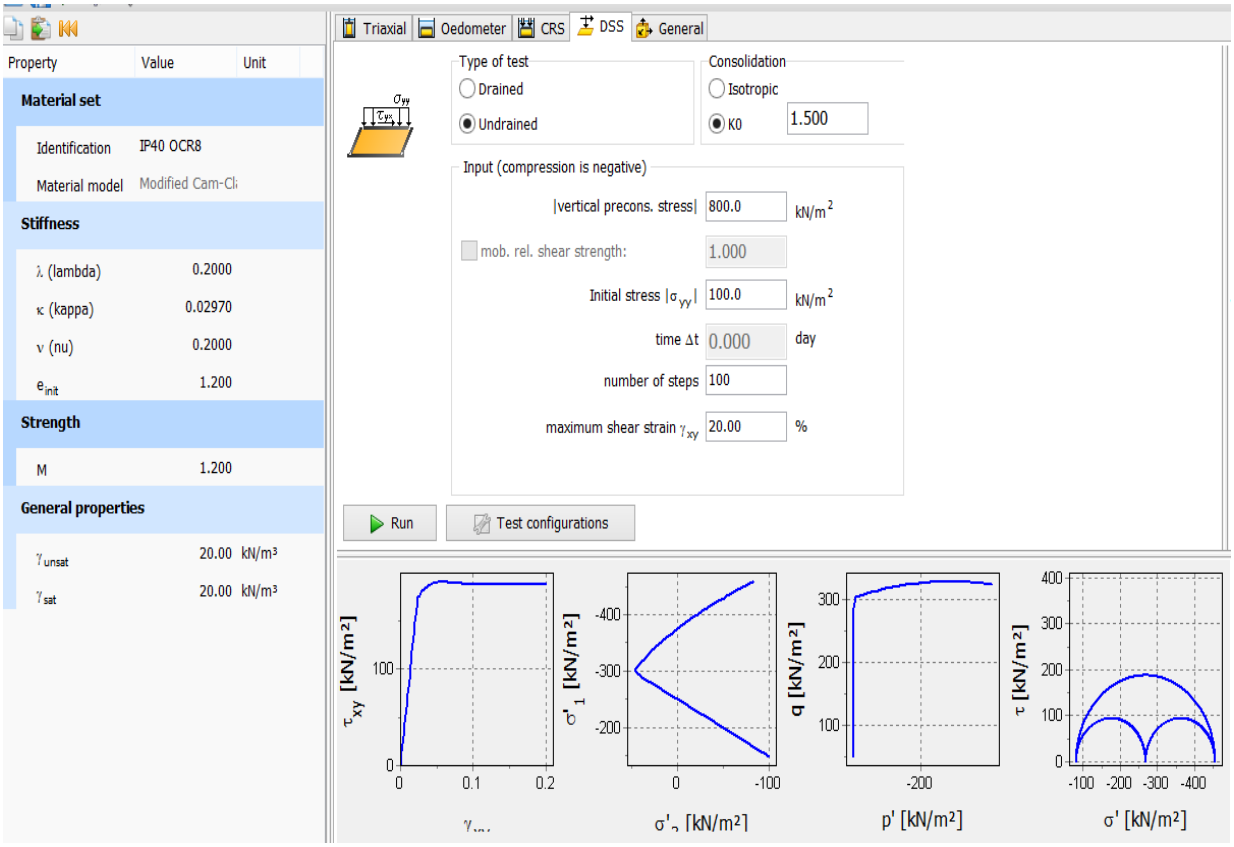

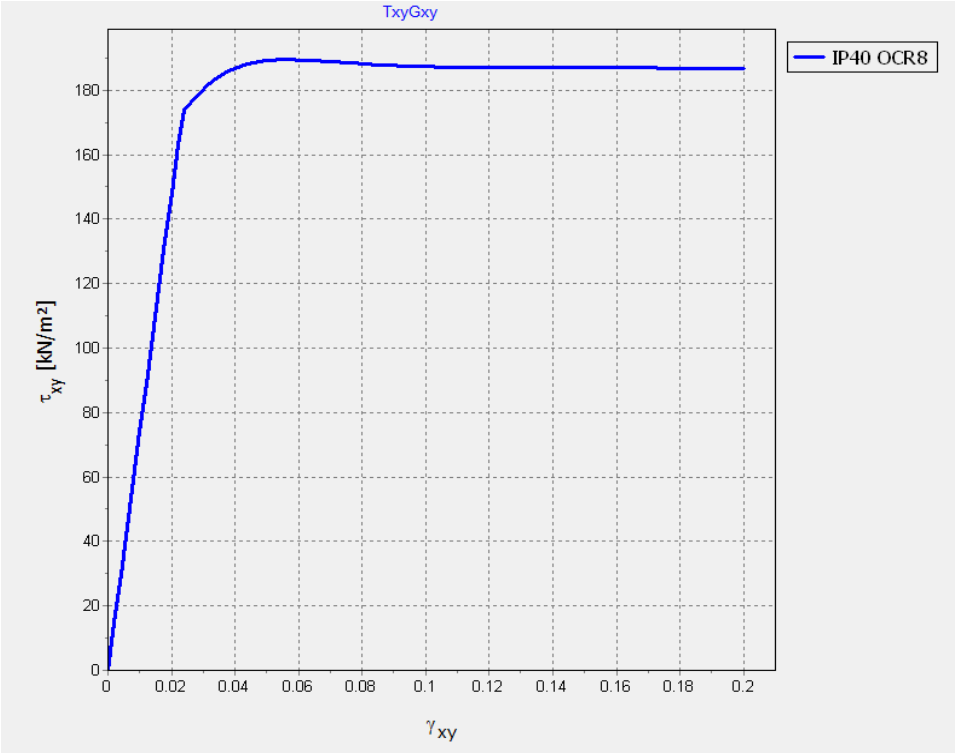

Figure A.4: Direct Simple Shear Test for case d)

Case d): s_{ud} = 189 kPa

Appendix B – Thin Slice Analysis

A numerical analysis assuming plane strain and axisymmetry is carried out in Plaxis 2D, by considering a thin slice. The results from the analysis was found to be highly dependent on the width (radius) of the model. A brief summary of the modelling procedure are presented here.

Plane strain is ensured by applying fixed boundaries in the vertical direction at the top and bottom of the thin slice. The stress state is simulated by adding vertical and horizontal load on a soil material with zero specific weight. Figure B.1 illustrate the model. The model is 0.1 m high. Different widths in the radial direction was tried to study any end effects.

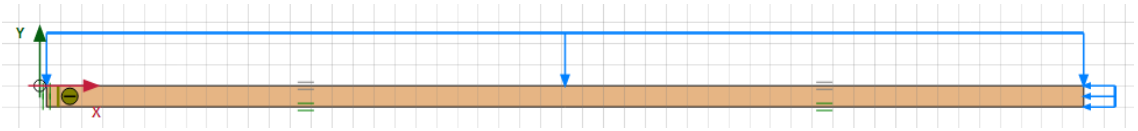

Figure B.1: Thin slice model

The soil parameters for the analysis are as determined Table 8.1, except that the specific weight of the material is set to be zero. The stresses and pore pressures at 10 m depth is investigated. As the ground water table is at the ground surface, the hydrostatic pressure at 10 m depth is 100 kPa. For case a), the initial effective stress state is σ_v' = 100 kPa and σ_r' = σ_θ' = 65 kPa (K_0' = 0.65). The following procedure is carried out in Plaxis 2D:

0. Initial Phase with drained material
1. Adding Load. The desired stress situation is created throughout the model by applying 200 kPa in the vertical direction and 165 kPa in the horizontal direction. GWT is 10 m above the thin slice.
2. The distributed vertical load is replaced by a line displacement boundary condition requiring fixity in the vertical direction. The horizontal line load of 165 kPa is applied throughout the analysis.
3. The drained soil material is replaced by an undrained soil material.
4. The Cavity Expansion is simulated by applying a prescribed displacement of 0.029 m outwards on the inner boundary of the axisymmetric model.
5. At last a consolidation phase is carried out. The pore pressure dissipation is set to carry on until the excess pore pressure is less than 1.0 kPa. (Loading type: minimum excess pore pressure)

A plot of the excess pore pressures with distance from the pile after cavity expansion, are shown in Figure B.2. The figure illustrate the impact of the model size. Results from a 2 m wide and a 5 m wide model are compared. Vertical deformations are not allowed in the "thin slice", as plane strain conditions are assumed. The stiffness of the model during cavity expansion is highly dependent on the width of the model. Thus, stress distributions in the soil after cavity expansion depends on the model size. In other words, the proposed procedure did not produce acceptable results.

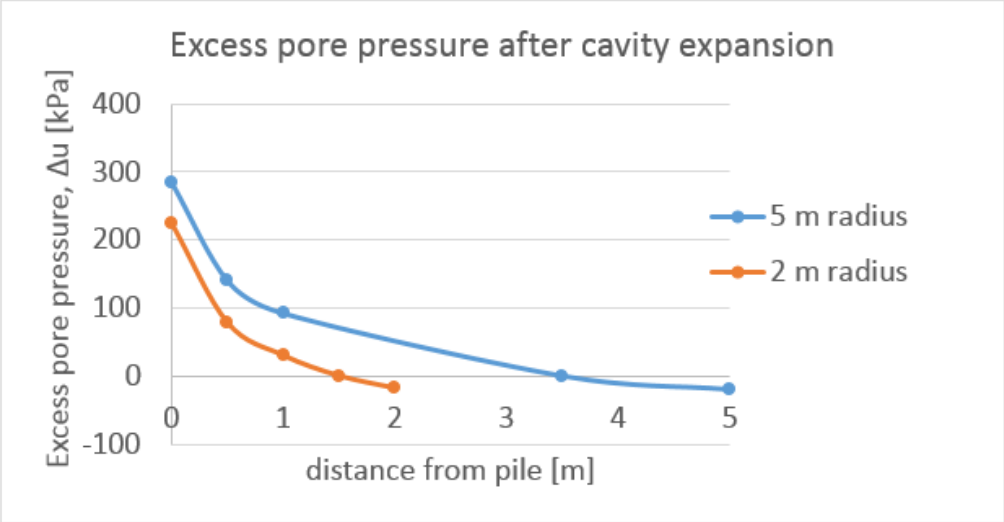

Figure B.2: Excess pore pressure with distance from pile

Appendix C - Stress changes from parametric study

The circumferential and vertical effective stresses from decreasing the compression index by a factor of five is compared to the stresses from the original analysis. The grey coloured plots are the results from the original analysis in section 8.3.2.

Note: Increasing κ by a factor of five for case b) and case d), produce similar stress changes as shown in section C.2 and C.4.

C.1 Circumferential and vertical effective stress changes for case a)

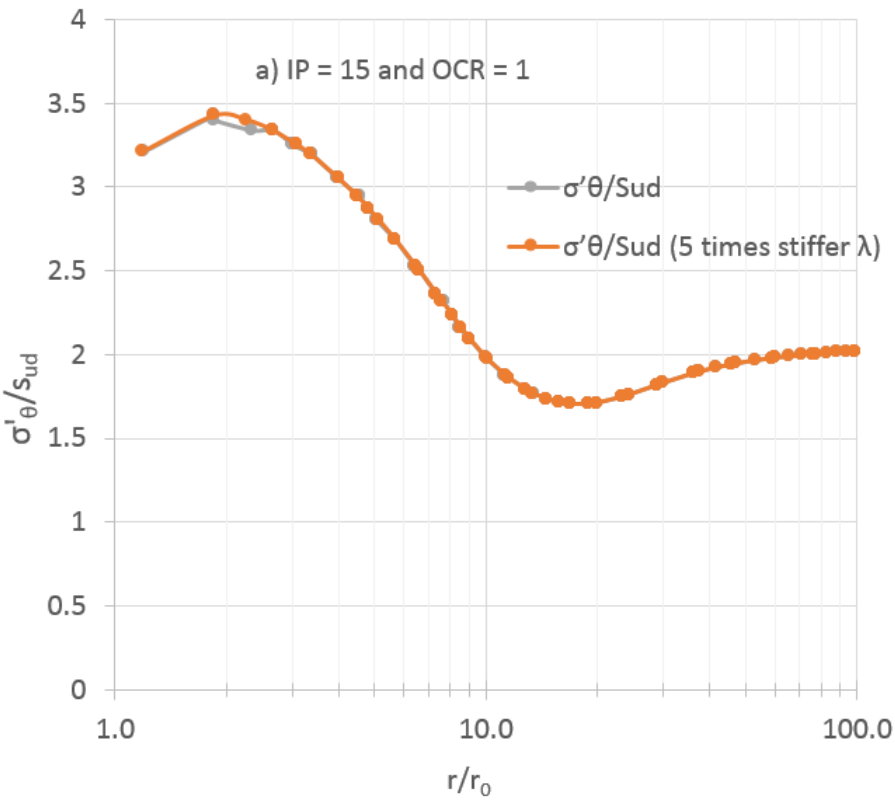

Figure C.1: Circumferential effective stress normalized by undrained shear strength, case a)

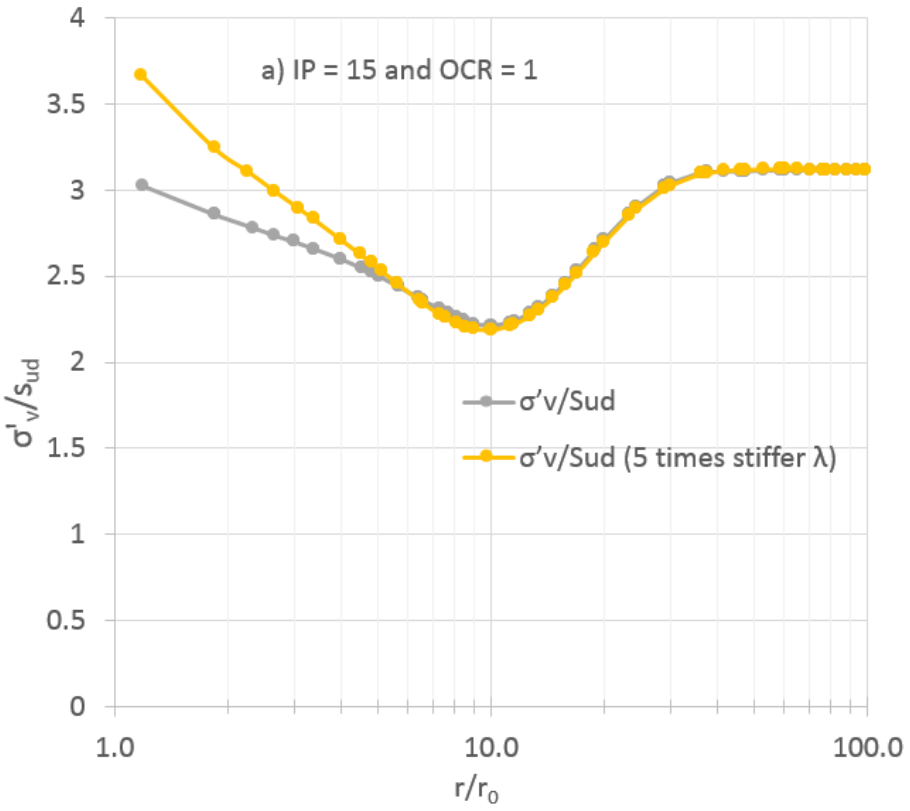

Figure C.2: Vertical effective stress normalized by undrained shear strength, case a)

C.2 Circumferential and vertical effective stress changes for case b)

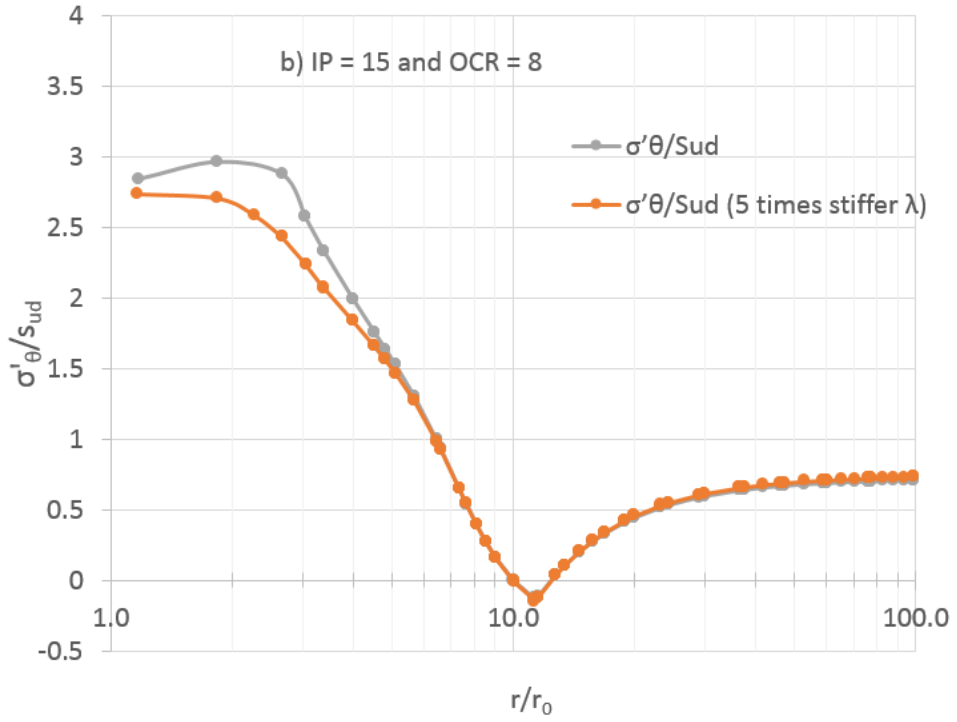

Figure C.3: Circumferential effective stress normalized by undrained shear strength, case b)

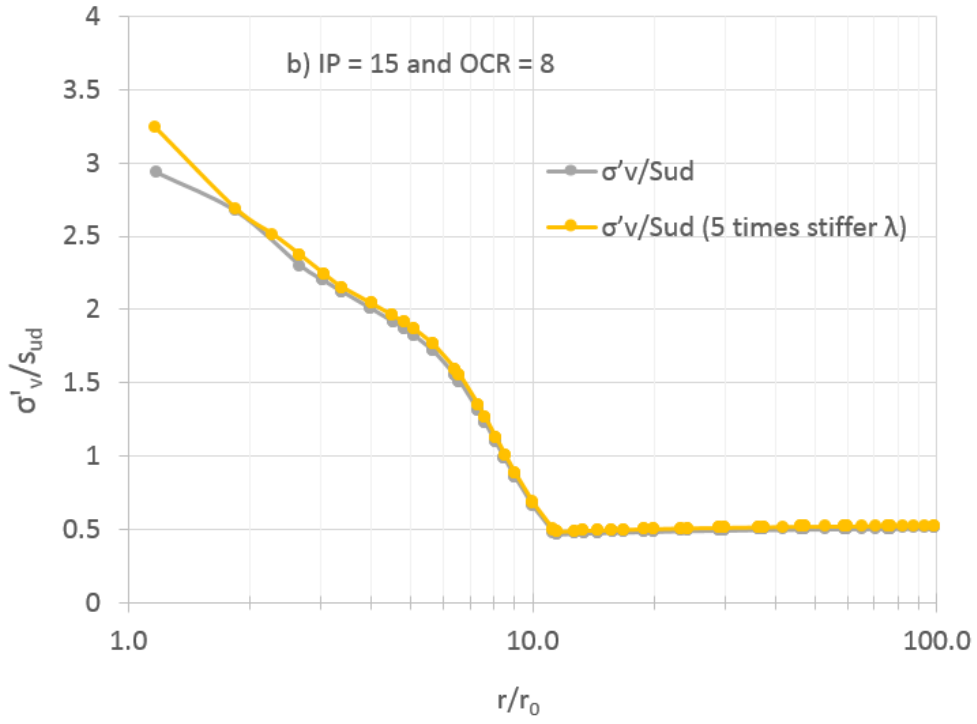

Figure C.4: Vertical effective stress normalized by undrained shear strength, case b)

C.3 Circumferential and vertical effective stress changes for case c)

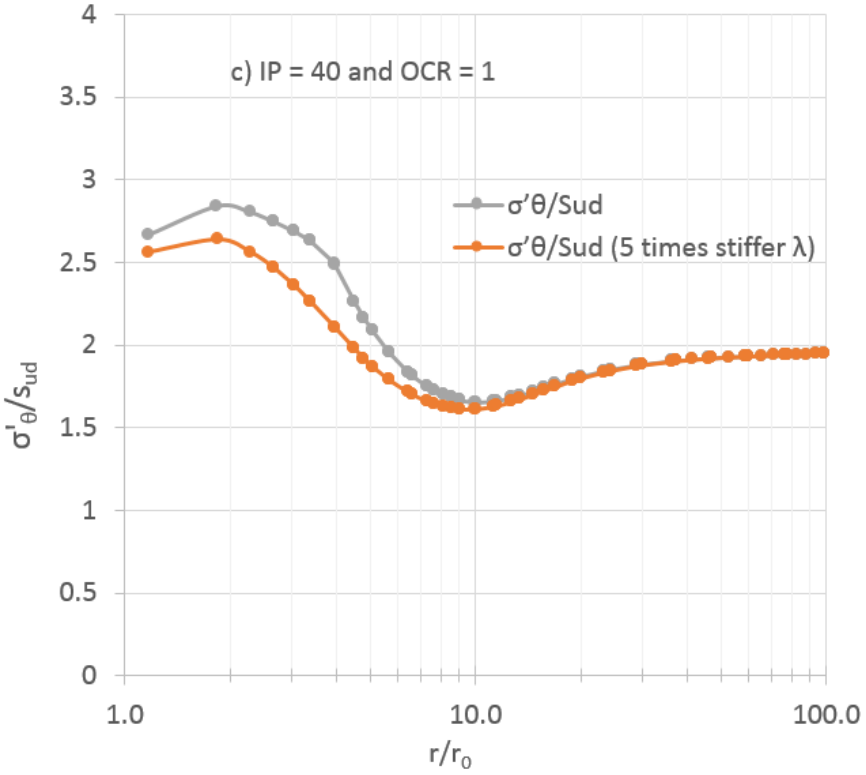

Figure C.5: Circumferential effective stress normalized by undrained shear strength, case c)

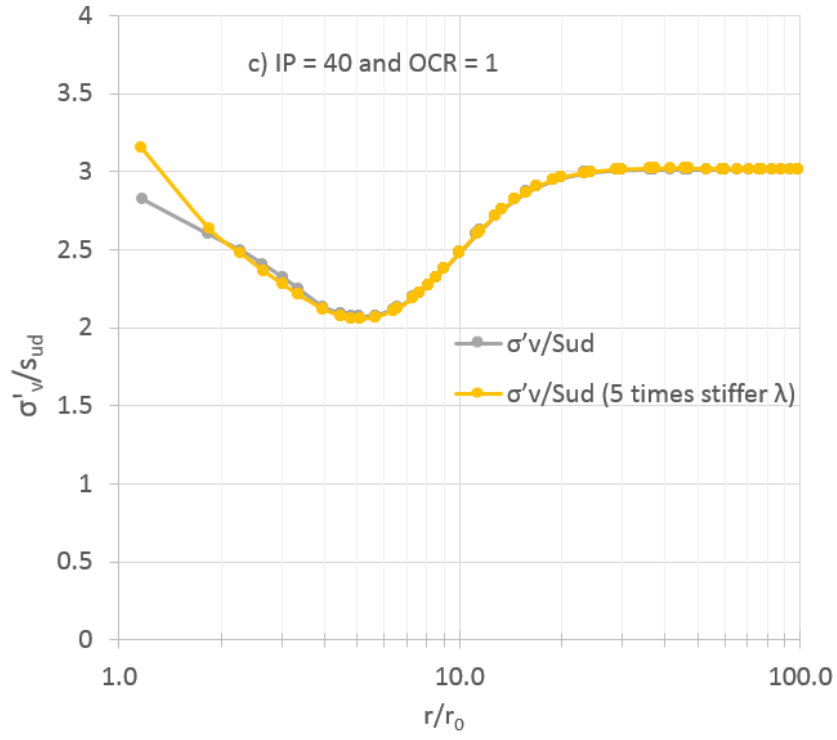

Figure C.6: Vertical effective stress normalized by undrained shear strength, case c)

C.4 Circumferential and vertical effective stress changes for case d)

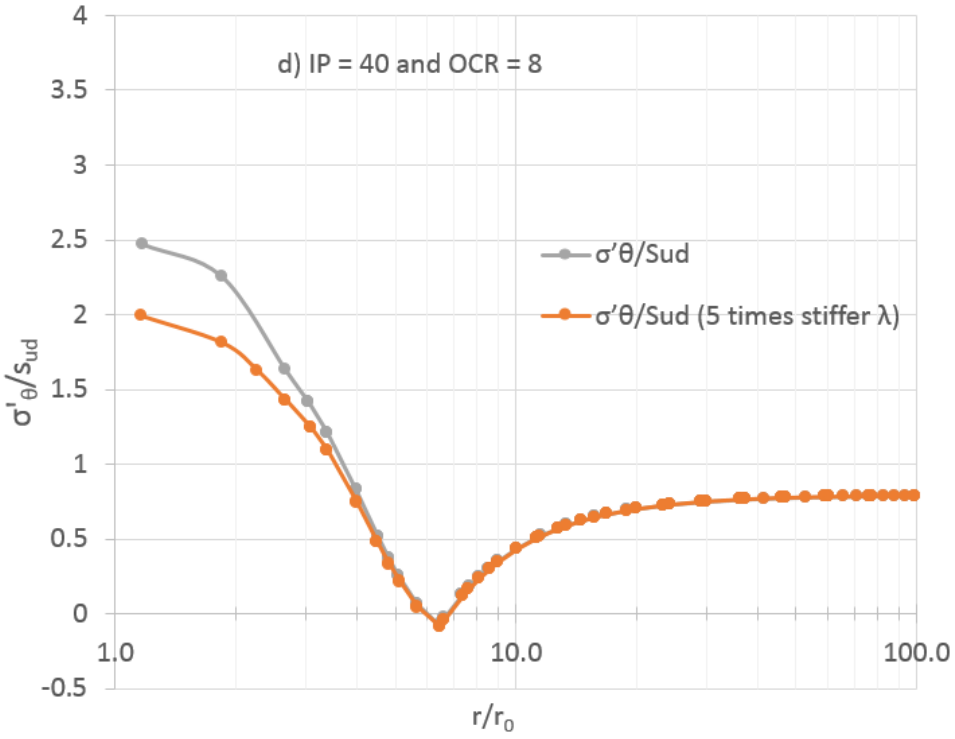

Figure C.7: Circumferential effective stress normalized by undrained shear strength, case d)

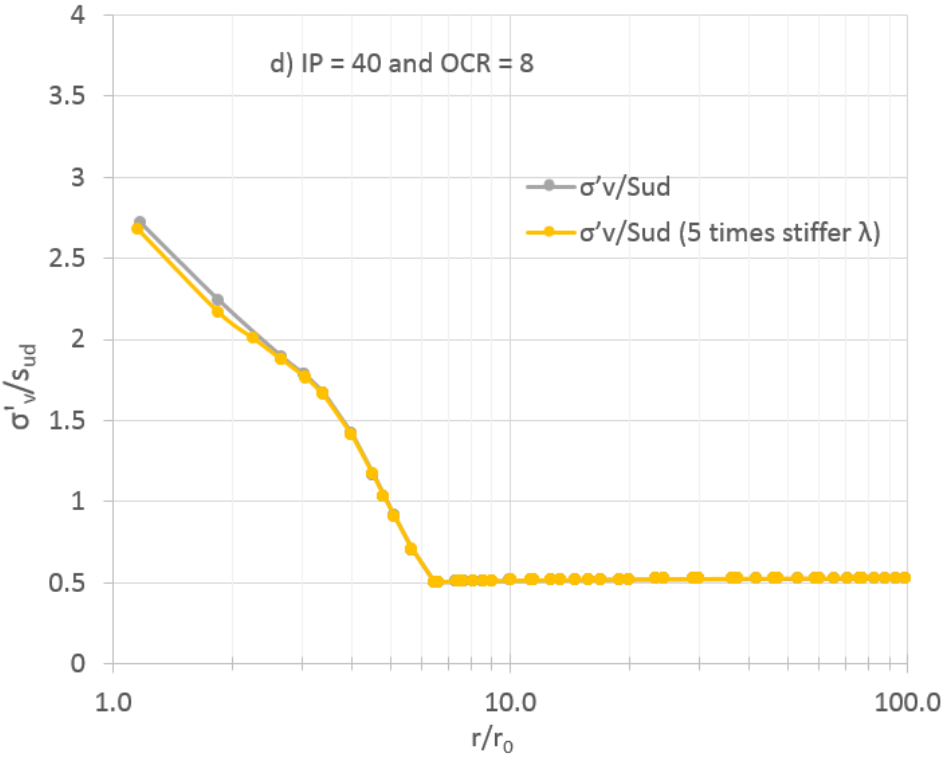

Figure C.8: Vertical effective stress normalized by undrained shear strength, case d)